HOKKAIDO UNIVERSITY

Title	Uncertainty-Aware Path Optimization and Multi-Scale Traffic Flow Modeling in Dynamic Transportation Networks
Author(s)	Wang, Yifan
Degree Grantor	北海道大学
Degree Name	博士(工学)
Dissertation Number	甲第16850号
Issue Date	2026-03-25
DOI	https://doi.org/10.14943/doctoral.k16850
Doc URL	https://hdl.handle.net/2115/99695
Type	doctoral thesis
File Information	Wang_Yifan_.pdf, 全文

Hokkaido University Collection of Scholarly and Academic Papers : HUSCAP

Uncertainty-Aware Path Optimization and Multi-Scale Traffic Flow Modeling in Dynamic Transportation Networks

YIFAN WANG

Graduate School of Engineering, Hokkaido University

NOV. 2025

Abstract

Uncertainty in transportation networks, arising from stochastic travel times, behavioral heterogeneity, and external environmental disturbances, has become a critical challenge for ensuring reliable network operation and efficient optimization. To address this issue, this dissertation establishes a comprehensive three-layer framework that integrates behavioral modeling, stochastic representation, and reliability-oriented optimization. The framework connects individual-level decision mechanisms with system-level optimization logic, providing a unified theoretical and methodological foundation for uncertainty-aware transportation system modeling.

At the behavioral level, a multi-class risk-sensitive path choice model (BST model) is developed to capture travelers' heterogeneous responses under non-extreme flood disturbances. The model introduces a risk-aversion coefficient to describe the degree of user sensitivity to uncertainty and constructs a composite stochastic utility function consisting of three components: perceived travel time, perceived flood risk, and path selection inertia. The first two components represent objective costs, while the third captures subjective psychological tendencies. Two independent stochastic terms, following Gumbel and uniform distributions, are introduced to represent cognitive uncertainty and behavioral asymmetry, allowing the derivation of a closed-form path choice probability. The model further defines dynamically adjusted sets of "acceptable" and "unacceptable" paths, ensuring that paths perceived as high-risk or psychologically rejected are excluded from the feasible choice set. Simulation results demonstrate that the model effectively reproduces users' risk-averse decision patterns and their impacts on the spatial and temporal evolution of network flow distributions.

At the stochastic representation level, a novel Fractional-Folding Moment Transform (FFFT) method is proposed for estimating fractional-order moments of random variables from a finite set of integer-order moments. Fractional moments provide a flexible and sensitive characterization of random processes, particularly under non-Gaussian, heavy-tailed, or long-memory distributions commonly observed in transportation systems. The FFMT method combines the Laplace transform with fractional calculus to derive both analytical and numerical expressions for fractional moments. Theoretical analyses establish explicit error bounds, parameter selection criteria, and the existence and uniqueness of optimal parameters. A short-memory principle is introduced to enhance computational efficiency. Numerical experiments verify that the FFMT method achieves superior stability and accuracy compared with traditional Taylor expansion and Monte Carlo methods, maintaining convergence even for complex and heavy-tailed distributions. This method provides a unified and efficient computational approach for representing stochastic travel time, enabling consistent information transfer between behavioral and optimization layers.

At the optimization level, the dissertation investigates reliable path optimization in correlated networks, focusing on both the mean–variance (m-v) and mean–standard deviation (m-s) formulations. The m-v problem, traditionally regarded as non-additive and non-linear under correlation, is reformulated as a linear programming model through the introduction of flow conservation constraints and an augmented hypergraph transformation. The constraint matrix is proven to be totally unimodular, guaranteeing the existence of integer optimal solutions and ensuring high computational efficiency. Building on this foundation, the m-s problem is formulated as a concave minimization problem, and a global optimization algorithm based on a linear programming framework is developed to ensure global optimality. Numerical results confirm that the proposed models and algorithms exhibit strong convergence, robustness, and scalability, providing a rigorous and efficient approach to reliable path optimization under correlated stochastic environments.

Through systematic integration, the three studies form a coherent and hierarchically connected mechanism. The behavioral model provides stochastic behavioral inputs, the FFMT method transforms these into measurable statistical

parameters, and the reliability optimization model applies them for system-level decision-making. The proposed multi-layer framework ensures logical consistency and continuous information transfer across behavioral, stochastic, and optimization layers, enabling a unified representation of uncertainty propagation and interaction within transportation systems.

In summary, this dissertation makes theoretical and methodological contributions in three aspects: risk-sensitive behavioral modeling, fractional-moment-based stochastic representation, and reliability-oriented path optimization. The proposed framework enhances the understanding of uncertainty mechanisms in transportation networks and offers practical decision-support insights for transportation planning, disaster management, and network resilience improvement.

Keywords

Transportation network uncertainty; Risk-sensitive path choice; Fractional moments; Stochastic travel time; Reliable path optimization; Network resilience.

Contents

Abstract 1

Keywords 3

1 Introduction 7

1.1 Background . . . 8

1.2 Literature Review . . . 10

1.2.1 Risk Perception and Stochastic User Equilibrium Models under Environmental Disturbances . . . 10

1.2.2 Fractural-Moment Modelling and Numerical Approaches for Stochastic Systems . . . 12

1.2.3 Reliable Path Optimization under Correlated Network Conditions . . . 14

1.2.4 Summary and Research Gaps . . . 15

1.3 Research Content . . . 16

1.3.1 Research Objectives . . . 16

1.3.2 Paper Structure . . . 17

2 Theoretical and Methodology Framework 19

2.1 Research Positioning and Overall Motivation . . . 20

2.2 Conceptual Framework . . . 20

2.2.1 Three-Layer Structural Framework . . . 21

2.2.2 Roles and Responsibilities of Each Layer . . . 22

2.3 Theoretical Linkages among the Three Studies . . . 22

2.3.1 Study I $\rightarrow$ Study II: Translating Behavioral Uncertainty into Stochastic Representation . . . 22

2.3.2 Study II $\rightarrow$ Study III: From Stochastic Representation to Reliability Optimization . . . 23

2.3.3 A Closed and Coherent Theoretical System . . . 23

3 Risk-Sensitive Path Selection and Stochastic Equilibrium Model 25

3.1 Overview and Research Objectives . . . 26

3.2 Path Cost Function . . . 26

3.2.1 User Classification and Path Flow . . . 26

3.2.2 Construction of Path Cost Function . . . 27

3.3 Network Equilibrium Model . . . 30

3.3.1 Path Selection Criteria . . . 30

3.3.2 Network Equilibrium Conditions . . . 33

3.4 Numerical Results . . . 33

3.4.1 Settings . . . 33

3.4.2 Results . . . 34

3.4.3 Results under Dynamic Non-Extreme Flood Scenarios . . . 38

3.5 Chapter Summary . . . 41

4 A Method for Estimating Travel Time Distribution Based on Fractional Moments **42**
4.1 Overview and Research Objectives . . . 43
4.2 Theoretical Framework of Fractional-Moment Computation . . . 44
4.3 Numerical Formulation and Error Analysis . . . 45
4.3.1 Numerical Formulation . . . 45
4.3.2 Error Analysis . . . 46
4.4 Parameter Optimization and Stability Analysis . . . 47
4.4.1 Parameter N . . . 47
4.4.2 Parameter h . . . 47
4.4.2.1 Existence and Uniqueness of h . . . 48
4.4.2.2 Calculation of the Optimal h . . . 53
4.5 Numerical Experiments . . . 55
4.5.1 Truncated Normal Distribution . . . 55
4.5.2 Lognormal Distribution . . . 56
4.5.3 Gamma Distribution . . . 58
4.5.4 Real-world Application Case . . . 59
4.6 Chapter Summary . . . 61

5 Reliable Shortest Path Optimization Model Under Relevant Risks **63**
5.1 Overview and Research Objectives . . . 64
5.2 Theoretical Framework and Model Formulation . . . 64
5.2.1 Notation and assumptions . . . 64
5.2.2 Shortest path problem . . . 65
5.3 Mean-Variance (M-V) Reliable Path Problem . . . 66
5.3.1 The m-v shortest path problem expressed in a hypergraph . . . 67
5.3.2 Optimality of the integer relaxation . . . 72
5.4 Mean-Standard-Deviation (M-S) Reliable Path Problem . . . 74
5.5 Numercial Experiments . . . 76
5.6 Chapter Summary . . . 79

6 Integrated Discussion and System Analysis **81**
6.1 Logical Consistency and Extended Results of the Multi-Layer Framework . . . 82
6.2 Interaction among Model Results . . . 82
6.3 Dynamic Closed-Loop Mechanism . . . 83
6.4 Integrated Experiment and Cross-Model Validation . . . 83
6.5 Theoretical and Practical Implications . . . 84
6.6 Summary . . . 84

7 Conclusion **85**
7.1 Summary of Findings . . . 86
7.2 Future Research Directions . . . 87

A The Notations Employed in Chapter 3 **88**

B Derivation Process of Calculation Method of t_{ima} **90**

C Proof of the Sub-additivity of Perceived Link Travel Time **92**

D Proof of the Expression of P_{imj} **94**

E Proof of the Expression of Φ_{imk} **96**

F Proof of Corollary 2.1 **98**

G Proof of Corollary 2.2 **100**

H Proof of Corollary 2.3 **102**

I Proof of Corollary 2.4 **104**

J Proof of Corollary 2.5 **106**

References **108**

Acknowledgments **114**

Chapter 1

Introduction

1.1 Background

(1) Fundamental Theory of Deterministic Path Choice and Network Equilibrium

In a transportation network, individual travelers typically select routes that minimize their perceived travel cost, commonly measured in terms of travel time, distance, monetary expenditure, or generalized disutility. Path-choice behavior interacts with the network's traffic-flow distribution through a feedback mechanism: increasing flow on a link raises its impedance (e.g., travel time or congestion level), which in turn influences subsequent route decisions. This endogenous interaction between individual decision-making and system performance constitutes the fundamental mechanism governing network operation and equilibrium formation, and implies that the transportation network evolves as an interdependent system rather than a static mapping of costs and flows.

Through successive iterations of such interactions, the system gradually approaches a stable state in which no traveler can further reduce personal cost by unilaterally changing routes. At this point, the network reaches an equilibrium flow pattern, either the User Equilibrium (UE), where all utilized routes have equal and minimal perceived costs, or the System Optimal (SO) state, in which total system cost is minimized. Deterministic traffic-assignment models grounded in these principles have therefore become the theoretical cornerstone for analyzing network efficiency and supporting traffic management and planning decisions.

Nevertheless, conventional deterministic models rely on restrictive assumptions, including a stable environment, perfectly known parameters, and fully rational travelers. In practice, transportation systems are exposed to various sources of fluctuation, such as weather conditions, traffic incidents, roadworks, and stochastic demand variations, which induce spatial and temporal variability in link performance. As a result, deterministic models are often insufficient to capture the inherent uncertainty and complex system behavior observed in real networks. Extending classical equilibrium frameworks to incorporate uncertainty and risk has therefore become a central direction in contemporary traffic-assignment research.

(2) Uncertainty and Risk Disturbances in Transportation Networks

Real-world transportation networks operate in complex and uncertain environments. With accelerated urbanization and the intensification of climate change, various disruptive events—such as extreme weather, flooding, traffic accidents, and sudden demand surges—have become more frequent and diverse. These disturbances affect link capacities and travel conditions, rendering travel times, impedances, and demands stochastic rather than deterministic. As a result, network operating states exhibit inherent variability, which is more appropriately represented by probability distributions than by fixed values.

To capture such uncertainty, the Stochastic Traffic Assignment (STA) framework has been developed as an extension of deterministic assignment models. Unlike deterministic formulations, STA treats travel time, impedance, or perceived cost as random variables and represents travelers' imperfect information and perception differences through probability distributions. Consequently, route choices are modeled probabilistically, reflecting bounded rationality and incomplete information in uncertain environments.

Under the stochastic assignment framework, the transportation system evolves toward an expected steady state in which no traveler can reduce expected travel cost by unilaterally changing routes, known as the Stochastic User Equilibrium (SUE). Compared with deterministic equilibrium, SUE captures not only randomness in network conditions but also the resulting heterogeneity in traveler behavior, thereby providing a more realistic description of network performance under uncertainty.

Nevertheless, while SUE accounts for stochastic variability in network conditions, it does not explicitly characterize how travelers' subjective risk perceptions and heterogeneous behavioral responses influence the evolution of network operating states and equilibrium outcomes. This limitation motivates further investigation into risk sensitivity and behavioral heterogeneity within stochastic equilibrium analysis.

(3) Risk Sensitivity and Behavioral Heterogeneity in Stochastic Equilibrium

Under stochastic conditions, travelers respond differently to uncertain travel times or costs. Some individuals prefer routes with shorter expected travel times despite high variability, whereas others prioritize stable and predictable routes even if their expected travel times are longer. Such diversity in psychological attitudes toward risk is pervasive in real transportation systems and plays a crucial role in shaping traffic-flow patterns and equilibrium outcomes. Differences in risk sensitivity imply that perceived route costs are not determined solely by expected values, but by a weighted combination of expectation and variability reflecting individual risk preferences. When a large proportion of travelers are risk-averse, traffic flows tend to distribute more evenly across alternative routes; conversely, when risk-seeking behavior dominates, flows may concentrate on a small number of routes with minimal expected costs, potentially increasing local congestion and network instability. Incorporating risk sensitivity into stochastic equilibrium models therefore enables a more realistic representation of travelers' decision-making processes and provides deeper insight into how network operating states and equilibrium structures emerge under uncertainty.

Moreover, travelers' risk perceptions are not static; they evolve with accumulated experience, information availability, and environmental context. This behavioral heterogeneity introduces additional layers of complexity into network dynamics, as adaptive decision-making continuously reshapes traffic-flow distributions and congestion patterns. Embedding risk sensitivity and behavioral diversity within stochastic assignment frameworks thus provides a behavioral foundation for analyzing the endogenous evolution of network operating states under uncertain conditions. This perspective constitutes the first research dimension of the present dissertation (Paper I).

(4) Numerical Characterization of Stochastic Variables via Fractional Moments

In stochastic traffic assignment and risk analysis, key network variables—such as travel times, link flows, and impedances—are inherently random. Their statistical characteristics (expectation, variance, higher-order moments, and distributional shape) directly affect system-performance evaluation, risk assessment, and route-reliability analysis. Empirical observations show that travel-time distributions in real networks often exhibit heavy tails, skewness, or multimodality, sometimes accompanied by non-Gaussian and long-memory properties. These features make conventional integer-order-moment methods inadequate for accurate or stable characterization, limiting the precision of stochastic analyses.

The Fractional-Moment approach extends the classical definition of moments to non-integer orders, allowing more flexible and continuous representation of random-variable characteristics. Fractional moments can capture fine-grained distributional information lying between the traditional mean and variance, and they are particularly effective in describing non-Gaussian or heavy-tailed behavior. Because of their robustness and expressive power, fractional-moment techniques have been widely adopted in signal processing, structural reliability, and complex-system modeling.

Nevertheless, computing fractional moments often involves intricate integral or differential operations, leading to high computational complexity and potential numerical instability. In large-scale transportation networks, where numerous random variables are interdependent, conventional numerical schemes struggle to balance accuracy and efficiency. Developing a stable, high-precision, and computationally tractable fractional-moment solution method is therefore essential for advancing stochastic network modeling. This challenge defines the second research dimension of the dissertation (Paper II), which proposes a numerical framework combining fractional-moment theory with efficient computation for accurate modeling of complex random variables.

(5) Reliable Path Optimization under Correlated Network Conditions

In stochastic transportation networks, link travel times or impedances are often correlated rather than independent. Correlations may arise from spatial proximity, similar environmental conditions, shared external disturbances, or synchronized fluctuations in travel demand. When such dependencies exist, the total travel time of a path is affected by the joint behavior of its constituent links, yielding a structured distribution that is more complex than the independent-link

assumption used in classical shortest-path models.

Traditional algorithms typically presume link independence and thus fail to capture the cumulative effects of these correlations, potentially underestimating overall uncertainty or overestimating route reliability. To provide more realistic reliability assessment, reliable-path optimization models incorporate inter-link correlations by explicitly modeling joint probability distributions or covariance structures. These models characterize how uncertainties propagate through the network and how correlated fluctuations affect total path travel times.

Within this framework, common reliability metrics include the **Mean-Variance (M-V)** and **Mean-Standard-Deviation (M-S)** formulations, which balance the expected travel cost against variability, reflecting users' or planners' preferences between efficiency and reliability. By introducing correlation structures into reliability analysis, these models extend stochastic-assignment and reliable-route theories, offering a more realistic foundation for route optimization under uncertainty. This constitutes the third research dimension of the dissertation (Paper III), focusing on the formulation and solution of reliable-path optimization problems under correlated network conditions.

(6) Integration and Overall Perspective

In summary, deterministic traffic-assignment models provide a fundamental framework for understanding route choice and equilibrium formation, but they rely on restrictive assumptions regarding environmental stability and traveler behavior. Real transportation systems are inevitably exposed to uncertain and disturbed conditions, under which travel costs, network performance, and user responses exhibit substantial variability.

Existing studies have addressed these challenges from multiple complementary perspectives, including behavioral modeling of risk perception, numerical characterization of stochastic variables, and optimization-based approaches for reliable routing under uncertainty. Together, these efforts highlight that traffic-flow patterns, congestion levels, and equilibrium outcomes are not static, but evolve through the interaction between uncertain conditions and heterogeneous traveler behavior.

This observation suggests the necessity of analytical frameworks capable of capturing the evolving nature of transportation networks under uncertainty, thereby motivating the subsequent review of related literature and the research framework developed in this dissertation.

1.2 Literature Review

1.2.1 Risk Perception and Stochastic User Equilibrium Models under Environmental Disturbances

(1) Disaster- and Disturbance-Induced Uncertainty in Transportation Networks

Urban transportation networks are increasingly exposed to a wide spectrum of environmental and operational disturbances such as heavy rainfall, localized flooding, snowstorms, and other adverse weather events. These disruptions can partially degrade the performance of road infrastructure and drainage systems, reduce network accessibility, and lead to indirect economic losses and safety concerns (Acosta-Coll et al., 2018; Gradeci et al., 2018; Wang et al., 2014). While catastrophic disasters may completely paralyze mobility, moderate-scale disturbances—those insufficient to shut down the entire system yet capable of impairing local traffic—can also produce long-lasting and spatially widespread effects on travel behavior.

During such events, travelers with different levels of risk sensitivity respond differently: risk-tolerant users may continue using affected routes, whereas risk-averse users will avoid them. Consequently, even within the same origin-destination (O-D) pair, the feasible path sets and flow distributions differ across user groups. Previous research on network vulnerability, accessibility, and resilience under disaster conditions (Sullivan et al., 2023; Ye and Kim, 2019; Zhou et al., 2022) has mostly focused on extreme events. Comparatively less attention has been devoted to moderate disturbances and their cumulative influence on route-choice dynamics and flow redistribution. Investigating traffic assignment under such stochastic perturbations therefore remains an important and practical research direction for understanding network

performance and management under everyday risk conditions.

(2) Reliability-Based Network Equilibrium

Travel-time reliability is a key determinant in travelers' route choices (Jackson and Jucker, 1982), especially when the network is affected by uncertain or disruptive events such as heavy rainfall, flooding, or earthquakes. Under such circumstances, travelers tend to avoid risk, and reliability often outweighs purely minimizing expected travel time (Liu et al., 2004). When uncertainty or partial disruption occurs, even if travelers do not cancel their trips, perceived risk and variability can significantly modify route choices and consequently alter the network-equilibrium state.

To better capture these effects, a wide variety of reliability-based network-equilibrium models have been proposed. Early studies introduced the travel-time budget concept (Lo et al., 2006) and developed within-budgeted-time equilibrium formulations. (Watling, 2006) incorporated stochastic travel-time components and late-arrival penalties into the path-cost function. The mean-excess traffic-equilibrium model (Chen and Zhou, 2010a) assumes travelers choose routes least affected by unreliability. Other researchers employed mean–variance or mean–standard-deviation formulations (de Palma and Picard, 2005; Nikolova and Stier-Moses, 2014) to represent users' preferences between efficiency and reliability. (Siu and Lo, 2014) analyzed joint route-and-departure-time choices considering punctuality requirements and reliability-risk trade-offs.

Several studies explicitly examined adverse weather or natural disasters as disturbance factors in reliability-based equilibrium. For example, (Sumalee et al., 2011) analyzed uncertainty in both demand and supply under severe weather and developed a reliability-based equilibrium model within a mean–variance framework; (Lam et al., 2008) incorporated stochastic rainfall effects into the route-cost function to capture weather-induced variability. Despite these advances, few works have systematically examined moderate or recurring disturbances that represent the majority of real-world operating conditions. Moreover, most existing models express uncertainty through a single random term in the path-cost function, which may be insufficient to capture multiple concurrent sources of variability—such as time fluctuations, perceived risk, and psychological factors—that jointly influence travelers' perceived costs. Extending the cost representation to include multiple stochastic components can therefore better reflect heterogeneous risk perceptions and multifaceted uncertainties in realistic networks.

(3) Bounded-Rationality Network Equilibrium

In actual networks, travelers have limited information, computational capability, and time, which constrains their ability to make fully rational decisions (Simon, 1955). The theory of bounded rationality assumes that travelers select optimal or near-optimal routes within a limited choice set, reflecting satisficing rather than perfect optimization. This behavioral assumption aligns more closely with observed decision-making and has led to numerous equilibrium formulations incorporating bounded rationality. (Di et al., 2013) investigated how bounded rationality influences network-equilibrium states; (Fosgerau and Small, 2013) examined congestion effects under bounded rationality; (Mahmassani and Liu, 1999) analyzed day-to-day adjustments during information acquisition; and (Siri et al., 2022) proposed and empirically validated a bounded-rationality day-to-day route-choice model.

These models typically introduce tolerance thresholds or indifference bands, allowing sub-optimal choices and thereby relaxing the strict conditions of UE or SO equilibrium. Under uncertain or perturbed network conditions, such tolerance reflects travelers' reluctance to use certain high-risk routes and their propensity to confine decisions within an acceptable range of perceived costs. However, few studies have explicitly linked these tolerance thresholds to both network disturbances and travelers' risk sensitivity. Additionally, in Logit-based assignment models, even highly unattractive routes often retain positive flow shares—a behavior inconsistent with reality during disruptions. By integrating bounded-rationality concepts with risk perception, it becomes possible to dynamically adjust feasible path sets according to both disturbance intensity and individual sensitivity, thereby yielding a more realistic representation of route choice and equilibrium under uncertain environments.

(4) Summary of Findings

Overall, the existing literature demonstrates substantial progress in modeling traveler behavior and network equilibrium under stochastic and disturbed conditions. Three major research streams can be identified:

a) studies on the influence of environmental and operational disturbances on network accessibility, vulnerability, and user risk perception;

b) reliability-based equilibrium models that incorporate stochastic travel times and risk preferences; and

c) bounded-rationality frameworks that account for travelers' limited decision-making capability.

Nevertheless, these research domains often remain disconnected. Few studies have integrated risk sensitivity, multiple uncertainty sources, and bounded rationality within a unified analytical framework. Bridging these aspects forms the first thematic focus of this dissertation, which seeks to establish a risk-sensitive stochastic-equilibrium model that consistently describes user behavior and network responses under general uncertain and disturbed conditions.

1.2.2 Fractural-Moment Modelling and Numerical Approaches for Stochastic Systems

The fractional-moment approach provides a flexible mathematical framework for representing the statistical properties of random variables beyond the limitations of integer-order moments. It has been widely applied in stochastic modeling, reliability analysis, and uncertainty quantification, offering greater descriptive capability for non-Gaussian, heavy-tailed, and long-memory phenomena. Over the past decades, three principal categories of approaches have been developed for computing fractional moments: analytical methods, numerical-integration methods, and Monte Carlo simulation methods. Each category exhibits unique advantages and inherent limitations, particularly regarding numerical stability, computational efficiency, and applicability to engineering problems.

(1) Analytical Methods

Analytical methods aim to derive explicit or semi-explicit expressions for fractional moments based on mathematical analysis. Representative techniques include direct analytical derivation, chaos-polynomial expansion, fractional-derivative formulations, and Taylor-series expansion.

The direct-derivation approach is conceptually the most straightforward, providing closed-form solutions for certain standard distributions. For example, analytical expressions for the fractional moments of lognormal and normal distributions can be directly obtained (Matsui and Pawlas, 2013). However, this method requires prior knowledge of the exact probability-density function (PDF) of the random variable and often involves further mathematical derivation, which limits its applicability when the PDF is complex or unknown.

The chaos-polynomial expansion method is another analytical approach capable of computing both fractional and integer moments. Lefebvre (T. Lefebvre, 2021) developed a method for calculating high-order integer moments using chaos polynomials, and the same principle was extended to fractional moments (Novák et al., 2024). Despite its mathematical rigor, this method is computationally demanding and resource-intensive, which restricts its use in large-scale engineering applications.

Many researchers have also derived analytical expressions for fractional moments using fractional-derivative techniques (Dremin, 1994; Laue, 1980; Trifche Sandev et al., 2011). Although these formulas are mathematically elegant, they are often impractical because of strict applicability conditions.

Among analytical techniques, the Taylor-expansion method is one of the most widely used in engineering (Cottone and Di Paola, 2009; Gzyl and Tagliani, 2010). It requires only the integer-order moments of the random variable and derives fractional moments through relatively simple calculations. Nevertheless, the method suffers from convergence issues similar to those of generalized Newton polynomials and often demands a large number of integer moments to ensure stable and accurate results (Gzyl and Tagliani, 2010). This high computational cost, together with potential fluctuations in high-order results, has limited the reliability of analytical fractional-moment computations in practice.

(2) Numerical-Integration Methods

The numerical-integration method provides an intuitive and effective alternative once the PDF of a random variable is known. Fractional moments can be computed through direct numerical integration, most commonly the Gaussian-Hermite integration (K. H. Biyari and W. C. Lindsey, 1993), or by employing Chebyshev-polynomial approximations (Benouini et al., 2019; Tagliani, 2011). Although conceptually simple, these methods present several practical difficulties. Because fractional moments involve non-integer powers, the numerical evaluation may suffer from instability or overflow, especially when dealing with extreme values or long-tailed distributions. This issue has been noted in financial engineering, where fractional moments are used to describe the tail behavior of asset returns (Consigli, 2002; Haas and Pigorsch, 2009).

Furthermore, the choice of integration intervals and boundary-handling strategies can significantly influence estimation accuracy, particularly in small-sample contexts where bias and noise are pronounced. In engineering reliability analysis, for example, data are often limited and uncertain, making it difficult for numerical-integration methods to accurately describe the characteristics of stress and strength distributions (Feng et al., 2024; Zhao et al., 2021). Consequently, while these techniques are intuitive, they may yield unstable or biased results in real-world stochastic modeling.

(3) Monte Carlo Simulation Methods

When accurate PDFs are unavailable but sample data exist, Monte Carlo simulation provides a convenient and widely used approach for computing fractional moments. This method generates random samples, computes the corresponding higher-order moments, and then estimates fractional moments from these results (Gelman, 1995). Because Monte Carlo sampling can be computationally intensive, various optimization strategies have been proposed to improve efficiency and accuracy. Xu and Dang (Xu and Dang, 2019) suggested using the Latinized partially stratified sampling method to enhance higher-order moment estimation. Other techniques such as bootstrap resampling and variance-reduction approaches further improve computational performance and precision (Frey and Burmaster, 1999; Salvat et al., 1999; Zhang and Pandey, 2013).

Despite these advantages, Monte Carlo simulations remain constrained by finite sample sizes, which may compromise the accuracy of fractional-moment estimation. Sampling bias and random noise can distort results, particularly for small or noisy datasets, leading to significant estimation errors. Thus, although straightforward and versatile, the Monte Carlo approach can yield unstable or biased outcomes when computing fractional moments for complex or high-variance distributions.

(4) Discussion and Research Gap

Analytical, numerical-integration, and simulation-based methods all provide feasible means to compute real-order moments, including both integer-order and fractional-order moments, but each exhibits inherent drawbacks. Integer-order moments are relatively simple to evaluate and numerically stable, whereas fractional-order moments, involving non-integer exponents, are far more sensitive to sample quality and prone to instability. Their calculation often demands complete knowledge of the underlying distribution, extensive data, or large computational resources. These factors significantly restrict the use of fractional moments in practical stochastic modeling.

Accordingly, a continuing need exists for efficient and robust algorithms that can derive fractional-order moments from known integer-order moments, thereby combining the stability of integer-moment computation with the descriptive strength of fractional moments. The Taylor-expansion approach offers one potential direction, though challenges regarding convergence, accuracy, and stability remain unresolved. Developing such improved numerical methods would enhance the practicality of fractional-moment analysis and provide a solid computational foundation for uncertainty quantification in engineering and transportation-system research.

1.2.3 Reliable Path Optimization under Correlated Network Conditions

The determination of the shortest or most reliable path is a fundamental issue in transportation network analysis. When the travel cost along a path is additive, defined as the sum of the travel costs of individual links, classical node-labeling algorithms such as Dijkstra's or Bellman–Ford can be effectively applied to identify the shortest path. However, when travel-time uncertainty is present, travelers often consider both the expected travel time and its reliability. As a result, reliable-path problems, where optimality is defined based on reliability criteria rather than purely additive cost, have become an important research focus.

Different formulations of reliable-path problems have been proposed depending on how travel-time reliability is defined and measured. The reliable path can be described as the path that minimizes a higher percentile of travel time (Frank, 1969a; Nie and Wu, 2009), maximizes the probability of on-time arrival (Y. Y. Fan et al., 2005; Nie and Fan, 2006; Nie and Wu, 2009), minimizes the mean-excess travel time (Chen and Zhou, 2010b), or minimizes a linear combination of the mean and the standard deviation or variance of travel time (Hall, 1983; Khani and Boyles, 2015; Lo and Tung, 2003; Xing and Zhou, 2011). These formulations represent different trade-offs between efficiency and risk aversion in travel decisions.

(1) Mean-Variance and Mean–Standard-Deviation Path Problems

Among the many approaches, the mean–variance (m–v) and mean–standard-deviation (m–s) reliable-path problems have received the most attention in the literature. In the m–v problem, path cost is expressed as a linear combination of the mean and variance of travel time, while in the m–s problem, the cost is defined as a linear combination of the mean and standard deviation. Although the m–v problem in a non-correlated network, where each link travel time is statistically independent, can be formulated as a mixed-integer quadratic programming problem, solving it in large networks remains computationally demanding.

(Sen et al., 2001) proposed a continuous relaxation method that generates a set of feasible paths from which the optimal m–v solution can be identified. For the m–s problem, (Khani and Boyles, 2015) developed an exact algorithm for non-correlated networks that iteratively solves subproblems formulated as m–v problems. (Chen et al., 2017) demonstrated that when path travel times follow a normal distribution, the m–s shortest-path problem is equivalent to the α-reliable-path problem. Other studies, including (Boyles and Waller, 2010; Chen et al., 2022; Y. Y. Fan et al., 2005; Khani and Boyles, 2015; Nie and Wu, 2009), typically assumed independent link travel times. Although this assumption simplifies model formulation and computation, it limits the representation of real-world traffic systems where dependencies between links are common.

(2) Correlated-Link Reliable Path Problems

Recognizing that link travel times are often correlated in real networks, subsequent studies incorporated statistical correlation into reliable-path formulations (Y.Y. Fan et al., 2005; Hutson and Shier, 2009; Nie and Fan, 2006; Sen et al., 2001; Shahabi et al., 2015, 2013). These studies primarily considered correlations between nearby or functionally connected links, allowing partial capture of spatial dependence but still facing significant computational challenges.

To solve reliable-path problems under correlated conditions, several optimization strategies have been proposed. (Xing and Zhou, 2011) introduced a Lagrangian relaxation method that decomposes the m–s problem into three simpler subproblems. (Zeng et al., 2015) developed a similar approach based on Cholesky decomposition, while (Zhang et al., 2017) further simplified the framework by reducing it to two subproblems without losing computational tractability. (Rostami et al., 2018) proposed a branch-and-bound algorithm that estimates both upper and lower bounds for the m–s shortest-path problem, improving global optimality assessment. (Zhang and Khani, 2019) introduced an approach combining Lagrangian substitution and eigendecomposition, further enhancing solution efficiency.

Although these methods provide valuable insights, reliable-path optimization with correlated travel times remains computationally complex. Many models assume linear correlation or rely on predefined covariance structures, which are difficult to estimate accurately in large or dynamic networks. Moreover, the influence of correlation among links

on the structure and uniqueness of optimal solutions has not been fully explored, particularly when both mean and variability measures are included in the objective function. These limitations continue to hinder practical implementation of correlated-link reliability models.

(3) Summary and Research Gaps

In summary, research on reliable-path optimization has progressed from traditional additive-cost shortest-path formulations toward models that account for stochasticity and link correlation. Early studies focused on independent travel times and introduced several reliability criteria, including percentile-based, probability-based, and moment-based measures. Later studies began to incorporate correlation among link travel times and to apply optimization frameworks such as Lagrangian relaxation, decomposition, and branch-and-bound search.

Despite these advances, reliable-path optimization under correlated conditions still faces both theoretical and computational challenges. Key issues include the difficulty of accurately modeling correlation structures, maintaining computational efficiency in large-scale networks, and ensuring global optimality in problems that combine multiple measures of reliability. Addressing these gaps requires unified frameworks that can effectively integrate correlated uncertainties into optimization while maintaining solvability and numerical stability.

1.2.4 Summary and Research Gaps

(1) Summary of Literature Findings

Existing research on transportation networks under uncertainty can be broadly divided into three interrelated areas: behavioral modeling, stochastic characterization, and reliable optimization. Studies in the first area, focusing on traveler behavior and risk perception, have provided valuable insights into how uncertainty and environmental disturbances influence route-choice behavior and network equilibrium. These models emphasize the role of risk sensitivity, perception heterogeneity, and bounded rationality in shaping stochastic user equilibrium.

The second area, centered on stochastic characterization, has explored various numerical and analytical approaches to describe the random nature of travel times and network flows. Fractional-moment modeling has emerged as a powerful tool for representing complex random variables, particularly those exhibiting non-Gaussian, heavy-tailed, or long-memory characteristics. These developments have enhanced the precision of uncertainty quantification in transportation systems but also revealed new challenges in computational stability and scalability.

The third area concerns reliable-path optimization, which extends traditional shortest-path problems to account for uncertainty and correlation among link travel times. Extensive research has examined mean–variance and mean–standard-deviation formulations, as well as percentile-based and probability-based reliability criteria. More recent studies have incorporated link correlations using Lagrangian-relaxation, decomposition, and global-optimization techniques, improving realism and model fidelity. Collectively, these research streams have significantly advanced the modeling and optimization of transportation systems under stochastic conditions.

(2) Identified Research Gaps

Despite substantial progress, the literature remains fragmented across behavioral, numerical, and optimization perspectives. First, behavioral models of risk-sensitive user equilibrium are often developed independently of network-optimization frameworks, leading to a lack of integration between user perception mechanisms and system-level performance analysis. Second, while fractional-moment methods offer theoretical advantages for accurately characterizing stochastic variables, their adoption in large-scale transportation models remains limited due to issues of convergence, numerical instability, and computational burden. Third, reliable-path optimization models that consider correlation among link travel times typically rely on simplified or fixed covariance structures, which restricts their applicability to dynamic and data-driven network environments. As a result, there remains no unified modeling framework capable of consistently linking traveler behavior, stochastic variable representation, and reliability-oriented optimization under

correlated uncertainty.

(3) Integrative Perspective of This Dissertation

Addressing these research gaps requires a holistic framework that bridges behavioral theory, stochastic modeling, and optimization under uncertainty. The present dissertation aims to establish such an integrated framework by connecting three complementary dimensions:

a) Behavioral dimension: modeling traveler risk sensitivity and stochastic user equilibrium under uncertain and disturbed conditions;

b) Numerical dimension: developing fractional-moment-based approaches to accurately and efficiently characterize stochastic properties of network variables;

c) Optimization dimension: formulating reliable-path optimization models that incorporate link correlations and ensure global solvability.

Through this integrative perspective, the dissertation seeks to provide a unified methodological foundation for understanding, modeling, and optimizing transportation-network performance under uncertainty and correlated risk. The following section (1.3) outlines the specific research objectives and the overall structure of this dissertation in accordance with this framework.

1.3 Research Content

1.3.1 Research Objectives

The overall objective of this dissertation is to establish a comprehensive framework for modeling the evolution of transportation network operating states and path decision-making mechanisms under uncertainty and risk conditions. The study aims to reveal how risk perception, stochastic disturbances, and link correlations collectively influence path choice behavior, travel time distributions, and the resulting network performance and reliability outcomes. Through a three-layered research design, the dissertation develops an integrated theoretical and methodological system that connects behavioral modeling, stochastic characterization, and reliability-oriented optimization, thereby providing a systematic foundation for analyzing and solving reliability problems in uncertain transportation networks.

To achieve this overall objective, the dissertation is organized around three interrelated research directions.

(1) Research Objective 1: Modeling path choice behavior under risk perception and disturbance response.

At the behavioral level, this study investigates how individual risk perception influences path choice behavior under non-extreme disturbance conditions. By incorporating risk sensitivity and behavioral heterogeneity, a risk-perception-based path choice model is established to capture the interaction among external disturbances, subjective perception, and flow distribution across the network. This research elucidates how heterogeneous traveler responses reshape traffic-flow patterns and contribute to the long-run formation of network operating states under uncertainty, providing the behavioral foundation for subsequent uncertainty characterization and decision analysis.

(2) Research Objective 2: Developing a fractional-moment-based stochastic traffic assignment method.

At the methodological level, this study focuses on efficiently and stably characterizing the statistical properties of travel time distributions. To address the limitations of conventional stochastic traffic assignment methods—such as high computational complexity and numerical instability in estimating higher-order moments—a fractional-moment framework combined with Padé approximation is proposed. This method enables accurate estimation of arbitrary-order fractional moments using only limited integer-moment information, ensuring both computational stability and numerical

precision. The resulting framework supports a consistent representation of uncertainty-induced variability in network operating states, thereby providing a reliable analytical basis for subsequent reliability analysis.

(3) Research Objective 3: Reliable path optimization under link correlation.

At the system-decision level, this research examines the reliable shortest-path problem in transportation networks with correlated link conditions. Considering that statistical dependencies among links may arise from spatial proximity or shared disturbance sources, a reliability-oriented path optimization model is developed to explicitly incorporate link correlation structures. The proposed model integrates correlation effects into the reliability-based optimization process, achieving a balanced consideration of expected performance and reliability. This study provides a decision-theoretic framework for selecting robust paths under evolving network conditions shaped by uncertainty and interdependence.

In summary, the three studies are logically sequential and methodologically complementary, forming a coherent research chain from risk-perception-based behavioral modeling to stochastic uncertainty characterization and finally to reliability-oriented path optimization under link correlation. Together, they establish a unified framework for understanding and modeling how transportation networks evolve in their operating states and decision outcomes under uncertainty, thereby offering both theoretical insights and methodological tools for reliability analysis and path optimization in complex environments.

1.3.2 Paper Structure

This dissertation is composed of seven chapters, and each chapter progressively addresses a specific aspect of the research problem, from behavioral modeling to stochastic quantification and reliability optimization. Together, they form a coherent and systematic investigation of uncertainty-aware traffic network modeling and reliable path analysis.

(1) Chapter 1: Introduction

This chapter introduces the background, motivation, and significance of studying uncertainty and risk in transportation networks. It provides a comprehensive review of related research on user behavior modeling, stochastic traffic assignment, and reliability-based optimization. The chapter concludes by defining the overall research objectives and outlining the structure of the dissertation.

(2) Chapter 2: Theoretical and Methodological Framework

This chapter establishes the theoretical foundation and overall methodology of the dissertation. It clarifies how the three core studies, namely risk sensitive path selection, fractional moment based uncertainty quantification, and reliable path optimization under link correlation, are conceptually and methodologically connected. A unified research roadmap is presented to illustrate the logical progression from behavioral responses to stochastic representation and system optimization, serving as the bridge between the introduction and the following chapters.

(3) Chapter 3: Risk-Sensitive Path Selection and Stochastic Equilibrium Model

This chapter corresponds to the first core study, which focuses on the behavioral level of analysis. It develops a risk-sensitive path choice and stochastic equilibrium model to describe how users respond to disturbances and how these behavioral responses shape flow propagation and equilibrium conditions within the network. The model identifies the behavioral origins of flow variability and provides the foundation for the stochastic quantification discussed in Chapter 4.

(4) Chapter 4: A Method for Estimating Travel Time Distribution Based on Fractional Moments

The second core study, presented in this chapter, deals with the mathematical representation and quantification of uncertainty. It proposes a fractional-moment-based approximation method for estimating travel-time distributions

with high accuracy and numerical stability. By combining analytical derivation and numerical computation, this method achieves a balance between theoretical rigor and computational feasibility, enabling efficient characterization of stochastic propagation that supports reliability analysis and optimization.

(5) Chapter 5: Reliable Shortest Path Optimization Model Under Link Correlation

This chapter presents the third core study, which focuses on reliability optimization when statistical correlations exist among network links. Considering that link travel times may be correlated due to spatial proximity or shared disturbance sources, a reliable shortest path model is formulated to incorporate link correlation into the optimization process. This study completes the research chain by integrating behavioral and stochastic findings into a reliability-oriented optimization framework.

(6) Chapter 6: Comprehensive Discussion

This chapter provides an integrative discussion of the three core studies, emphasizing their interconnections and mutual reinforcement. It examines how risk-sensitive behavioral mechanisms influence the formation of travel-time distributions, how the fractional-moment approach enhances the estimation of reliability metrics, and how stochastic information supports reliable path optimization. The potential closed-loop interactions among the three components are also discussed, highlighting the systematic nature of the proposed framework.

(7) Chapter 7: Conclusion

The final chapter summarizes the major findings and contributions of the dissertation. It highlights the theoretical and methodological advancements achieved across the three research dimensions: behavioral modeling, stochastic quantification, and reliability optimization. The chapter concludes with a discussion of future research directions, including possible extensions to dynamic environments, large-scale applications, and data-driven modeling approaches.

Chapter 2

Theoretical and Methodology Framework

2.1 Research Positioning and Overall Motivation

Uncertainty in transportation networks does not arise from a single source; rather, it emerges through the interaction of multiple layers of mechanisms. Traveler responses to disturbances, the propagation of stochastic travel times through network structures, and reliability-oriented decision behaviors jointly shape how traffic-flow patterns, congestion levels, and overall network performance evolve under uncertain conditions. In this sense, uncertainty is not merely a source of randomness, but a driving factor that induces endogenous evolution in transportation network operating states.

At the behavioral level, existing research has extensively examined travelers' risk perception, behavioral heterogeneity, and bounded rationality, revealing the fundamental origins of uncertainty in route choice. However, such models often remain at the individual decision level and do not explicitly explain how heterogeneous responses accumulate and translate into network-scale operating states. At the stochastic representation level, many studies rely on explicit distributional assumptions or computationally intensive high-order moment estimation, which obscures the link between behavioral mechanisms and system-level uncertainty. At the optimization level, reliable path models frequently depend on exogenously specified travel-time distributions, without explicitly accounting for how such distributions emerge from traveler behavior and network interactions.

Motivated by these limitations, this dissertation aims to construct a unified theoretical chain that integrates uncertainty generation, stochastic representation, and reliability-oriented decision-making, with a particular emphasis on how uncertainty and traveler behavior jointly drive the evolution of network operating states. The proposed framework ensures that uncertainty is modeled consistently across three complementary layers:

(a) **Study I (Behavioral Layer): Where does uncertainty originate?**

This study focuses on risk sensitivity and perceptual bias under non-extreme disturbances, revealing how heterogeneous traveler responses generate variability in route choice and initiate the long-run evolution of traffic-flow patterns under persistent external conditions.

(b) **Study II (Stochastic Representation Layer): How can uncertainty be mathematically described and quantified?**

This study develops a fractional-moment-based representation method to characterize complex or unknown travel-time distributions, transforming behavior-induced uncertainty into stable, computable, and distribution-free statistical descriptors suitable for network-level analysis.

(c) **Study III (Decision Layer): How should reliable decisions be made under uncertainty?**

This study formulates a reliability-oriented path optimization model that incorporates link correlations and leverages the statistical descriptors derived from Study II to jointly consider expected performance and reliability under correlated network conditions.

These three studies do not operate independently; rather, they form a strict causal sequence in which behavior-induced uncertainty reshapes network operating states, is systematically characterized in the stochastic layer, and is ultimately embedded in reliability-based decision-making. Together, they constitute a coherent and closed modeling framework for analyzing the evolution of transportation networks under uncertainty, thereby providing a solid foundation for the theoretical developments presented in the subsequent sections.

2.2 Conceptual Framework

This section presents the overall conceptual structure of the framework developed in this dissertation. Motivated by the multi-layered nature of uncertainty in transportation systems, the proposed framework incorporates three interrelated layers—behavioral generation, stochastic representation, and reliability-oriented decision-making. Together, these layers provide a coherent and causally ordered foundation for understanding how uncertainty arises, how it can be mathematically represented, and how it should be incorporated into reliable path-selection decisions.

2.2.1 Three-Layer Structural Framework

(1) Behavioral Generation Layer (Study I)

The behavioral layer focuses on how travelers respond to non-extreme disturbances such as localized congestion, minor weather variations, or small-scale incidents. Under such conditions, travelers do not behave as fully rational agents; instead, risk sensitivity, perceptual bias, and behavioral heterogeneity lead to fluctuations in route choices. These behavioral variations constitute the initial and fundamental source of uncertainty within the network.

This layer addresses the question:

Where does uncertainty originate?

It provides the behavioral foundation for the subsequent modeling layers.

(2) Stochastic Representation Layer (Study II)

As behavior-driven uncertainty propagates through network topology and flow interactions, it manifests as stochastic travel-time and path-cost distributions. These distributions often exhibit complex, non-Gaussian, or unknown statistical characteristics that cannot be reliably captured by conventional methods relying on explicit distributional assumptions. To overcome these limitations, the second layer employs a fractional-moment-based approach that reconstructs key statistical descriptors—such as mean, variance, covariance, and fractional moments—from limited integer-moment information. This method provides a stable and distribution-free representation of uncertainty suitable for network analysis and reliability evaluation.

This layer addresses the question:

How can uncertainty be mathematically expressed and quantified?

It functions as the analytical bridge between behavioral mechanisms and decision models.

(3) Reliability-Oriented Decision Layer (Study III)

When travel times are random and statistically correlated across links, traditional shortest-path models fail to account for reliability considerations. Reliable path selection requires balancing expected performance with robustness under uncertainty, especially when link correlations arise from spatial proximity or shared disturbance sources.

Drawing upon the statistical descriptors provided by the stochastic representation layer, the third layer develops an optimization model that explicitly incorporates link correlation and jointly optimizes expected cost and reliability.

This layer answers the question:

How should reliable decisions be made under uncertainty?

(4) Logical Integration Across Layers

The three layers form a strictly ordered and functionally complementary chain:

- the behavioral layer generates uncertainty;
- the stochastic layer formalizes and quantifies it;
- the decision layer utilizes these representations for reliability optimization.

Together, they establish a closed and coherent framework that links uncertainty generation, propagation, and application.

2.2.2 Roles and Responsibilities of Each Layer

To avoid treating the three studies as parallel or disconnected topics, Table 2-1 clarifies the specific tasks and functions associated with each layer.

Table 2-1: Task–Question–Study Structure Across the Three Modeling Layers

Layer	Primary Task	Core Question	Corresponding Study
Behavioral Generation	Explain the origin of behavioral uncertainty	Where does uncertainty come from?	Study I
Stochastic Representation	Provide mathematical representations of uncertainty	How can uncertainty be quantified?	Study II
Reliability Optimization	Support optimal decisions under uncertainty	How to make reliable decisions?	Study III

A critical point is worth emphasizing: Study II is not a computational tool for Study I or Study III. It is an independent analytical layer that converts behavior-induced randomness into generalizable statistical descriptors suitable for reliability-oriented optimization. This structured division of roles forms the conceptual foundation of the dissertation and guides the theoretical development in the following sections.

- patterns of variability in route-choice probabilities,
- travel-time fluctuations induced by risk-sensitive behavior, and
- flow randomness resulting from behavioral heterogeneity.

It is essential to emphasize that Study II does not use the numerical outputs of Study I as computational inputs. The connection between the two studies is theoretical rather than technical: Study II builds on the mechanism revealed in Study I—that uncertainty is behaviorally generated—and provides a stable, distribution-free stochastic representation framework capable of expressing this uncertainty in a mathematically tractable form.

Thus, the relationship can be summarized as follows:

- Study I explains why uncertainty arises;
- Study II formalizes how such uncertainty can be mathematically represented.

2.3 Theoretical Linkages among the Three Studies

This section clarifies the theoretical relationships among the three studies of this dissertation. Although each study focuses on a distinct analytical layer—behavioral generation, stochastic representation, and reliability-oriented optimization—they form a coherent chain through an explicit "input–output" relationship. Their interdependence lies not in computational requirements but in the progression of concepts, assumptions, and theoretical functions. Together, they constitute a complete sequence from the generation of uncertainty to its representation and final application in decision-making.

2.3.1 Study I → Study II: Translating Behavioral Uncertainty into Stochastic Representation

Study I reveals the behavioral origins of uncertainty in transportation networks. By modeling travelers' responses to non-extreme disturbances—such as localized congestion or minor weather variability—it demonstrates how risk sensitivity, perceptual bias, and behavioral heterogeneity lead to fluctuations in route choices, flow distributions, and travel times. The primary conceptual outputs of Study I include:

- patterns of variability in route-choice probabilities,
- travel-time fluctuations induced by risk-sensitive behavior, and
- flow randomness resulting from behavioral heterogeneity.

It is essential to emphasize that Study II does not use the numerical outputs of Study I as computational inputs. The connection between the two studies is theoretical rather than technical: Study II builds on the mechanism revealed in Study I—that uncertainty is behaviorally generated—and provides a stable, distribution-free stochastic representation framework capable of expressing this uncertainty in a mathematically tractable form.

Thus, the relationship can be summarized as follows:

- Study I explains why uncertainty arises;
- Study II formalizes how such uncertainty can be mathematically represented.

This constitutes a fundamental cross-layer transformation from behavioral mechanisms to analytical characterization.

2.3.2 Study II → Study III: From Stochastic Representation to Reliability Optimization

Study II produces a set of statistical descriptors that characterize complex travel-time distributions without assuming a specific probability form. These descriptors include:

- the mean travel time (μ),
- variance (σ^2),
- link-to-link covariance structures, and
- fractional-moment features.

Study III uses these statistical descriptors as essential inputs to develop a reliable path optimization model that explicitly incorporates link correlation. In this sense: Study II provides the theoretical foundation—not a computational tool—for Study III to conduct reliability-oriented decision-making.

Their relationship can be described as:

- Study II defines how uncertainty is quantified;
- Study III determines how decisions should be optimized under such quantified uncertainty.

This linkage completes the conceptual transition from stochastic description to decision formulation.

2.3.3 A Closed and Coherent Theoretical System

Taken together, the three studies form a comprehensive closed-loop structure:

(a) **Generation of uncertainty (Study I):**
Behavioral mechanisms—risk sensitivity, perceptual bias, and heterogeneity—introduce randomness into the network.

(b) **Representation of uncertainty (Study II):**
The stochastic characteristics generated by behavior are transformed into computable and distribution-free statistical descriptors.

(c) **Decision-making under uncertainty (Study III):**
These descriptors are incorporated into a reliability-oriented optimization framework that balances expected cost and reliability.

This closed-loop hierarchy highlights that uncertainty propagates across behavioral, analytical, and decision layers, with each layer providing indispensable theoretical support for the next. The three studies are therefore not parallel contributions but mutually dependent components of an integrated framework for modeling uncertain transportation systems.

Chapter 3

Risk-Sensitive Path Selection and Stochastic Equilibrium Model

3.1 Overview and Research Objectives

In complex transportation systems, external disturbances are ubiquitous and often unavoidable. Such disturbances—including adverse weather conditions, unexpected incidents, infrastructure degradation, and fluctuations in travel demand—affect link capacities and travel conditions, thereby influencing travelers' risk perception and route choice behavior. Under uncertainty, the transportation network should be understood not as a static system, but as one whose operating states—such as traffic-flow distributions and congestion patterns—evolve endogenously through the interaction between external conditions and heterogeneous traveler responses.

With the growing impacts of climate change, weather-related disturbances have become one of the most influential factors affecting the long-term operational stability of urban transportation networks. In particular, medium- and low-intensity disturbances, while less destructive than extreme events, occur more frequently and persist over longer periods. Such disturbances do not completely disrupt travel activities, but continuously influence user behavior and network performance, making them especially relevant for analyzing the long-run evolution of traffic systems under uncertainty.

Among various disturbance types, flooding represents a direct and illustrative example. Flooding can reduce effective road capacity, slow vehicle speeds, and increase travel times, thereby altering travelers' routing decisions. Under non-extreme flood conditions, although moderate water accumulation degrades road usability, most travelers continue their trips while exhibiting stronger risk-avoidance tendencies and increased behavioral heterogeneity. This partial-impact setting, in which travel is sustained but route choice behavior is systematically modified, provides a representative context for studying risk-sensitive path choice and equilibrium formation under persistent external disturbances.

Based on this perspective, this chapter adopts non-extreme flooding as a typical disturbance scenario and develops a risk-sensitive stochastic equilibrium model to characterize the long-run interaction between user heterogeneity, disturbance intensity, and traffic-flow redistribution. Travelers are categorized according to their levels of risk sensitivity, and a link-based traffic assignment framework with a cost function incorporating Binary Stochastic Terms (BST) is proposed to describe heterogeneous route choice behavior. The generalized cost function consists of three components: travel time, flood risk, and path choice inertia. Flood risk is quantified using inundation length, depth, and flow velocity along each link, reflecting objective external conditions, while path choice inertia captures travelers' subjective psychological tendencies when facing uncertainty. Both flood risk and inertia are modeled as stochastic variables to represent perceptual ambiguity and behavioral variability.

Furthermore, the model introduces the concept of an acceptable path set, within which travelers of different risk sensitivities select routes consistent with their individual risk tolerance. Paths deemed unacceptable receive no flow, ensuring behavioral consistency at the individual level. Equilibrium conditions are then formulated to allow acceptable path sets and flow patterns to adjust endogenously to disturbance intensity and user risk preferences. Through this framework, the chapter aims to reveal how risk-sensitive behavior drives the evolution of stochastic equilibrium states in transportation networks under non-extreme flooding, thereby providing a behavioral foundation for subsequent analyses of uncertainty propagation and reliable path optimization.

3.2 Path Cost Function

The notations employed in Chapter 3 are shown in Appendix A.

3.2.1 User Classification and Path Flow

Users within each O-D pair are categorized into different types based on their risk sensitivity, denoted as ρ_{im}, where m represents the user type. User risk sensitivity represents the degree of concern towards risks, with higher sensitivity indicating greater aversion to risks. Users with different levels of risk sensitivity will perceive different travel costs for the same paths and will make different path choices accordingly. This study assumes that the demand for O-D pair Q_i, $i \in I$, is a random variable, denoted as $Q_i \sim (q_i, \sigma_i^2)$. Employing Q_{im} represents the demand for different types of users within the same O-D pair. Q_{im} is stochastic, denoted as $Q_{im} \sim (q_{im}, \sigma_{im}^2)$, and Q_{im} is independent of each other. Then

the following relationship holds:

$$Q_i = \sum_{m \in M_i} Q_{im}, \quad \forall i \in I. \tag{3-1}$$

$$Q_{im} = P_{im} \cdot Q_i, \quad \forall i \in I,\ \forall m \in M_i. \tag{3-2}$$

$$q_{im} = P_{im} \cdot q_i, \quad \forall i \in I,\ \forall m \in M_i. \tag{3-3}$$

$$\sigma_{im}^2 = \mathrm{var}[Q_{im}] = P_{im}^2 \cdot \mathrm{var}[Q_i] = P_{im}^2 \cdot \sigma_i^2, \quad \forall i \in I,\ \forall m \in M_i. \tag{3-4}$$

were P_{im} represents the proportion of Q_{im} occupied in Q_i. F_{imj} denotes the stochastic traffic flow on the path $j \in J_i$ belonging to Q_{im}, denoted as $F_{imj} \sim (f_{imj}, \sigma_{imj}^2)$. Introducing P_{imj} to denote the proportion of traffic flow among different paths within Q_{im}, which is interpreted as the probability of user type m selection among different paths within Q_{im}, the following relationship can be obtained:

$$Q_{im} = \sum_{j \in J_i} F_{imj}, \quad \forall i \in I,\ \forall m \in M_i. \tag{3-5}$$

$$F_{imj} = P_{imj} \cdot Q_{im}, \quad \forall i \in I,\ \forall m \in M_i,\ \forall j \in J_i. \tag{3-6}$$

$$f_{imj} = P_{imj} \cdot q_{im}, \quad \forall i \in I,\ \forall m \in M_i,\ \forall j \in J_i. \tag{3-7}$$

$$\sigma_{imj} = \sqrt{\mathrm{var}[F_{imj}]} = \sqrt{\mathrm{var}[P_{imj} \cdot Q_{im}]} = P_{imj} \cdot \sigma_{im}, \quad \forall i \in I,\ \forall m \in M_i,\ \forall j \in J_i. \tag{3-8}$$

$$\mathrm{cov}[F_{imj}, F_{imk}] = \mathrm{cov}[P_{imj} \cdot Q_{im}, P_{imk} \cdot Q_{im}] = P_{imj} \cdot P_{imk} \cdot \sigma_{im}^2, \quad \forall i \in I,\ \forall m \in M_i,\ \forall j, k \in J_i. \tag{3-9}$$

F_{ij} represents the total stochastic traffic flow on the path $j \in J_i$, as $F_{ij} \sim (f_{ij}, \sigma_{ij}^2)$, and V_a represents the total stochastic flow on the link a, as $V_a \sim (v_a, \sigma_a^2)$. The following relationship holds:

$$f_{ij} = \sum_{m \in M_i} f_{imj}, \quad \forall i \in I,\ \forall j \in J_i. \tag{3-10}$$

$$\mathrm{var}[F_{ij}] = \sigma_{ij}^2 = \sum_{m \in M_i} \mathrm{var}[F_{imj}] = \sum_{m \in M_i} \sigma_{imj}^2, \quad \forall i \in I,\ \forall j \in J_i. \tag{3-11}$$

$$\mathrm{cov}[F_{ij}, F_{ik}] = \sum_{m \in M_i} \mathrm{cov}[F_{imj}, F_{imk}] = \sum_{m \in M_i} P_{imj} P_{imk} \sigma_{im}^2, \quad \forall i \in I,\ \forall j, k \in J_i. \tag{3-12}$$

$$V_a = \sum_{i \in I} \sum_{j \in J_i} \delta_{aj} F_{ij}, \quad \forall a \in A. \tag{3-13}$$

$$v_a = \sum_{i \in I} \sum_{j \in J_i} \delta_{aj} f_{ij}, \quad \forall a \in A. \tag{3-14}$$

$$\sigma_a^2 = \sum_{i \in I} \sum_{j \in J_i} \delta_{aj}\, \mathrm{var}[F_{ij}] + \sum_{i \in I} \sum_{j \in J_i} \sum_{\substack{k \in J_i \\ k \neq j}} \delta_{aj} \delta_{ak}\, \mathrm{cov}[F_{ij}, F_{ik}], \quad \forall a \in A. \tag{3-15}$$

$$\mathrm{cov}[V_a, V_b] = \sum_{i \in I} \sum_{j \in J_i} \sum_{k \in J_i} \delta_{aj} \delta_{bk}\, \mathrm{cov}[F_{ij}, F_{ik}], \quad \forall a, b \in A. \tag{3-16}$$

3.2.2 Construction of Path Cost Function

The acquisition of link travel times is based on the BPR function, as depicted below:

$$T_a = t_a^0 \left(1 + \beta \left(\frac{V_a}{C_a}\right)^{\lambda}\right), \quad \forall a \in A, \tag{3-17}$$

where t_a^0 is the free flow travel time on the link a. T_a is stochastic, then the mean $E[T_a]$ and variance $\mathrm{var}[T_a]$ can be obtained:

$$E[T_a] = t_a^0 + \frac{t_a^0 \beta}{C_a^\lambda} E[V_a^\lambda], \quad \forall a \in A, \tag{3-18}$$

$$\mathrm{var}[T_a] = \left(\frac{t_a^0 \beta}{C_a^\lambda}\right)^2 \left(E[V_a^{2\lambda}] - (E[V_a^\lambda])^2\right), \quad \forall a \in A. \tag{3-19}$$

(1) Perceived Path Travel Time

In the context of non-extreme flood, risk sensitivity significantly affects users' perception of travel time. Users with higher risk sensitivity tend to dislike risks more, leading them to perceive longer travel times and thus prioritize reliability in their travels. To reflect the impact of risk sensitivity on users' perception of travel time, this study adopts the approach of link-based travel time reliability measures based on the sub-additivity property, as the corresponding reliability-based travel time calculation formulas used by (Xu et al., 2017). Then this study constructs the mathematical expressions that represents the relationship between risk sensitivity and perceived travel time. Let t_{ima} represent the perceived link travel time for m-type users within an O-D pair under their own risk sensitivity influence. The way t_{ima} represents the user-perceived link travel time and its specific calculation expression are as follows (the detailed derivation of the calculation expression can be found in Appendix B):

$$\Pr(T_a < t_{ima}) \geq \rho_{im}, \quad \forall i \in I,\ \forall m \in M_i,\ \forall a \in A. \tag{3-20}$$

$$t_{ima} = E[T_a] + \sqrt{\frac{\rho_{im}}{1-\rho_{im}}} \cdot \sqrt{\mathrm{var}[T_a]}, \quad \forall i \in I,\ \forall m \in M_i,\ \forall a \in A. \tag{3-21}$$

By directly summing t_{ima}, the perceived path travel time for type m users can be obtained, denoted as t_{imj}. The specific expression is as follows:

$$t_{imj} = \sum_{a \in A} \delta_{aj}\, t_{ima}, \quad \forall i \in I,\ \forall m \in M_i,\ \forall j \in J_i. \tag{3-22}$$

The method represented by Equations (3-20), (3-21), and (3-22) for calculating the perceived path travel time of users is termed the "link-based method". In contrast, the more commonly used "path-based method" involves first calculating the corresponding path travel time and then determining the user's perceived path travel time based on this, as shown below:

$$\begin{cases} E[T_{ij}] = \sum_{a \in A} \delta_{aj} E[T_a], \\ \mathrm{var}[T_{ij}] = \sum_{a \in A} \sum_{b \in A} \delta_{aj}\delta_{bj}\, \mathrm{cov}[T_a, T_b], \\ \Pr\left(T_{ij} < t_{imj}^{(\text{path-based})}\right) \geq \rho_{im}, \\ t_{imj}^{(\text{path-based})} = E[T_{ij}] + \sqrt{\frac{\rho_{im}}{1-\rho_{im}}} \cdot \sqrt{\mathrm{var}[T_{ij}]}. \end{cases} \tag{3-23}$$

for all $i \in I,\ j \in J_i,\ m \in M_i,\ a \in A$.

Whether adopting a link-based or path-based method, the key lies in the use of the calculation method proposed in Appendix B for user-perceived travel time, as indicated by $E[\cdot] + \sqrt{\rho_{im}/(1-\rho_{im})} \cdot \sqrt{\mathrm{var}[\cdot]}$, for simplicity, $\rho(\cdot)$ is used to represent it. Under the impact of flood disasters, longer travel times imply a greater likelihood of users encountering danger. Therefore, perceived travel time not only carries the characteristics of time cost but also embodies a distinctive risk attribute. When considering the risk attribute of perceived travel time, the calculation method represented by $\rho(\cdot)$ serves as a risk measure. For a reasonable risk measure, sub-additivity is a necessary condition. Hence, ensuring that $\rho(\cdot)$ possesses sub-additivity to reflect the risk characteristics of perceived travel time provides additional advantages. Let X represent the travel time T_a for link a, and Y represent the travel time T_b for link b. The travel time T_{ij} for path j, composed of links a and b, is given by $X + Y$. Thus, the following relationship holds (the proof process is provided in

Appendix C):

$$\rho(X+Y) \le \rho(X) + \rho(Y). \tag{3-24}$$

The left side of Equation (3-24) can be regarded as the "path-based method", while the right side can be regarded as the "link-based method". Equation (3-24) demonstrates that the method represented by $\rho(\cdot)$ for calculating perceived travel time satisfies the "sub-additivity of risk measure". Thus, the mathematical expression $\rho(\cdot)$ proposed in this study for calculating perceived travel time not only effectively quantifies the impact of risk sensitivity on users' perceptions but also helps to reflect the risk characteristics of perceived travel time under flood conditions. Additionally, the relationship expressed by Equation (3-24) can be interpreted as the perceived travel time along a path not exceeding the sum of perceived travel times across all links within that path. Moreover, whether using a link-based or path-based method, both approaches employ mathematical expression $\rho(\cdot)$. However, considering the computational feasibility and tractability for large-scale network applications, this study adopts the link-based method to calculate the final perceived path travel time.

(2) Perceived Path Flood Risk

Flood risk on a specific link within the road network is determined by the velocity, depth, and length of flooding on that link. Leveraging mechanical principles, (Martínez-Gomariz et al., 2023; Wang et al., 2021) conducted a study on the stability of vehicles under the influence of flood depth and flow velocity, providing corresponding analytical expressions. Let ϑ_a denote the degree of objective risk for a vehicle to lose stability under certain flood depths and flow velocities on the link a, which can be calculated using the following formula:

$$\vartheta_a = \min\left(1,\ \frac{U_{af}}{U_{ac}}\right), \quad \forall a \in A, \tag{3-25}$$

$$U_{ac} = w_1 \left(\frac{h_{af}}{h_c}\right)^{w_2} \sqrt{2gl_c\left(\frac{\rho_c h_c}{\rho_f h_{af}} - R_f\right)}, \quad \forall a \in A. \tag{3-26}$$

were h_{af} and U_{af} represent the flood depth and flood velocity on link a, respectively. These two key parameters directly influence the risk of vehicle instability caused by flooding on the link. The flood conditions in this study are assumed, so the values of h_{af} and U_{af} are also predefined. However, in practical applications of the model, these parameter values can be adjusted according to actual flood conditions. The remaining parameters in the equation represent empirical values, the specific meanings of which can be found in Appendix A.

Given l_{af} representing the proportion of the link's inundation length to its total length, a larger l_{af} amplifies the danger of flooding, thereby increasing the objective flood risk for users. To maintain the uniformity of units among the elements in the cost function and considering the inherent risk characteristics of travel time on the link, travel time is introduced as the basis for calculating flood risk. Thus, for m type users, the objective flood risk on link a and path j, denoted as r_{ima} and r_{imj} respectively, follow the expressions below:

$$r_{ima} = (1 + l_{af}) \cdot \vartheta_a \cdot t_{ima}, \quad \forall i \in I,\ \forall m \in M_i,\ \forall a \in A, \tag{3-27}$$

$$r_{imj} = \sum_{a \in A} \delta_{aj}\, r_{ima}, \quad \forall i \in I,\ \forall m \in M_i,\ \forall j \in J_i. \tag{3-28}$$

When the flood conditions on links within a path become more severe, the value of $(1 + l_{af}) \cdot \vartheta_a$ increases, leading to a higher r_{ima} value. Similarly, if the risk sensitivity of users in the current category increases, the value of t_{ima} will rise, further resulting in a larger r_{ima}. This indicates that the flood risk of a link is influenced by the objective flooding conditions on the link as well as the user's risk sensitivity, exhibiting a relationship akin to direct proportionality. Given the inherent uncertainty and vagueness in users' perceptions of objective flood risk, a stochastic distribution is used to capture this uncertainty. Assuming perceived path flood risk for m type users within Q_i is R_{imj}. Let $-R_{imj}$ follows a Gumbel distribution, denoted as $-R_{imj} \sim EV(-r_{imj}, 1)$. In this context, a larger value of r_{imj} shifts the probability density curve of R_{imj} to the right, increasing the probability of higher perceived path flood risk. Perceived flood risk

among different paths is mutually independent.

(3) Path Selection Inertia

Path costs play a pivotal role in users' path judgment and selection processes. Among these costs, travel time and flood risk are inherent components that consistently influence user behavior. Additionally, subjective psychological factors can shape user decisions during these processes. When a user determines that one path, such as path 1, is acceptable and can be chosen, there will be the user's subjective psychological tendency on path 1. Judgment and selection behavior must be based on comparison between path 1 and other paths. In such cases, another path, such as path 2, serves as an anchor for comparison with path 1, and subjective tendencies toward path 1 do not extend to path 2 during the current evaluation and selection process. This asymmetry tendency in path selection is referred to as "path selection inertia", denoted by ε_{imj}. It is worth noting that the concept of "path selection inertia" defined in this study aims to describe the user's tendency toward a particular path in their path selection behavior and is unrelated to the commonly used concept of "inertia" in dynamic traffic assignment. The psychological path selection inertia is incorporated into the cost function, thereby affecting users' path selection behavior. Subjective psychological perceptions of users inherently involve uncertainty and ambiguity. To capture this uncertainty, the path selection inertia of users is assumed to follow a uniform distribution. When users have higher risk sensitivity, they become more selective and cautious in their path selections. Consequently, the upper limit of path selection inertia for these users will be lower. Thus, for m type users within Q_i, the expression for path selection inertia ε_{imj} is given as follows:

$$\varepsilon_{imj} \sim \text{Uniform}[0,\ \bar{\varepsilon}_{imj}], \quad \forall i \in I,\ \forall m \in M_i,\ \forall j \in J_i, \tag{3-29}$$

$$\bar{\varepsilon}_{imj} = (1 - \rho_{im}) \cdot t_{imj}, \quad \forall i \in I,\ \forall m \in M_i,\ \forall j \in J_i. \tag{3-30}$$

In real-world scenarios, flood conditions in road networks and users' subjective perceptions are highly varied. Thus, the two random variables in the cost function—perceived flood risk and path selection inertia—may follow any distribution. Consider a probability density function curve based on perceived flood risk and path cost. Path selection inertia, reflecting the user's preference for a path, shifts this curve to the left (reducing the cost). The extent of this shift is determined by the boundary of path selection inertia, within which any shift value is possible. Consequently, this study uses a uniform distribution to represent path selection inertia. On the other hand, selecting Gumbel and uniform distributions for the two stochastic terms in the cost function ensures that the corresponding path selection probability expressions have closed-form solutions. Then, in the context of non-extreme flood, the perceived path cost for users encompasses three elements: perceived path travel time, perceived path flood risk, and path selection inertia. For m-type users, risk sensitivity consistently influences the costs associated with a path. This is because all three cost components—travel time, flood risk, and path selection inertia—are inherently associated with risk. Risk sensitivity reflects the user's attitude toward risk, thereby affecting the specific values of these cost components. A higher level of risk sensitivity leads to greater perceived travel time and flood risk. It also signifies a more cautious attitude, which results in a lower value of path selection inertia. For instance, when the risk sensitivity is equal to 1, it indicates that the user evaluates and selects paths with extreme caution and rationality, effectively eliminating path selection inertia. The perceived cost C_{imj} on the path j for m type users within Q_i satisfies:

$$C_{imj} = t_{imj} + R_{imj} - \varepsilon_{imj}, \quad \forall i \in I,\ \forall m \in M_i,\ \forall j \in J_i. \tag{3-31}$$

3.3 Network Equilibrium Model

3.3.1 Path Selection Criteria

Under non-extreme flood conditions, certain paths may be deemed too dangerous by users and thus classified as completely unacceptable. Consequently, users will not choose these unacceptable paths. Therefore, when making path

selection, users will evaluate paths based on specific path selection criteria to identify acceptable and unacceptable paths. Users will then make their selections only from among their acceptable paths. Let $\bar{J}_{im}$ be the set of acceptable paths for m type users within Q_i, which is a subset of J_i. Conversely, let $\tilde{J}_{im}$ represent the set of unacceptable paths for m type users within Q_i, which is a subset of J_i.

(1) Definition and Selection of Acceptable Paths

Users determine the acceptability of paths through a comparison of path costs. During this comparison process, both perceived path travel time and perceived path flood risk are present for the paths. In the context of path selection inertia, it is not symmetrically applied to the costs of both paths during one comparison action. Instead, it is only applied to the path that the user subjectively intends to evaluate for acceptability and selection, while the other path, used as a reference for comparison, is not assigned path selection inertia. For example, for m-type users, when determining whether path j is acceptable, they compare the cost of path j with another path, denoted as path k. When m-type users subjectively assess whether path j is acceptable, they develop a psychological inclination towards path j, resulting in the application of path selection inertia to path j. In contrast, the path k being compared, does not have the user's inclination and therefore does not undergo path selection inertia. If, at this point, the cost of path j is not greater than the cost of path k, then path j is considered acceptable to m type users relative to path k. Similarly, if the user wants to determine whether path k is acceptable, path k will also receive the user's psychological inclination during this assessment, and path j will not have the user's inclination.

In other words, if the cost of path j, which includes path selection inertia, is not greater than the cost of path k, which excludes path selection inertia, then the path j is considered acceptable for m-type users and has the potential to be selected. The specific expression is as follows:

$$t_{imj} + R_{imj} - \varepsilon_{imj} \le t_{imk} + R_{imk}, \quad \forall i \in I,\ \forall m \in M_i,\ \forall j \in \bar{J}_{im},\ \forall k \in J_i. \tag{3-32}$$

This judgment method can only determine that path j is an acceptable path for m-type users, but it cannot determine that path k is unacceptable. Therefore, after m-type users have evaluated all paths, their acceptable path set may include multiple paths, each being acceptable in comparison to the others. When the acceptable path set for m-type users includes both path j and k, the following relationship holds:

$$\begin{cases} t_{imj} + R_{imj} - \varepsilon_{imj} \le t_{imk} + R_{imk}, & \forall i \in I,\ \forall m \in M_i,\ \forall j,k \in \bar{J}_{im}, \\ t_{imk} + R_{imk} - \varepsilon_{imk} \le t_{imj} + R_{imj}, & \forall i \in I,\ \forall m \in M_i,\ \forall j,k \in \bar{J}_{im}. \end{cases} \tag{3-33}$$

Once the acceptable path set is determined, users will select a path from within their acceptable path set. The judgment method provided by equation (3-32) is used to define whether a path is considered acceptable, which essentially involves comparing the costs between two paths. The selection proportion of m type users for a particular path from the set of acceptable paths is determined by comparing that path with all the remaining paths in the acceptable set, following the judgment method represented by equation (3-32). For example, for a path j in the set of acceptable paths, if path j is compared with all other remaining paths in the set using the comparison method from equation (3-32), the greater the probability that path j satisfies the definition of an acceptable path, the more advantageous path j is relative to other acceptable paths, and therefore, more users will choose path j.

Let Y_{imj} represent the probability that a certain acceptable path (path j), when subjected to path selection inertia, has a cost no greater than all other acceptable paths without the path selection inertia. The expression for this probability

is given as follows (the detailed derivation process is shown in Appendix D):

$$\begin{aligned} Y_{imj} &= \Pr\left(t_{imj} + R_{imj} - \varepsilon_{imj} \le t_{imk} + R_{imk},\ \forall k \in \bar{J}_{im} \text{ and } j \ne k\right) \\ &= \frac{1}{\bar{\varepsilon}_{imj}} \ln\left(1 + \frac{\left(e^{\bar{\varepsilon}_{imj}} - 1\right) e^{-(t_{imj}+r_{imj})}}{\sum_{k \in \bar{J}_{im}} e^{-(t_{imk}+r_{imk})}}\right), \quad \forall i \in I,\ \forall m \in M_i,\ \forall j \in \bar{J}_{im}. \end{aligned} \tag{3-34}$$

When the value of Y_{imj} is larger, it implies that for m type users, this path has a lower cost compared to other acceptable paths. Consequently, more users are likely to choose this path. Let P_{imj} represent the proportion, for this user category within this O-D pair i, that selects acceptable path j, the closed-form calculation equation for P_{imj} is obtained:

$$P_{imj} = \frac{Y_{imj}}{\sum_{k \in \bar{J}_{im}} Y_{imk}}, \quad \forall i \in I,\ \forall m \in M_i,\ \forall j \in \bar{J}_{im}. \tag{3-35}$$

The method proposed in this paper for determining and selecting acceptable paths, as well as the method for determining unacceptable paths to be discussed later, both hinge on the asymmetric application of path selection inertia. The essence of path selection inertia lies in the user's psychological preference during the path comparison process. Since subjective psychological factors in the comparison process are inherently biased, path selection inertia is necessarily asymmetric when focusing on the micro-level comparison between paths, whether in the judgment or selection phase. However, from a more macro perspective, the user's path comparison behavior is not a one-time occurrence limited to a single path; rather, the user applies this biased comparison process to all possible paths and, after evaluating each option, ultimately selects the most satisfactory path. Thus, on a macro level, every path undergoes the influence of path selection inertia fairly, making the application of path selection inertia effectively "symmetric" at that stage.

(2) Definition of Unacceptable Paths

The definition of acceptable paths, along with their corresponding mathematical expressions, is used to determine the assignment proportions of user demand within the acceptable path set. However, prior to path flow assignment, it is essential to establish the composition of the acceptable path set. To avoid situations where two highly dangerous paths are incorrectly classified as acceptable based on comparisons using equation (3-33), introduce the definition of unacceptable paths. This definition is supplemented with specific analytical expressions to facilitate judgment. Based on the judgment method provided by the unacceptable path definition, users classify paths that do not meet the unacceptable criteria as acceptable paths. This ensures a well-defined path set for subsequent assignment of user demand, which is carried out using the definition of acceptable paths. Unacceptable paths are determined through cost comparison with acceptable paths, for users, an unacceptable path invariably fails to meet the criteria defining acceptable paths entirely. When a user applies path selection inertia to a particular path (path k) and its cost remains strictly higher than that of another acceptable path (path j) without path selection inertia, path k is considered unacceptable for the user. Specifically, for m-type users within Q_i, an unacceptable path k, when compared to other acceptable paths j, must satisfy the following relationship:

$$t_{imk} + R_{imk} - \varepsilon_{imk} > t_{imj} + R_{imj}, \quad \forall i \in I,\ \forall m \in M_i,\ \forall j \in \bar{J}_{im},\ \forall k \in \tilde{J}_{im}. \tag{3-36}$$

Equation (3-36) provides the logic for determining unacceptable paths. However, in practical applications, due to the presence of various random components in path costs, it is not feasible to directly determine whether a path is unacceptable by comparing cost values. Considering the stochastic nature of these components, use the probability of equation (3-36) being satisfied to identify unacceptable paths. Let Φ_{imk} represent the probability that equation (3-36) holds when compared to the path with the highest cost in the set of acceptable paths, and Φ_{imk} is referred to as the "degree of unacceptability" of path k. When utilizing the maximum cost from the set of acceptable paths, due to the presence of random variables, the selection is made based on the corresponding mean values for each path. Under non-extreme flood

conditions, the magnitude of the perceived path cost also reflects the level of danger associated with the path. A higher path cost indicates greater inherent risk. If the likelihood of equation (3-36) being satisfied is higher, it implies that the path is more dangerous compared to other paths. When the danger level of the path exceeds the user's danger tolerance, the path will be abandoned, and the user will deem it unacceptable. In this process, the parameter Φ_{imk}, which represents the degree of unacceptability, can be used to reflect the path's danger level. The specific expression for Φ_{imk} is as follows (the derivation process of Φ_{imk} is detailed in Appendix E):

$$\begin{aligned}\Phi_{imk} &= \Pr\left(t_{imk} + R_{imk} - \varepsilon_{imk} > \max_{j \in \bar{J}_{im}} \left(t_{imj} + R_{imj}\right)\right) \\ &= \frac{1}{\bar{\varepsilon}_{imk}} \frac{e^{t_{imj}+r_{imj}-t_{imk}-r_{imk}} + 1}{e^{t_{imj}+r_{imj}-t_{imk}-r_{imk}} + e^{-\bar{\varepsilon}_{imk}}}, \quad \forall i \in I,\ \forall m \in M_i,\ \forall k \notin \bar{J}_{im}.\end{aligned} \tag{3-37}$$

The user's psychological tolerance for danger can be represented by a psychological threshold, denoted as τ_{im}, which is determined by the users' risk sensitivity: the higher the risk sensitivity, the more selective the users are in their path selection, making paths more likely to be deemed unacceptable. Then τ_{im} holds the following relationship:

$$\tau_{im} = 1 - \rho_{im}, \quad \forall i \in I,\ \forall m \in M_i. \tag{3-38}$$

In other words, when the unacceptability degree Φ_{imk} of path k exceeds the psychological threshold τ_{im} of m type users, path k is considered unacceptable for these users. Then for m-type users, path k is considered unacceptable when the following relationship is satisfied:

$$\Phi_{imk} \geq \tau_{im}, \quad \forall i \in I,\ \forall m \in M_i,\ \forall k \in \tilde{J}_{im}. \tag{3-39}$$

3.3.2 Network Equilibrium Conditions

The network equilibrium conditions for the BST model is formulated as follows:

a) For user category m within the same O-D pair i, the proportion of traffic on the any acceptable path is denoted as P_{imj}. This proportion, P_{imj}, is determined by the probability Y_{imj}, which represents the likelihood that the path cost with selection inertia less than or equals to the cost without selection inertia of other alternative acceptable paths.

b) τ_{im} denotes the psychological threshold, which is directly related to the users' risk sensitivity and equals $1 - \rho_{im}$.

c) The probability that the cost with selection inertia for user category m on any unacceptable path is strictly greater than the maximum cost without tolerance factor among all acceptable paths, is not strictly greater than the psychological threshold τ_{im}.

Utilizing these road network equilibrium conditions, the corresponding mathematical model for the network equilibrium state is as follows:

$$\begin{cases} F_{imj} > 0 \iff F_{imj} = P_{imj}\, Q_{im}, & \forall i \in I,\ \forall m \in M_i,\ \forall j \in \bar{J}_{im}, \\ F_{imk} = 0 \iff \Phi_{imk} \geq \tau_{im}, & \forall i \in I,\ \forall m \in M_i,\ \forall k \in \tilde{J}_{im}. \end{cases} \tag{3-40}$$

3.4 Numerical Results

3.4.1 Settings

This case employs the Nguyen and Dupuis network as the traffic network for the application of the BST model, as illustrated in Figure 3-1. The network comprises 13 nodes and 19 links. A subset of links in this network is affected by non-extreme flood, represented by the blue regions. In this network, there are two O-D pairs, and the demand for each

O-D pair follows a normal distribution. Furthermore, users within each O-D pair are classified into different categories based on their risk sensitivity. The specific demand distribution characteristics and user classification parameters can be found in Table 3-1.

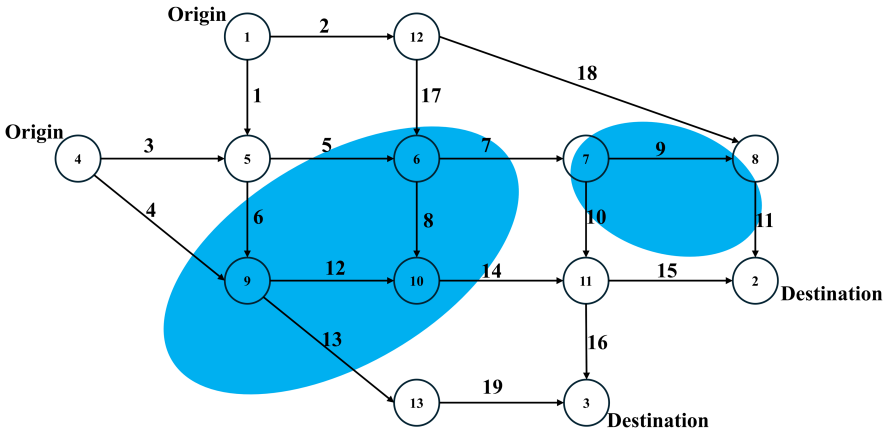


Figure 3-1: The Nguyen and Dupuis network with two distinct flooded regions

Table 3-1: Characteristics of O-D pairs and user classification features

O-D pair	Mean [pcu/hour]	Standard deviation	User type Q_{im}	Proportion P_{im}	Risk sensitivity ρ_{im}
(1, 3)	700	140	Q_{11}	0.2	0.3
			Q_{12}	0.6	0.5
			Q_{13}	0.2	0.7
(4, 2)	400	80	Q_{21}	0.3	0.5
			Q_{22}	0.7	0.7

Table 3-2 provides information on the flood characteristics of links affected by flooding, where all links have a free-flow travel time of 3 and a capacity of 500. Considering the non-extreme flooding background in this paper, the flood parameter settings on each link will not introduce extreme risks that would lead users to abandon their travel plans. To calculate the objective risk associated with flooding on the links, it is necessary to provide characteristic parameters such as the average length and height of vehicles on the links, as s

3.4.2 Results

The determination of acceptable path sets for users of different categories is not an instantaneous process; it involves dynamic comparisons over iterations to eventually confirm their respective acceptable path sets, leading to equilibrium on the acceptable path sets. The iterative evolution of acceptable path sets for a total of five user categories within the two O-D pairs is presented in Table 3-5.

Figures 3-2 and 3-3 illustrate the corresponding dynamic iteration process of acceptable paths for users within two O-D pairs. Then a clear depiction of the users' path selection process during dynamic iteration emerges. The information in Figure 3-2 and Figure 3-3 clearly illustrates the dynamic selection process. In each iteration, users of the corresponding categories compare the remaining non-acceptable paths in the network. They judge and choose whether to add an acceptable path. This process continues until there is no further change in the acceptable path set for all users. Then users are assigned only on these acceptable paths, satisfying the principles of network equilibrium conditions of the

Table 3-2: Values of link characteristic parameters under flood conditions

Link number	l_{af} (%)	h_{af} (m)	U_{af} (m·s^{-1})	Link number	l_{af} (%)	h_{af} (m)	U_{af} (m·s^{-1})
1	0	0	0	11	70	0.5	6
2	0	0	0	12	100	0.3	5
3	0	0	0	13	70	0.4	6
4	20	0.4	4	14	30	0.3	5
5	70	0.3	5	15	0	0	0
6	80	0.6	6	16	0	0	0
7	60	0.2	5	17	10	0.3	4
8	100	0.3	5	18	0	0	0
9	100	0.3	5	19	0	0	0
10	50	0.6	5				

Table 3-3: Values of vehicle parameters on the links

w_1	w_2	h_c (m)	g (m·s^{-2})	l_c (m)	ρ_c (kg·m^{-3})	ρ_f (kg·m^{-3})	R_f
0.35	-0.45	1.6	9.8	5	190	1000	0.55

Table 3-4: Path and link sequences

O-D pair	Path number	Link sequence
(1, 3)	1	1-6-13-19
	2	2-17-8-14-16
	3	2-17-7-10-16
	4	1-6-12-14-16
	5	1-5-7-10-16
	6	1-5-8-14-16
(4, 2)	7	3-5-7-9-11
	8	3-5-7-10-15
	9	3-5-8-14-15
	10	3-6-12-14-15
	11	4-12-14-15

Table 3-5: Dynamic evolution process of acceptable path sets

Evolution Process	Acceptable path set of Q_{11}	Acceptable path set of Q_{12}	Acceptable path set of Q_{13}	Acceptable path set of Q_{21}	Acceptable path set of Q_{22}
The Initial State	∅	∅	∅	∅	∅
As the Algorithm Iterations Increase	1	1	1	11	11
	1, 3	1, 3	1, 3	11, 8	11, 8
	1, 3, 5	1, 3, 5	1, 3	11, 8, 9	11, 8
	1, 3, 5, 2	1, 3, 5, 2	1, 3	11, 8, 9, 10	11, 8
	1, 3, 5, 2, 6	1, 3, 5, 2, 6	1, 3	11, 8, 9, 10	11, 8
Complete Equilibrium in the Road Network	1, 3, 5, 2, 6, 4	1, 3, 5, 2, 6, 4	1, 3	11, 8, 9, 10	11, 8

proposed model. In each new path selection process, users consistently demonstrate their instinct to avoid risks. Taking the example of the three categories of users within the O-D pair (1, 3), in the first two iterations of Figure 3-2, all three categories of users chose paths 1 and 3 as their acceptable paths. This is because, among all paths, only paths 1 and 3 can avoid flooded links 8 and 12, where the flood situation is most dangerous. In the next iteration, the Q_{13} users no longer add new acceptable paths. Only the Q_{11} and Q_{12} users choose to add new acceptable paths. This is because Q_{13} users are more sensitive to risks, and for them, the remaining paths are considered too dangerous. Therefore, they do not accept new paths. This phenomenon reflects the realistic behavior of users with high-risk sensitivity in the context of a flood disaster. Observing Figure 3-3 and Table 3-5, it illustrates the path selection process for users within the O-D pair (4, 2). For all users in the O-D pair (4, 2), reaching the destination implies crossing both the left and right flooded areas. No matter which path it is, each path includes links submerged in the left flood zone. In this situation, the safest approach is to prioritize paths with minimal impact from the left flood zone, meaning selecting links with the least danger among those submerged by the left flood. Simultaneously, users aim to choose links unaffected by the right flood zone as much as possible. Based on this consideration, the optimal choice for users in the O-D pair (4, 2) is expected to be Path 11, as it minimizes exposure to the left flood zone while avoiding the most dangerous links. The model's simulation results align with this optimal path selection strategy. The suboptimal choice would be Path 8, as it circumvents the riskier links (8, 9, and 12) in the left flood zone. When further selecting additional acceptable paths, users' risk sensitivity comes into play. The Q_{22} users, with higher risk sensitivity, choose not to accept the remaining high-risk paths. Consequently, their acceptable paths remain Paths 11 and 8. In contrast, the Q_{21} users, less concerned about risks, can accept even riskier paths, such as Paths 9 and 10. These results strongly demonstrate the model's capability to effectively simulate users' dynamic path selection behavior in the context of a flood disaster.

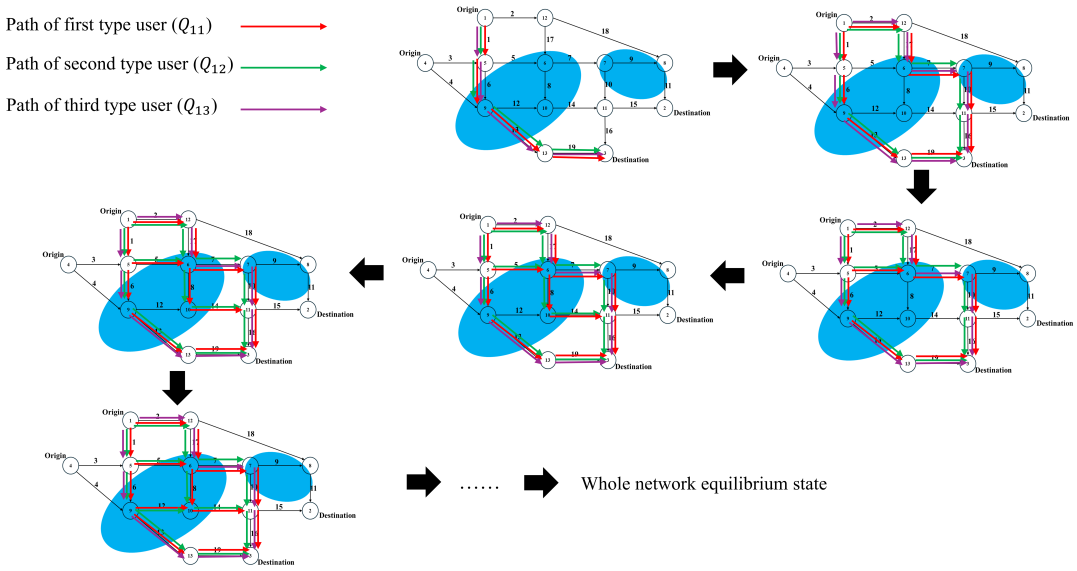


Figure 3-2: Dynamic Evolution of Acceptable Path Set for Users within O-D Pair (1, 3)

Based on Table 3-5, users Q_{11} and Q_{13} began the iterative process of determining their acceptable path sets, starting with Path 1 as their first acceptable path. During the first judgment, Path 3 was included in the acceptable path set for both Q_{11} and Q_{13}. In the second judgment, Q_{11} added Path 5 to its acceptable path set, whereas Q_{13} did not accept any new paths. Figure 4 illustrates the path cost composition for both user types during the first and second judgments. For simplicity, the random variables representing perceived flood risk (R_{imj}) and path selection inertia (ε_{imj}) are denoted by r_{imj} and $E[\varepsilon_{imj}]$, respectively. It can be observed that the acceptable path costs for Q_{13} are consistently higher than those for Q_{11} during both the first and second judgments. This discrepancy arises from the higher risk sensitivity of Q_{13}, leading them to perceive greater path costs, including travel time and flood risk. In the first judgment, apart from Path 1 (already classified as acceptable), Path 3 had the lowest cost among the remaining paths, significantly lower than the cost of Path 1. Thus, both Q_{11}, with lower risk sensitivity, and Q_{13}, with higher risk sensitivity, selected Path 3 as

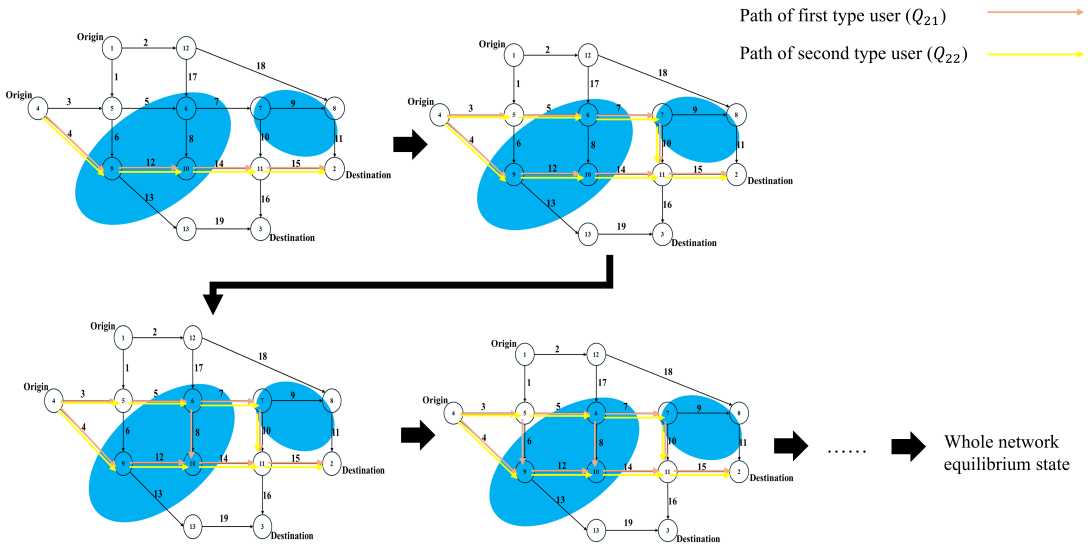


Figure 3-3: Dynamic Evolution of Acceptable Path Set for Users within O-D Pair (4, 2)

their new acceptable path in this round. Following the same logic, during the second judgment, Path 5 had the lowest cost among the remaining paths that were not yet acceptable. Users then evaluated whether Path 5 could be included in their acceptable path sets. For Q_{11}, Path 5 had a cost 1.1 units higher than Path 3, but this increase in cost was within their tolerance, prompting them to accept Path 5. The higher cost represents additional risk, but due to Q_{11}'s lower risk sensitivity, they were willing to accept Path 5 as a new acceptable path. For Q_{13}, the cost difference between Path 5 and Path 3 was only 0.4 units—substantially smaller than for Q_{11}—yet Q_{13} rejected Path 5. This is because Q_{13}'s high risk sensitivity renders even small increases in risk cost unacceptable, leading them to classify Path 5 as an unacceptable path. This behavior reflects the model's ability to effectively simulate the path selection behavior of users with varying risk sensitivities in a flood scenario. As shown in Figure 5, after Q_{13} finalized their acceptable path set as Path 1 and Path 3, they began making choices exclusively within this set. For clarity, the path costs are represented by t_{imj}, r_{imj}, and ε_{imj}. It can be observed that through iterative path selection, the flow no longer changes after a certain point, indicating that Q_{13}'s demand achieves equilibrium within their acceptable path set.

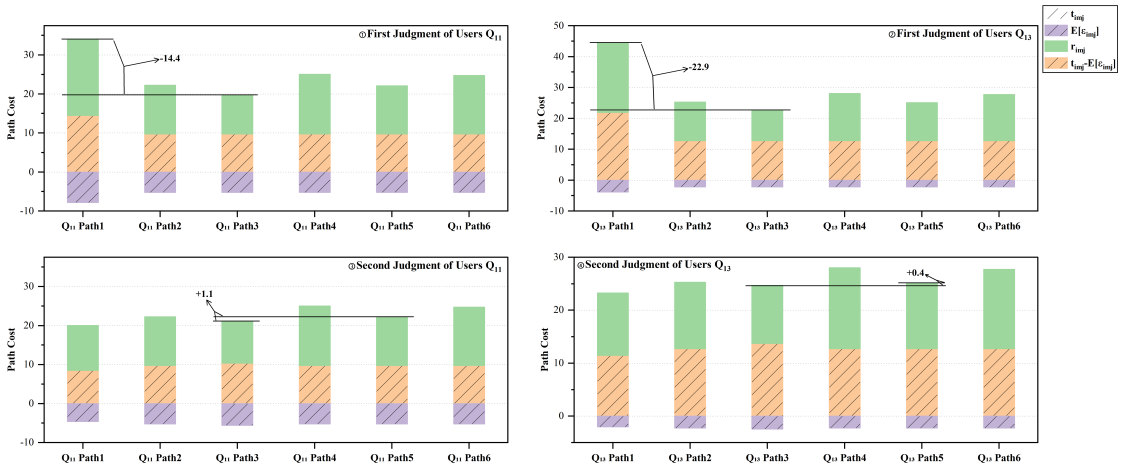


Figure 3-4: Path costs for users Q_{11} and Q_{13} during the first and second acceptable path judgments

Once all user types across all O-D pairs have determined their acceptable path sets, they proceed to make path choices within the same network until the entire network reaches an equilibrium state. Path flows are iteratively reassigned until reaching equilibrium using the MSA algorithm. To illustrate network convergence through changes in path flow, the gap function method is applied to evaluate the convergence of the 11 paths in the network. The path flow-based gap function is defined as follows:

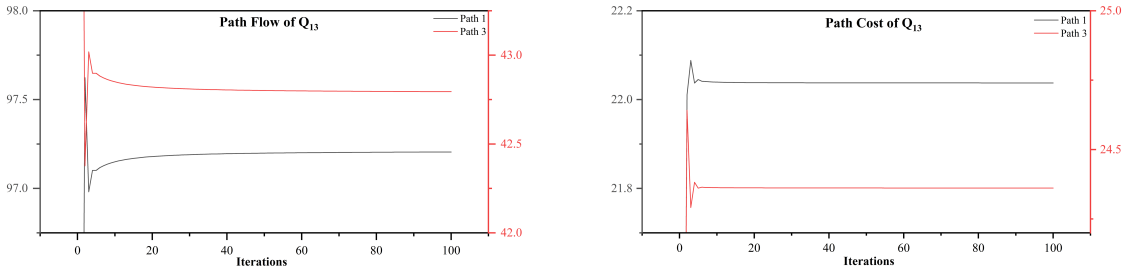


Figure 3-5: Changes in flow and cost within the acceptable path set of users Q_{13} during MSA iterations

$$\text{Relative Flow Gap}_k^n = \frac{f_k^n - f_k^{n-1}}{f_k^{n-1}} \tag{3-41}$$

where k represents the path, and f_k^n denotes the flow on path k at the n-th iteration. This function quantifies the difference in flow assignments for each path between successive iterations. As iterations progress, the gap values approaching zero indicate stabilizing path flow assignments and that the network is nearing equilibrium. Figure 3-6 shows the flow gap changes for all 11 paths across iterations. The results demonstrate that as iterations increase, the flow gap values for all paths converge to zero, signifying that the network has reached equilibrium after users finalize their acceptable path sets and iteratively select paths.

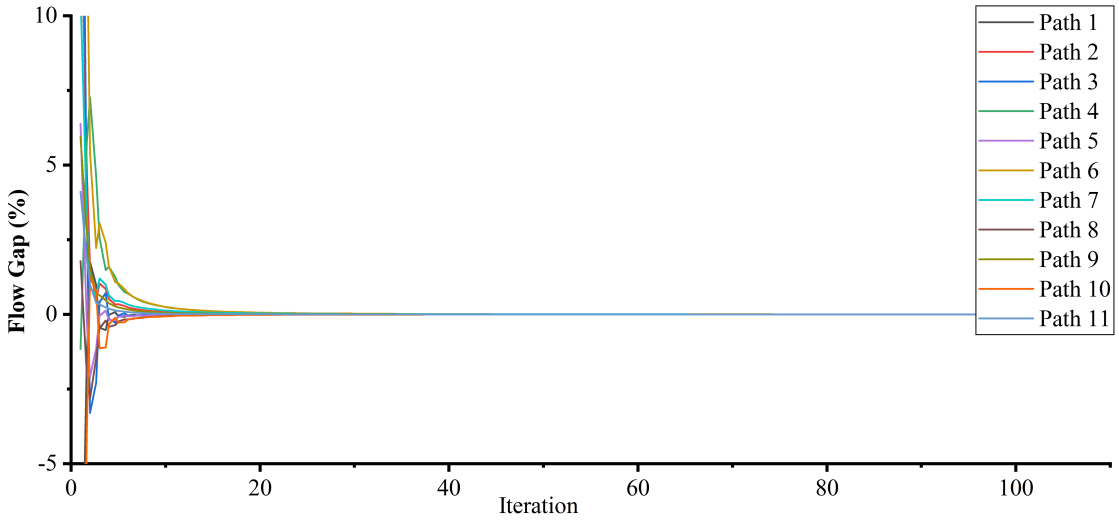


Figure 3-6: Fluctuations in relative path flow gaps across iterations

3.4.3 Results under Dynamic Non-Extreme Flood Scenarios

To investigate path choice behavior under dynamic non-extreme flood conditions, numerical experiments were conducted on the Sioux Falls network, which consists of 24 nodes and 76 links. The network topology and the spatial distribution of waterlogging are illustrated in Figure 3-7, where inundation impacts are confined to a subset of links and do not induce large-scale network disruption, consistent with the characteristics of non-extreme flooding.

The temporal evolution of waterlogging is represented using a discrete time framework. As shown in Figure 3-8, the flooding process spans a total duration of 10 days and is divided into successive time nodes t, each corresponding to an 8-hour interval. The dynamic non-extreme flood event is characterized by five successive stages: onset, development, peak inundation, recession, and dissipation. Specifically, the flood initiates at $t = 1$, gradually intensifies and reaches its peak at $t = 19$, then recedes after $t = 22$, with waterlogging effects fully dissipating by $t = 28$, before the event ends at $t = 30$. This temporal structure provides a clear basis for examining path choice evolution across different phases of the flood event.

Travel demand is specified for the O–D pair $(1, 20)$ and follows a normal distribution with a mean of 1000 and a

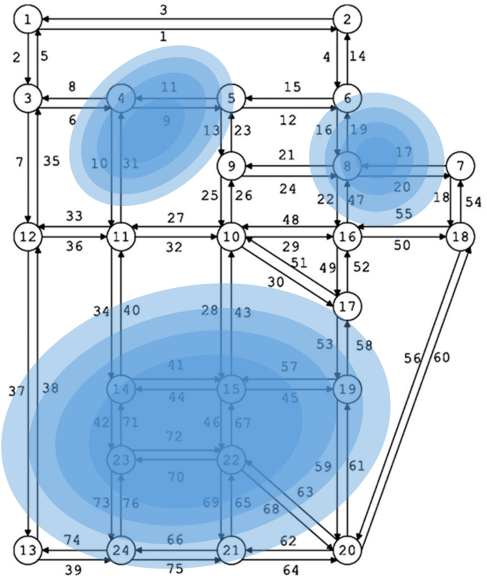


Figure 3-7: The Sioux-falls network with three distinct waterlogging regions

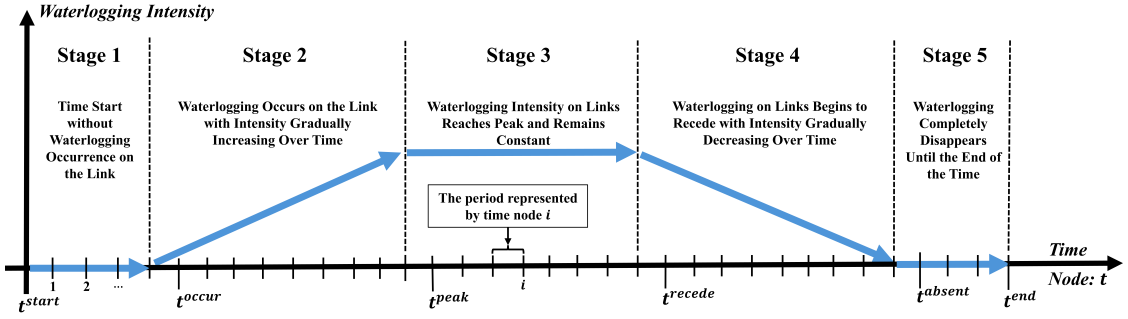


Figure 3-8: Temporal sequence of road network waterlogging event

standard deviation of 200. The demand consists of three user classes with heterogeneous risk sensitivities. These user groups account for 20%, 60%, and 20% of the total demand, respectively, with corresponding risk sensitivity parameters of 0.2, 0.5, and 0.8, representing low-, medium-, and high-risk-averse users. This user classification is consistent with that adopted in the static analysis, ensuring that observed differences in path choice behavior can be attributed to temporal flood dynamics rather than changes in behavioral assumptions.

Based on the above temporal configuration and user classification, the following subsection analyzes representative path-level results to illustrate how different user groups adapt their routing decisions across time nodes t under dynamic non-extreme flooding conditions.

To examine the dynamic evolution of users' acceptable path sets under the joint influence of risk sensitivity and time-varying waterlogging, Figure 3-9 presents the composition of acceptable paths for the highly risk-averse user group Q_{13} at three representative time nodes, $t = 9$, $t = 10$, and $t = 11$. These time nodes correspond to the transitional phase during which waterlogging intensity increases toward the peak stage.

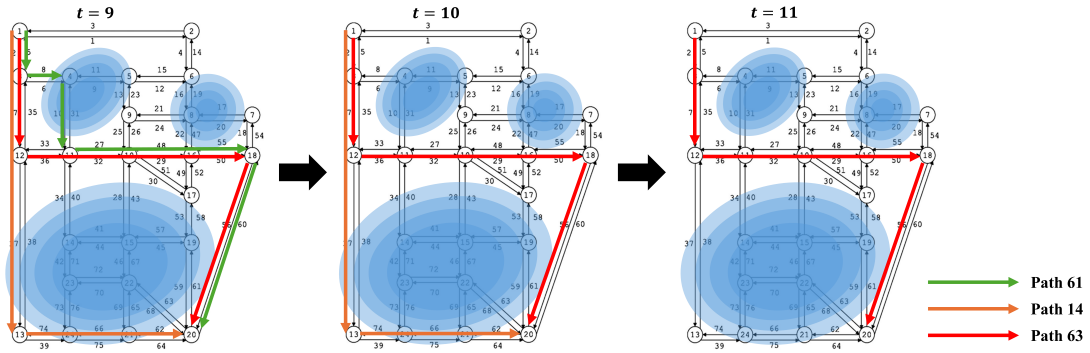


Figure 3-9: Acceptable Paths for User Q_{13} at Time Nodes $t = 9, 10, 11$

At $t = 9$, User Q_{13} identifies three acceptable paths, namely Paths 61, 14, and 63. As waterlogging intensifies over time, the user's acceptable path set gradually contracts. At $t = 10$, Path 61 is excluded because, relative to Path 14, it traverses links located closer to the core of the waterlogged region, resulting in a higher associated waterlogging risk. In contrast, Path 14 only passes through the peripheral area of the waterlogging zone, leading to a comparatively lower risk level. Consequently, Paths 14 and 63 remain acceptable, while Path 61 is eliminated from the choice set.

At $t = 11$, as waterlogging intensity further increases, even the residual risk associated with Path 14 exceeds the tolerance threshold of User Q_{13}, causing this path to be excluded as well. As a result, Path 63 becomes the sole acceptable option for this user group. Notably, Path 63 is unaffected by waterlogging throughout the considered period, rendering it acceptable even for highly risk-sensitive users.

A horizontal comparison across user groups reveals distinct behavioral responses driven by heterogeneous risk sensitivities. Unlike User Q_{13}, the less risk-averse users Q_{11} and Q_{12} exhibit greater tolerance toward waterlogging-induced risks. Accordingly, at $t = 11$, Path 14 remains acceptable for these user groups, while it is rejected by User Q_{13}. Overall, these results demonstrate that the proposed model effectively captures users' adaptive path judgment behavior, characterized by progressive risk avoidance as waterlogging conditions deteriorate over time.

3.5 Chapter Summary

This chapter developed a network equilibrium model to investigate risk-sensitive path choice behavior under external disturbances, using non-extreme flooding as a representative scenario. The model captures travelers' heterogeneous risk preferences and introduces the concept of acceptable and unacceptable path sets to characterize behavioral differences between risk-averse and risk-neutral users. Based on an enhanced generalized cost function, the model jointly considers travel time, flood risk, and path choice inertia, where travel time and flood risk reflect objective disturbance effects, while path choice inertia represents subjective psychological tendencies. By incorporating Binary Stochastic Terms (BST) into the cost function, the model accounts for both external uncertainty and perceptual ambiguity, enabling a more realistic representation of traveler decision-making under uncertain conditions.

The results demonstrate that the proposed framework effectively reproduces heterogeneous path choice behavior under non-extreme disturbances. Higher levels of risk sensitivity encourage travelers to select safer routes, which in turn redistributes traffic flows and alters the resulting equilibrium structure of the network. As disturbance intensity and user risk preferences vary, acceptable path sets and corresponding flow patterns adjust endogenously, revealing how risk perception drives the evolution of network operating states under persistent external conditions.

Overall, by focusing on non-extreme flooding as a typical disturbance scenario, this chapter provides a micro-level behavioral explanation of how risk perception and environmental uncertainty jointly shape route choice decisions and the formation of stochastic equilibrium states in transportation networks. These findings establish a behavioral foundation for subsequent analysis of uncertainty propagation, supplying key behavioral parameters and mechanisms for the fractional-moment-based modeling framework developed in the next chapter, which further examines the statistical characterization and stability of traffic flow fluctuations under uncertainty.

Chapter 4

A Method for Estimating Travel Time Distribution Based on Fractional Moments

4.1 Overview and Research Objectives

Uncertainty in travel time constitutes a fundamental source of performance variability and reliability fluctuation in transportation networks. As network flow distributions are influenced by heterogeneous user perceptions of risk and external disturbances, the resulting path and link travel times often exhibit complex stochastic patterns. Such randomness manifests not only in low-order statistics such as means and variances but also in the nonlinearity, asymmetry, and heavy-tailed characteristics of the underlying distributions. Conventional methods that rely solely on a limited number of integer moments or assume specific distributional forms (e.g., normal or log-normal) are often insufficient to capture the non-Gaussian and nonlinear nature of travel time distributions observed in real networks, leading to inaccurate reliability evaluation and optimization outcomes.

In conventional traffic assignment modeling, travel times are typically represented by empirical impedance functions such as the Bureau of Public Roads (BPR) function:

$$T_a = t_a^0 \left(1 + \beta \left(V_a / C_a\right)^{\lambda}\right) \tag{4-1}$$

where V_a and C_a denote the flow and capacity of link a, and λ is an empirical parameter. Since λ usually takes non-integer values between 3 and 5, the presence of stochastic variables—such as random flow, capacity, or disturbance intensity—naturally introduces non-integer power terms of random variables. For instance, when V_a or C_a is assumed to be random, the computation of expected travel time, variance, or reliability measures inevitably involves expressions like $E[(V_a/C_a)^{\lambda}]$, which correspond to fractional moments of the underlying random variables. Consequently, the fractional-moment problem arises as a direct mathematical manifestation of stochastic propagation in transportation networks.

This problem becomes even more pronounced when both behavioral uncertainty (arising from heterogeneous user perceptions) and environmental randomness (e.g., capacity reduction or external perturbation) coexist. In such cases, travel time is no longer a simple function of deterministic inputs but a nonlinear transformation of random variables with non-integer exponents. Analytical integration becomes intractable, and conventional high-order moment methods tend to suffer from instability or divergence, especially in high-dimensional or data-limited settings. Hence, developing a numerically stable and computationally efficient approach for evaluating fractional moments is essential for accurately characterizing stochastic network performance.

To address this challenge, this chapter develops a fractional-moment-based method for estimating travel time distributions. The proposed approach enables the stable and efficient computation of arbitrary-order fractional moments using a limited set of integer moments, providing a versatile mathematical tool for quantifying complex stochastic characteristics. Compared with traditional approaches, the fractional-moment method achieves higher precision and robustness while avoiding explicit integration or distributional assumptions, making it particularly suitable for large-scale or partially observed transportation systems.

From the overall perspective of this dissertation, the study presented in this chapter corresponds to the second analytical layer—mathematrical characterization and propagation of uncertainty. Building upon the behavioral-level findings in Chapter 3, which revealed how individual risk perception and disturbance responses induce stochastic flow distributions and travel time variability, this chapter translates such behavioral uncertainty into quantifiable stochastic characteristics. By applying a fractional-moment modeling framework, the study extracts stable and computationally tractable statistical indicators that serve as the analytical foundation for subsequent reliability optimization and network performance evaluation.

Specifically, this chapter integrates the Laplace transform and fractional calculus to establish a unified analytical and numerical framework that links the probability density function of a random variable to its fractional moments. Based on this framework, a general numerical solution method, referred to as the Fractional-Folding Moment Transform (FFMT), is proposed. The FFMT method recursively derives fractional moments from integer moments without requiring explicit probability distributions, thereby achieving a balance between computational accuracy and efficiency. In addition, by

deriving the corresponding error bounds and optimal parameter conditions, the method is demonstrated to be numerically stable and broadly applicable to positive random variables commonly encountered in engineering and transportation modeling.

Accordingly, the main objectives of this chapter are as follows:

- To clarify the theoretical and practical origins of the fractional-moment problem in stochastic traffic modeling.
- To develop a general and numerically stable method for estimating fractional moments of travel time distributions.
- To verify the theoretical validity and computational precision of the proposed method, providing reliable stochastic inputs for subsequent reliability-oriented optimization.

In summary, the fractional-moment framework proposed in this chapter not only extends the mathematical tools for representing uncertainty in transportation networks but also establishes a methodological bridge between behavioral randomness and reliability analysis. It provides a robust and theoretically grounded means of quantifying stochastic propagation, thereby laying the analytical and computational foundation for the reliability-oriented models developed in the following chapters.

4.2 Theoretical Framework of Fractional-Moment Computation

Given any random variable V that may occur in engineering applications, where the value of this random variable is strictly positive, and its corresponding probability density function is denoted as $p(V)$, this paper considers only this univariate probability density function. The Laplace transform of the function $p(V)$ can be obtained as follows:

$$\mathcal{L}\{p(V)\}(s) = \int_0^\infty p(V)\, e^{-sV}\, dV \tag{4-2}$$

Definition 2.1: For complex numbers with a positive real part, the gamma function is defined via a convergent improper integral (Remmert, 1998):

$$\Gamma(\zeta) = \int_0^\infty t^{\zeta-1} e^{-t}\, dt, \qquad \Re(\zeta) > 0 \tag{4-3}$$

For every positive integer n, given the fact that $\Gamma(1) = 1$, $\Gamma(n) = (n-1)!$ holds.

Definition 2.2: Given an arbitrary real number z, where $z \in \mathbb{R}$, and a non-integer number λ, where $\lambda \in \mathbb{R}^+$ and $\lambda \notin \mathbb{N}$. Subsequently, by combining the Cauchy formula with the concept of iterative integrals, the corresponding generalized fractional-order integral can be expressed by the following formula (Nonnenmacher and Metzler, 1995):

$$I_z^\lambda f(t) = \frac{1}{\Gamma(\lambda)} \int_z^t (t-\tau)^{\lambda-1} f(\tau)\, d\tau \tag{4-4}$$

Definition 2.3: Given an arbitrary real number z, where $z \in \mathbb{R}$, and a non-integer number λ, where $\lambda \in \mathbb{R}^+$ and $\lambda \notin \mathbb{N}$. Let $k = \lceil \lambda \rceil$, $\zeta = k - \lambda$, hence $k - 1 < \lambda < k$. The left Riemann–Liouville (R-L) fractional derivative of order λ is defined by (Luchko, 2023):

$$\left({}_z^{RL}D_t^\lambda f\right)(t) = D^k\left[I_z^\zeta f(t)\right] = \frac{1}{\Gamma(\zeta)} \frac{d^k}{dt^k} \int_z^t (t-\xi)^{\zeta-1} f(\xi)\, d\xi \tag{4-5}$$

Setting $z \to -\infty$ and applying the R-L type λ-order derivative to Equation (4-2), the following relationship can be obtained:

$$\left({}_{-\infty}^{RL}D_s^\lambda \mathcal{L}\{p(V)\}(s)\right) = \int_0^\infty p(V) \left[\frac{1}{\Gamma(\zeta)} \frac{d^k}{ds^k} \int_{-\infty}^s (s-\xi)^{\zeta-1} e^{\xi V}\, d\xi\right] dV \tag{4-6}$$

Definition 2.4: If $f : \mathbb{R}_+ \to \mathbb{R}$, then given an arbitrary real number z, where $z \in \mathbb{R}$, and a non-integer number λ, where $\lambda \in \mathbb{R}^+$ and $\lambda \notin \mathbb{N}$. Let $k = \lceil \lambda \rceil$, $\zeta = k - \lambda$, $k - 1 < \lambda < k$. The left Caputo fractional derivative is defined as:

$$\left({}_{z}^{C}D_{t}^{\lambda}f\right)(t) = I_{t}^{\zeta}\left[\frac{d^{k}f(t)}{dt^{k}}\right] = \frac{1}{\Gamma(\zeta)}\int_{z}^{t}(t-\xi)^{\zeta-1}f^{(k)}(\xi)\,d\xi \tag{4-7}$$

Corollary 2.1: Given a non-integer number λ, $\lambda \in \mathbb{R}^{+}$ and $\lambda \notin \mathbb{N}$, as $z \to -\infty$, the left R-L fractional-order derivative is equivalent to the left Caputo fractional-order derivative. The specific proof can be found in Appendix F:

$$\left({}_{-\infty}^{RL}D_{t}^{\lambda}f(t)\right) = \left({}_{-\infty}^{C}D_{t}^{\lambda}f(t)\right) \tag{4-8}$$

Based on Corollary 2.1, Equation (4-5) can be further transformed into:

$$\left({}_{-\infty}^{RL}D_{s}^{\lambda}\mathcal{L}\{p(V)\}(s)\right) = \int_{0}^{\infty}\left({}_{-\infty}^{C}D_{s}^{\lambda}e^{sV}\right)p(V)\,dV \tag{4-9}$$

Corollary 2.2: Given $f(t) = e^{\varepsilon t}$, as $z \to -\infty$, $\varepsilon > 0$, then for $\lambda \in \mathbb{C}$ with $\Re(\lambda) > 0$, the following holds (proof in Appendix G):

$$\left({}_{-\infty}^{C}D_{t}^{\lambda}e^{\varepsilon t}\right) = \varepsilon^{\lambda}e^{\varepsilon t} \tag{4-10}$$

Applying Corollary 2.1 to Equation (4-7) and setting $s = 0$, the following relationship can be obtained:

$$\begin{aligned}\left({}_{-\infty}^{RL}D_{s}^{\lambda}\mathcal{L}\{p(V)\}(s)\right)\Big|_{s=0} &= \int_{0}^{\infty}V^{\lambda}\,e^{0\cdot V}\,p(V)\,dV \\ &= \int_{0}^{\infty}V^{\lambda}p(V)\,dV = E\left[V^{\lambda}\right]\end{aligned} \tag{4-11}$$

The relationship presented in Equation (4-11) represents the analytical solution expression contained within the FFMT method, indicating that the non-integer order moments of a positive random variable can be computed using $\left({}_{-\infty}^{RL}D_{s}^{\lambda}\mathcal{L}\{p(V)\}(s)\right)\Big|_{s=0}$. However, the mathematical expression of the left R-L fractional derivatives is not suitable for practical applications. Therefore, this chapter proceeds to derive a more practical numerical solution expression.

4.3 Numerical Formulation and Error Analysis

4.3.1 Numerical Formulation

Definition 2.5: Given an arbitrary real number z, where $z \in \mathbb{R}$, and a non-integer number λ, where $\lambda \in \mathbb{R}^{+}$ and $\lambda \notin \mathbb{N}$. The left Grunwald–Letnikov (G-L) fractional derivative ${}_{z}^{GL}D_{t}^{\lambda}f$ of order λ of a function $f(t)$ is defined by (Podlubny, 1998):

$$\begin{aligned}\left({}_{z}^{GL}D_{t}^{\lambda}f\right)(t) &= \lim_{h\to 0}\frac{1}{h^{\lambda}}\sum_{i=0}^{\infty}(-1)^{i}\binom{\lambda}{i}f(t-ih) \\ &= \lim_{\substack{h\to 0 \\ n=(t-z)/h}}\frac{1}{h^{\lambda}}\sum_{i=0}^{n}(-1)^{i}\binom{\lambda}{i}f(t-ih)\end{aligned} \tag{4-12}$$

Corollary 2.3: Given the assumption that the function $f(t)$ possesses a continuous derivative of order $m+1$, the G-L fractional derivative is congruent to the R-L fractional derivative (proof in Appendix H):

$$\left({}_{z}^{GL}D_{t}^{\lambda}f(t)\right) = \left({}_{z}^{RL}D_{t}^{\lambda}f(t)\right) \tag{4-13}$$

Remark 2.1: For $t \gg z$, from the expression of the coefficients in the G-L fractional derivative, for large t the role of the history of the behavior of $f(t)$ near the lower terminal can be neglected. This results in the establishment of the "short memory principle," indicating that the operator ${}_{z}^{GL}D_{t}^{\lambda}$ only necessitates considering the behavior of $f(t)$ within the recent past.

Defined within the interval $[t-L,\ t]$, where L represents the memory length, the "short memory principle" can be

articulated as follows:

$$\left({}_{-\infty}^{GL}D_t^{\lambda} f(t)\right) \approx \left({}_{t-L}^{GL}D_t^{\lambda} f(t)\right) \tag{4-14}$$

Based on Definition 2.5, Corollary 2.3, and Remark 2.1, the following relationship can be derived:

$$\begin{aligned}\left({}_{-\infty}^{RL}D_s^{\lambda}\mathcal{L}\{p(V)\}(s)\right)\Big|_{s=0} &= \left({}_{-\infty}^{GL}D_s^{\lambda}\mathcal{L}\{p(V)\}(s)\right)\Big|_{s=0} \\ &\approx \left({}_{s-L}^{GL}D_s^{\lambda}\mathcal{L}\{p(V)\}(s)\right)\Big|_{s=0} \\ &= \frac{1}{h^{\lambda}}\sum_{i=0}^{N}(-1)^i\binom{\lambda}{i}\mathcal{L}\{p(V)\}(s-ih)\Big|_{s=0} \\ &= E[V^{\lambda}]\end{aligned} \tag{4-15}$$

In this case, Equation (4-15) still contains the term $\mathcal{L}\{p(V)\}(s-ih)$, which remains unsuitable for practical applications. Through further derivation, a numerical solution expression suitable for practical computation is obtained, as stated in the following corollary.

Corollary 2.4: For the random variable V, assuming arbitrary distributions, the values of non-integer order moments $E[V^{\lambda}]$ can be obtained through the following numerical solution expression (proof in Appendix I):

$$E[V^{\lambda}] = \sum_{j=0}^{N}\frac{(-1)^{N-j}(\lambda-N)}{\lambda-j}\binom{\lambda}{N}\binom{N}{j}h^{j-\lambda}E[V^j] \tag{4-16}$$

where $N = \lfloor L/h \rfloor$, and L is the memory length, and

$$\binom{\lambda}{i} = \frac{\lambda(\lambda-1)(\lambda-2)\cdots(\lambda-i+1)}{i!} = \frac{\Gamma(\lambda+1)}{\Gamma(\lambda+1-i)\,i!}.$$

The equation in Corollary 2.4 is the core formula of the FFMT method, indicating that for random link flow, regardless of the distribution, obtaining its corresponding integer-order moments enables the calculation of the corresponding non-integer order moments via Equation (4-16).

4.3.2 Error Analysis

The parameter N in the numerical solution expression is highly worthy of elucidation, as it holds significant intrinsic meaning. According to the definition, N adheres to the following relationship:

$$N = \lfloor L/h \rfloor \tag{4-17}$$

where h represents the step length, provided directly with a requirement of h being sufficiently small. Another critical parameter is L, representing the memory length. The value of L plays a crucial role in determining the error size associated with the left Grunwald–Letnikov fractional derivatives method. In essence, this method incurs some inaccuracy as a penalty; hence, the value of L should be selected cautiously to ensure the error remains within the specified range.

Corollary 2.5: Given $|f(t)| \le M$, $a + L < b$, and L as the memory length. Given a required accuracy ε, ε can impose a direct impact on the memory length. If $\Delta(t) \le \varepsilon$, then ε further determines the memory length L (proof in Appendix J):

$$L \ge \left(\frac{M}{\varepsilon\,|\Gamma(1-\lambda)|}\right)^{1/\lambda} \tag{4-18}$$

Thus far, this part has elucidated and derived the analytical solution expression for arbitrary-order moments utilizing R-L fractional derivatives and the Laplace transform. Simultaneously, based on this computational principle and employing G-L fractional derivatives, a numerical solution expression for computing arbitrary-order moments of random

variables has been proposed, along with the corresponding calculation formulas.

4.4 Parameter Optimization and Stability Analysis

For convenience, the formula in Corollary 2.4 is represented using the following functional expression:

$$f_{N,h}(\lambda, V) = \sum_{j=0}^{N} \left[(-1)^{N-j} \cdot \frac{\lambda - N}{\lambda - j} \cdot \binom{\lambda}{N} \right] \binom{N}{j} E[V^j] \, h^{j-\lambda} \tag{4-19}$$

In the practical application of the function $f_{N,h}(\lambda, V)$ to calculate the corresponding $E[V^\lambda]$, the values of the random variable V and the fractional order λ are given and are considered as independent variables of the function $f_{N,h}(\cdot)$. Consequently, the function's output is the corresponding dependent variable. To obtain the result of $E[V^\lambda]$ once the values of the independent variables V and λ are established, there are two corresponding parameters in the function $f_{N,h}(\cdot)$ that need to be determined: N and h.

Corollary 2.4 provides a numerical solution expression, which inherently contains some error. According to the short memory principle, the memory length L significantly impacts the error magnitude of the numerical solution expression, and the memory length L is directly related to the parameters N and h. Therefore, the values of the parameters N and h in the function $f_{N,h}(\cdot)$ will significantly affect the accuracy of the computational results.

Once V and λ in the function $f_{N,h}(\cdot)$ are determined, there exist specific corresponding values of N and h that minimize the numerical solution error. The parameter N represents the number of integer-order moments used. Essentially, Corollary 2.4 can be understood as linearly combining these N integer-order moments in appropriate proportions to obtain the desired computational result. This appropriate proportion can be represented by h.

4.4.1 Parameter N

The determination of the parameter N is directly related to the independent variable λ in the function $f_{N,h}(\cdot)$. Using a finite number of integer-order moments to achieve accurate computational results can effectively save computational resources. When the number of integer-order moments exceeds λ, it includes sufficient information from the integer-order moments to obtain sufficiently accurate λ-order moments. Therefore, the optimal strategy for determining the value of N is to set N as the smallest integer greater than λ. Based on this, when λ varies within the corresponding integer interval, denoted as $(i, i+1)$ and $i = \lfloor \lambda \rfloor$, the value of N remains unchanged. Similarly, even if the independent variable V in function $f_{N,h}(\cdot)$ changes, it will not affect the value of N. The equation for N is as follows:

$$N = \lceil \lambda \rceil \tag{4-20}$$

4.4.2 Parameter h

Once the values of the independent variables V and λ for the function $f_{N,h}(\cdot)$ are determined, the corresponding value of the parameter N can be identified. At this point, there is an optimal value for the parameter h that minimizes the result error in the function $f_{N,h}(\cdot)$. The FFMT method essentially involves linearly combining N integer-order moments in appropriate proportions to obtain the desired fractional-order moment.

When the independent variable V of the function $f_{N,h}(\cdot)$ remains constant, and the fractional order λ varies within the integer interval $(i, i+1)$, the integer-order moments used for linear combination stay the same. Using the same optimal h value in this scenario ensures a stable and sufficiently accurate result. However, if the independent variable V of the function $f_{N,h}(\cdot)$ changes, even if λ remains unchanged, the integer-order moments used for the linear combination will change significantly. In this case, using the same optimal h value will not ensure minimal error, indicating a change in the optimal h value. Thus, when the independent variable V of the function $f_{N,h}(\cdot)$ changes, the optimal value of the parameter h also changes. Similarly, when the fractional order λ crosses its corresponding integer interval $(i, i+1)$, the optimal value of the parameter h changes.

Considering that the only known conditions are the values of the integer-order moments of the corresponding random variables, the method to determine the optimal parameter h will only rely on these integer-order moments. Let P be a very small constant. Then set $\lambda' = i + P$. When the difference between the value of the function $f_{N,h}(\lambda', V)$ and the value of $E[V^i]$ is minimized, the corresponding h value must be optimal, minimizing the computational error of the function $f_{N,h}(\cdot)$.

Given a new function $g_{\lambda',V}(h)$, as shown below, representing the difference between the function $f_{N,h}(\lambda', V)$ and the corresponding $E[V^i]$, with h as the independent variable. To find the optimal parameter h, it is necessary to identify the value of h that corresponds to the minimum of the function $g_{\lambda',V}(\cdot)$.

4.4.2.1 Existence and Uniqueness of *h*

Before using function $g_{\lambda',V}(\cdot)$ to determine the optimal h value, it is essential to prove the existence and uniqueness of the minimum in function $g_{\lambda',V}(\cdot)$. When the value of N is either odd or even, it corresponds to different patterns. Therefore, when discussing the characteristics of function $g_{\lambda',V}(h)$, N will be classified and discussed based on its parity.

(1) *N* is Odd

A new function $G_{\lambda',V}(h)$ is defined, with h serving as the independent variable. The first derivative of function $G_{\lambda',V}(h)$ with respect to h is denoted as function $g_{\lambda',V}(h)$. And C represents an arbitrary constant. The expression for function $G_{\lambda',V}(h)$ is formulated as follows:

$$\begin{aligned} G_{\lambda',V}(h) = &\sum_{j=0}^{N} \left[\frac{(-1)^{N-j}(\lambda' - N)}{(\lambda' - j)(\, j - \lambda' + 1\,)} \binom{\lambda'}{N} \binom{N}{j} V^j \right] h^{\,j-\lambda'+1} \\ &- E[V^i]\, h + C \end{aligned} \tag{4-21}$$

For simplicity, let

$$\alpha_j = \frac{(-1)^{N-j}(\lambda' - N)}{(\lambda' - j)(\, j - \lambda' + 1\,)} \binom{\lambda'}{N} \binom{N}{j} V^j, \qquad T_j(h) = h^{\,j-\lambda'+1}.$$

In this case, function $G_{\lambda',V}(h)$ can be expressed as:

$$\begin{aligned} G_{\lambda',V}(h) = &(\alpha_0 T_0 + \alpha_1 T_1 + \cdots + \alpha_{N-2} T_{N-2}) \\ &+ \left(\alpha_{N-1} T_{N-1} + \alpha_N T_N - E[V^i]\, h\right) + C \end{aligned} \tag{4-22}$$

As h approaches 0, with T_0 being the highest-order term and $\alpha_0 < 0$, it can be inferred the limit of function $G_{\lambda',V}(h)$:

$$\lim_{h \to 0} G_{\lambda',V}(h) = -\infty \tag{4-23}$$

Considering the random variable V, which has a range of $(0, +\infty)$ and corresponds to the probability density function $p(V)$, then the validity of the relationship

$$\frac{V^N}{N} - d\left(\frac{V^N}{N}\right) > 0$$

implies the derivation of the following:

$$\begin{aligned} &\frac{V^N}{N} - d\left(\frac{V^N}{N}\right) > 0 \;\Rightarrow\; \left| \frac{V^{N+1}}{N+1} - V^N \right|_0^{+\infty} > 0 \\ &\Rightarrow \int_0^{+\infty} (V^N - NV^{N-1})\, dV > 0 \\ &\Rightarrow \int_0^{+\infty} V^N p(V)\, dV - \int_0^{+\infty} NV^{N-1} p(V)\, dV > 0 \\ &\Rightarrow E[V^N] - NE[V^{N-1}] > 0 \end{aligned} \tag{4-24}$$

Relaxing specific coefficients, the relationship still holds true:

$$
\begin{aligned}
& E[V^N] - NE[V^{N-1}] > 0 \\
& \Rightarrow (N-j)E[V^{j+1}] - (j+1)E[V^j] > 0 \\
& \Rightarrow \frac{(j+1)!(N-j-1)!\,E[V^j]}{j!(N-j)!\,E[V^{j+1}]} < 1 \\
& \Rightarrow \frac{(\lambda'-j-2)(j+1)!(N-j-1)!\,E[V^j]}{(\lambda'-j)\,j!(N-j)!\,E[V^{j+1}]} < 1 \\
& \Rightarrow \frac{\dfrac{N-\lambda'}{(\lambda'-j)(\lambda'-j-1)}\binom{\lambda'}{N}\binom{N}{j}E[V^j]}{\dfrac{N-\lambda'}{(\lambda'-j-1)(\lambda'-j-2)}\binom{\lambda'}{N}\binom{N}{j+1}E[V^{j+1}]} < 1
\end{aligned}
\tag{4-25}
$$

Now considering j ranges from 0 to $N-2$, based on the structural formula of α_j, it is evident that α_j is negative when j is even and positive when j is odd. Assuming j is even, and the range of h is $(0, 1]$ in conjunction with Equation (4-25), the following relationship can be derived:

$$
\frac{\alpha_j}{\alpha_{j+1}} > -1 \quad \Rightarrow \quad \frac{\dfrac{d}{dh}\left(\alpha_{j+1}T_{j+1}(h)\right)}{\dfrac{d}{dh}\left(-\alpha_j T_j(h)\right)} < 1 \tag{4-26}
$$

Then considering the remaining terms in function $G_{\lambda',V}(h)$, denoted by function $S_{\lambda',V}(h)$, excluding C, it can be represented as follows:

$$
S_{\lambda',V}(h) = \alpha_{N-1}h^{N-\lambda'} + \alpha_N h^{N-\lambda'+1} - E[V^{N-1}]\,h \tag{4-27}
$$

Given the very small value of P, function $S_{\lambda',V}(h)$ can be approximated as an upward-opening quadratic function, where $S_{\lambda',V}(0) = 0$, and its minimum value is negative, located at

$$
h = \frac{E[V^{N-1}] - \alpha_{N-1}}{2\alpha_N}.
$$

Then the following relationship can be derived:

$$
\begin{aligned}
& \alpha_0\left(\frac{E[V^{N-1}] - \alpha_{N-1}}{2\alpha_N}\right)^{-\lambda'+1} - \lim_{h\to 0} G_{\lambda',V}(h) \\
& - \left[\alpha_{N-1}\left(\frac{E[V^{N-1}] - \alpha_{N-1}}{2\alpha_N}\right)^{N-\lambda'} + \alpha_N\left(\frac{E[V^{N-1}] - \alpha_{N-1}}{2\alpha_N}\right)^{N-\lambda'+1}\right. \\
& \left. - E[V^{N-1}]\cdot\frac{E[V^{N-1}] - \alpha_{N-1}}{2\alpha_N}\right] > 0
\end{aligned}
\tag{4-28}
$$

Based on Equations (4-26) and (4-28), for the function $G_{\lambda',V}(\cdot)$, when N is odd, within the range $(0, 1]$, it is impossible to find two distinct values of h ($h_1 \neq h_2$) such that $G_{\lambda',V}(h_1) = G_{\lambda',V}(h_2)$. Therefore, according to the Rolle's lemma, it can be concluded that there are no zeros of the function $g_{\lambda',V}(h)$ within the range $(0, 1]$.

Then for simplicity, let

$$
K_j = (-1)^{N-j}(N-\lambda')\binom{\lambda'}{N}\binom{N}{j}E[V^j], \qquad U_j(h) = h^{j-\lambda'}.
$$

Then function $g_{\lambda',V}(h)$ can be expressed as:

$$
g_{\lambda',V}(h) = K_0U_0 + K_1U_1 + \cdots + K_NU_N \tag{4-29}
$$

In this case, for the function $g_{\lambda',V}(h)$, as h approaches 0, the highest-order term corresponds to U_0. Considering the parity of N, it can be deduced that K_0 is greater than 0 in this scenario. Therefore, the limit of function $g_{\lambda',V}(h)$ can be derived as follows:

$$\lim_{h\to 0} g_{\lambda',V}(h) = +\infty \tag{4-30}$$

At this juncture, within the range of $(0, 1]$, it has been proved that the function $g_{\lambda',V}(h)$ does not have any zeros. Consequently, it can be inferred that the value of the function $g_{\lambda',V}(h)$ at $h = 1$ is greater than 0, i.e., $g_{\lambda',V}(1) > 0$. To further ascertain the characteristics of the function $g_{\lambda',V}(h)$, the first derivative of function $g_{\lambda',V}(h)$ is provided as follows:

$$g^{(1)}_{\lambda',V}(h) = \sum_{j=0}^{N} \left[(-1)^{N-j}(N-\lambda')\binom{\lambda'}{N}\binom{N}{j}E[V^j] \right] h^{j-\lambda'-1} \tag{4-31}$$

For the sake of simplicity, let

$$I_j = (-1)^{N-j}(N-\lambda')\binom{\lambda'}{N}\binom{N}{j}E[V^j], \qquad C_j(h) = h^{j-\lambda'-1}.$$

Then function $g^{(1)}_{\lambda',V}(h)$ can be expressed as:

$$g^{(1)}_{\lambda',V}(h) = I_0C_0 + I_1C_1 + \cdots + I_NC_N \tag{4-32}$$

Following the same principles of computation as with $\lim_{h\to 0} G_{\lambda',V}(h)$, and considering that the value of I_0 is negative, the limit of the function $g^{(1)}_{\lambda',V}(h)$ as h approaches 0 is

$$\lim_{h\to 0} g^{(1)}_{\lambda',V}(h) = -\infty.$$

Considering j within the range $[0, N]$, assuming j is even, I_j is always negative, and I_{j+1} is always positive. Then the conclusion from Equation (4-24) can be used to derive the following relationship:

$$\begin{aligned}
&E[V^N] - NE[V^{N-1}] > 0 \\
&\Rightarrow (N-j)E[V^{j+1}] - (j+1)E[V^j] > 0 \\
&\Rightarrow \frac{(j+1)!(N-j-1)!\,E[V^j]}{j!(N-j)!\,E[V^{j+1}]} < 1 \\
&\Rightarrow \frac{(N-\lambda')\binom{\lambda'}{N}\binom{N}{j}E[V^j]}{(N-\lambda')\binom{\lambda'}{N}\binom{N}{j+1}E[V^{j+1}]} < 1 \\
&\Rightarrow \frac{I_j}{I_{j+1}} > -1
\end{aligned} \tag{4-33}$$

According to the result of Equation (4-33), it is evident that the value of the function $g^{(1)}_{\lambda',V}(h)$ at $h = 1$ is greater than 0, i.e., $g^{(1)}_{\lambda',V}(1) > 0$. According to the Bolzano–Cauchy theorem, it can be deduced that within the range $(0, 1)$, there must exist at least one value of h for which the function $g^{(1)}_{\lambda',V}(h)$ equals 0. Building upon the conclusion of Equation (4-33) and incorporating the characteristics of C_j, the following relationship can be further derived:

$$\frac{I_j}{I_{j+1}} > -1 \quad \Rightarrow \quad 0 < \frac{\dfrac{d}{dh}(I_{j+1}C_{j+1}(h))}{\dfrac{d}{dh}(-I_jC_j(h))} < 1 \tag{4-34}$$

Then it is evident that the function $g^{(1)}_{\lambda',V}(h)$ has only one zero within the interval $(0, 1]$. Continuing to utilize the results of Equation (4-33) and incorporating the characteristics of $C_j(h)$, given that the range of j is $[0, N]$, with N being

an even number, and for h in the range $(1, +\infty)$, the following relationship can be derived:

$$0 > \frac{I_j C_j(h)}{I_{j+1} C_{j+1}(h)} > -1 \tag{4-35}$$

Based on the results of Equation (4-35), it is evident that within the range of h within $(1, +\infty)$, the value of the function $g^{(1)}_{\lambda',V}(h)$ is always greater than 0. Thus, it has been demonstrated that the shape of the function $g_{\lambda',V}(h)$ approximately resembles an upward-opening quadratic function. The function $g_{\lambda',V}(h)$ necessarily has a single minimum within the range $h \in (0, +\infty)$, and the corresponding value of h that yields this minimum is certainly located within the range $(0, 1)$. Consequently, this also indicates that for the formula in Corollary 2.4, when N is an odd number, there exists an optimal value of h that minimizes the corresponding computational error, as shown in Figure 4-1.

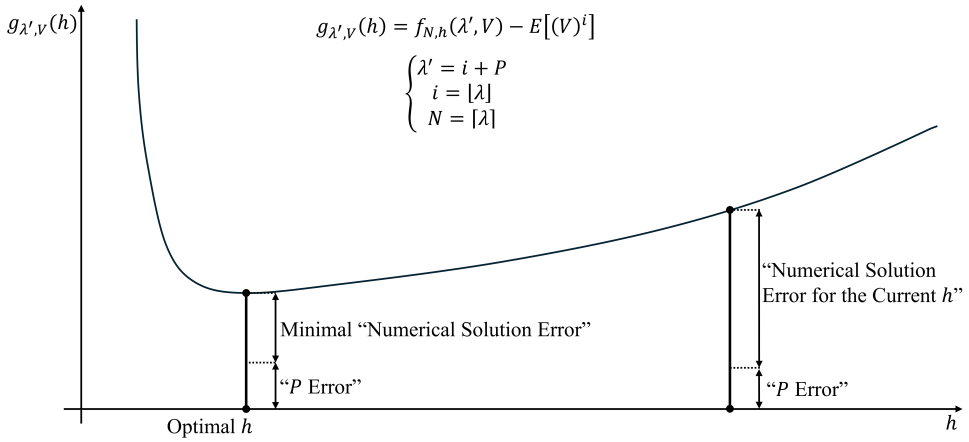


Figure 4-1: The approximate shape of function $g_{\lambda',V}(h)$ and the corresponding sources of computational error when N is odd

As shown in Figure 4-1, the value of function $g_{\lambda',V}(h)$ represents the corresponding computational error. It is evident that there will always be a computational error regardless of the value of h, but the magnitude of this error will vary with changes in h. This study assumes that the computational error itself consists of two parts: P error and numerical solution error. Although the value of P used in variable λ' for function $g_{\lambda',V}(h)$ is very small, it is never zero. Therefore, even if the formula in Corollary 2.4 yields a totally accurate result, the value of function $g_{\lambda',V}(h)$ will not be zero after using λ', but greater than zero. This part of the computational error is caused by P, which is referred to as P error. P error is solely related to the value of P and represents the difference between $E[V^{i+P}]$ and $E[V^i]$ when applying function $g_{\lambda',V}(h)$. It is an objective error that is independent of the values of N and h. In contrast, the other part of the computational error represented by function $g_{\lambda',V}(h)$ is the numerical solution error. This error originates from the formula in Corollary 2.4 itself, as the formula in Corollary 2.4 is a numerical solution expression and inherently has computational errors. This part of the error is referred to as the numerical solution error. Based on the previous analysis, it has been established that when λ and N are determined, the magnitude of the numerical solution error is related to the value of h, so there exists an optimal h value that minimizes the current numerical solution error. The purpose and significance of finding the optimal h value lie in this context, which is to minimize the numerical solution error component of the computational error represented by the function $g_{\lambda',V}(h)$. The optimal h value corresponds to the h value at which function $g^{(1)}_{\lambda',V}(h)$ equals zero. Therefore, when calculating the optimal h value for odd N, it is only necessary to determine the h value corresponding to $g^{(1)}_{\lambda',V}(h) = 0$. This corresponds to the following relationship:

$$\begin{aligned} g^{(1)}_{\lambda',V}(h) = 0 \quad &\Rightarrow \quad \sum_{j=0}^{N} (-1)^{N-j} (N - \lambda') \binom{\lambda'}{N} \binom{N}{j} E[V^j] h^{j-\lambda'-1} = 0 \\ &\Rightarrow \quad \sum_{j=0}^{N} (-1)^{N-j} \frac{E[V^j]}{j!\,(N-j)!} h^j = 0 \end{aligned} \tag{4-36}$$

From the result of Equation (4-36), it is evident that the optimal h value is independent of P. When the values

of V and N corresponding to function $g_{\lambda',V}(h)$ remain unchanged, the optimal h value is fixed regardless of the initial value of P. This in turn implies that the role of the current optimal h value is to minimize the numerical solution error, thereby maximizing computational accuracy of the FFMT method, and it does not affect the P error. Moreover, the fact that the optimal value of h is independent of P indicates that once the optimal value of h is determined using λ', the corresponding integer-order moments for linear combination remain unchanged even if P varies within the range $(0, 1)$. Consequently, even if λ varies within the respective integer interval $(i, i+1)$, the same optimal value of h ensures that the error in the FFMT results remains stable and relatively low.

(2) N is Even

When N is even, based on the function $g_{\lambda',V}(h)$, assuming j is within the range $[0,\ N-1]$, and combining with the result of Equation (4-25), the following relationship can be obtained when h is within the range $(0, 1]$:

$$0 < \frac{\dfrac{d\big(K_{j+1}\,U_{j+1}(h)\big)}{dh}}{\dfrac{d\big(-K_j\,U_j(h)\big)}{dh}} < 1 \tag{4-37}$$

Similarly, for the function $g_{\lambda',V}(h)$, within the range of $j \in [0,\ N-1]$, when the independent variable h ranges from $(1, +\infty)$, the following relationship can be derived:

$$-1 < \frac{K_j\,U_j(h)}{K_{j+1}\,U_{j+1}(h)} < 0 \tag{4-38}$$

Then, for the remaining terms of the function $g_{\lambda',V}(h)$, with the independent variable h in the range $(0, +\infty)$, the following relationship holds:

$$\frac{d\big(K_N\,U_N(h) - E[V^{N-1}]\,h\big)}{dh} > 0 \tag{4-39}$$

Based on the above conclusions, it can be determined that when N is even, the function $g_{\lambda',V}(h)$ is always increasing over the interval $(0, +\infty)$. On the other hand, considering the limits of the function $g_{\lambda',V}(h)$, denoted as

$$\lim_{h\to 0} g_{\lambda',V}(h) = -\infty, \qquad \lim_{h\to +\infty} g_{\lambda',V}(h) = +\infty,$$

it follows that within the range $(0, +\infty)$, there must exist a value of h such that $g_{\lambda',V}(h) = 0$. This zero-point h must satisfy the following relationship:

$$\sum_{j=0}^{N} \frac{(-1)^{N-j}\,\big((i+P)' - N\big)}{(i+P)' - j} \binom{(i+P)'}{N} \binom{N}{j} E[V^j]\,h^{\,j-(i+P)'} = E[V^i] \tag{4-40}$$

For Equation (4-40), regardless of whether the corresponding h value can be obtained, it is evident that the h value is significantly influenced by P. From the previous analysis, it is clear that P can only affect the P error, i.e., the value of $E[V^{i+P}] - E[V^i]$, and cannot influence the numerical solution error. The purpose and significance of constructing the function $g_{\lambda',V}(h)$ is to find the optimal h value that minimizes the current numerical solution error. This optimal h value should only relate to the current V and N and is not influenced by P, and the numerical solution error will never be zero. Based on this, when N is even, directly calculating the optimal h value through the approach of Equation (4-40) is unreasonable. This is because the optimal h is directly related to the value of P, and when P changes, the corresponding optimal h value will change drastically. Consequently, this optimal h lacks stability, meaning that the method of determining the optimal h through the function $g_{\lambda',V}(h)$ is unstable and cannot be effectively applied in practice.

Additionally, when the optimal h value is directly related to the value of P, any change in λ within the respective interval implies a change in P, meaning this optimal h cannot ensure the stability of the FFMT method's computational

error, leading to a significant increase in error. Therefore, when N is even, Equation (4-40) should be further modified to make the calculated optimal h independent of P. Thus, when N is even, the function $g_{\lambda',V}(h)$ is modified as follows:

$$\begin{aligned} g_{\lambda',V}(h) &= \sum_{j=1}^{N} \frac{(-1)^{N-j}(\lambda'-N)}{\lambda'-j}\binom{\lambda'}{N}\binom{N}{j}E[V^j]\,h^{j-\lambda'} - E[V^i] \\ &= K_1U_1 + K_2U_2 + \cdots + K_NU_N \end{aligned} \tag{4-41}$$

The form of function $g_{\lambda',V}(h)$ proposed in Equation (4-41) effectively addresses the described issues, allowing for the calculation of the optimal h value that is not influenced by P. The modification to the form of Equation (4-41) is necessary because the first term (K_0U_0) of the original function $g_{\lambda',V}(h)$ does not contain significant integer-order moment information. Consequently, when λ varies within the corresponding integer interval, the first term K_0U_0 has minimal impact on the final computational result. Therefore, removing the first term to obtain the optimal h still ensures that the error of the FFMT method remains within a low range.

Additionally, after removing the first term, the curve shape of the new function $g_{\lambda',V}(h)$ resembles that of the function when N is odd, with only one minimum value. This similarity ensures that the optimal h value, unaffected by P, can be effectively obtained. The trend and sign change patterns of each term are consistent with those of the function $g_{\lambda',V}(h)$ when N is odd. The characteristics of the function $g_{\lambda',V}(h)$ in Equation (4-41) remain consistent with those when N is odd.

Therefore, the method for calculating the corresponding optimal h value is the same as when N is odd. The corresponding expression is as follows:

$$\sum_{j=1}^{N}(-1)^{N-j}\frac{E[V^j]}{j!\,(N-j)!}h^j = 0 \tag{4-42}$$

Thus far, the analysis has focused on the characteristics of the function $g_{\lambda',V}(h)$ corresponding to different parity of N, as well as the existence and uniqueness of the corresponding optimal h. Furthermore, the validity of the method proposed in this paper for obtaining the optimal h value through the function $g_{\lambda',V}(h)$ has been demonstrated.

4.4.2.2 Calculation of the Optimal *h*

Based on the preceding argumentation, letting

$$Q_j = \frac{(-1)^{N-j}E[V^j]}{j!\,(N-j)!},$$

the expression for calculating the optimal h as described above can be understood as solving the corresponding N-order univariate equation, as shown below:

$$\begin{cases} Q_1h + Q_2h^2 + \cdots + Q_Nh^N - \dfrac{1}{N!} = 0, & \text{for } N \text{ is Odd}, \\ Q_1h + Q_2h^2 + \cdots + Q_Nh^N = 0, & \text{for } N \text{ is Even}. \end{cases} \tag{4-43}$$

The methods for solving high-order univariate equations can be broadly classified into two categories: algebraic methods for analytical solutions and numerical solution methods. According to Galois Theory, for high-order univariate equations of degree 5 or higher, it is impossible to express solutions using a finite number of arithmetic operations and radicals. Given that N in Equation (4-43) can indeed be greater than 5, it is evident that using algebraic methods to obtain an analytical solution for Equation (4-43) is impractical. Considering that the h value calculated through Equation (4-43) does not require high precision—accuracy to four decimal places is sufficient to ensure the precision of the FFMT method's computational results—using numerical solution methods to solve Equation (4-43) is evidently more appropriate. And since Equation (4-43) contains only one unknown variable, applying relevant numerical solution techniques is straightforward. There are numerous well-known numerical methods for solving high-order univariate

equations, including the bisection method, secant method, fixed-point iteration method, Newton-Raphson iteration method, and Taylor series expansion method. Considering that the optimal h does not require high precision to ensure the error level of the FFMT method, the more convenient and intuitive Taylor series expansion method is used here to solve Equation (4-43) to obtain the optimal h. For the sake of clarity, the function $q(h)$ corresponding to Equation (4-43) is given by the following expression:

$$q(h) = \begin{cases} Q_1 h + Q_2 h^2 + \cdots + Q_N h^N - \dfrac{1}{N!}, & \text{for } N \text{ is Odd}, \\ Q_1 h + Q_2 h^2 + \cdots + Q_N h^N, & \text{for } N \text{ is Even}. \end{cases} \tag{4-44}$$

Subsequently, a series of θ_i ($i = 0, 1, 2, \ldots, 8, 9$) are provided, where except for $\theta_0 = 0.01$, the remaining θ_i values are given by $\theta_i = 0.1\,i$. The Taylor series expansion method is then used to approximate the function $q(h)$ at different θ_i points, expanding it into the corresponding quadratic functions:

$$q(h) = q(\theta_i) + q^{(1)}(\theta_i)\,(h - \theta_i) + \frac{q^{(2)}(\theta_i)}{2}\,(h - \theta_i)^2 \tag{4-45}$$

Using Equation (4-45), the roots corresponding to $q(h) = 0$ for the Taylor series expansion at different θ_i points can be conveniently obtained. These roots are denoted by h_i^T, and the specific expression for h_i^T is given as follows:

$$h_i^T = \frac{-b_i \pm \sqrt{b_i^2 - 4a_i c_i}}{2a_i} \tag{4 - 46a}$$

$$a_i = \frac{q^{(2)}(\theta_i)}{2} \tag{4 - 46b}$$

$$b_i = q^{(1)}(\theta_i) - \theta_i\, q^{(2)}(\theta_i) \tag{4 - 46c}$$

$$c_i = q(\theta_i) - q^{(1)}(\theta_i)\theta_i + \frac{\theta_i^2}{2} q^{(2)}(\theta_i) \tag{4 - 46d}$$

The method for obtaining h_i^T is based on the root-finding formula for a quadratic equation, where $q^{(n)}(\cdot)$ represents the n-th derivative of the function $q(h)$. When the difference between θ_i and h_i^T is minimized, then this h_i^T value is the optimal h sought. Given a function $y(h_i^T)$, denoted as $y(h_i^T) = |\theta_i - h_i^T|$, the optimal h value can be expressed by the following relationship:

$$\text{Optimal } h = \arg\min\ y(h_i^T) = \arg\min\ |\theta_i - h_i^T| \tag{4 - 47}$$

The h_i^T values in Equation (4-47) correspond to the real roots of Equation (4-45). If no real roots exist, the corresponding imaginary roots h_i^T are not adopted. The advantage of using the above method to calculate the optimal h value lies in the elimination of the need for multiple iterations. Only 10 computations are required to obtain the corresponding optimal h value, significantly reducing the computational cost of the FFMT method in practical applications. On the other hand, for the Taylor series expansion of the function $q(h)$, in addition to being expanded into the form of a quadratic equation as in Equation (4-45), it can also be expanded into the form of a cubic equation, denoted as

$$q(h) = q(\theta_i) + q^{(1)}(\theta_i)(h - \theta_i) + \frac{q^{(2)}(\theta_i)}{2}(h - \theta_i)^2 + \frac{q^{(3)}(\theta_i)}{6}(h - \theta_i)^3.$$

The cubic equation also has a root-finding formula, which allows for the roots to be obtained very conveniently. Increasing the number of terms in the Taylor expansion (such as using the cubic equation) can further improve the accuracy of the final optimal h value. It should be noted that the use of the Taylor expansion method to obtain the optimal h value here is due to its intuitive nature. However, in practical applications, more efficient solution methods may exist depending on

the specific application environment and the nature of the random variables. Developing tailored solution methods for particular application settings can significantly enhance the computational efficiency of the FFMT method. Nevertheless, this aspect is not the focus of the present study, and therefore, it is not discussed further here.

At present, this study has provided the method for determining the values of parameters N and h. When applying the formula from Corollary 2.4 in practical scenarios, it is only necessary to determine the values of N and h using the described method. Then, by combining these with the given integer-order moments of the corresponding random variable V and the values of the fractional order λ, the result $E[V^{\lambda}]$ can be calculated.

4.5 Numerical Experiments

In the numerical experiments, it is assumed that the random variable V follows various types of probability distributions. The proposed FFMT method is employed to compute the corresponding fractional moments, and its effectiveness is validated through numerical experiments. To provide a clear and reliable benchmark for validation, the fractional moments of different types of random variables V are calculated using either direct numerical integration or closed-form analytical expressions, whenever available. These results are treated as the *true values* and are used as references for comparison with the results obtained by the FFMT method. The accuracy of the FFMT method is evaluated by the approximation error, which is defined as the difference between the fractional moments computed by the FFMT method and the corresponding true values. In addition, since the Taylor expansion method is widely adopted in engineering practice for the computation of fractional moments and similarly relies on known integer-order moments, it is selected as a comparative benchmark. Accordingly, the numerical results also report the error levels of fractional moments obtained using the Taylor expansion method under identical conditions. For consistency and fairness in comparison, the number of expansion terms used in the Taylor expansion method is set equal to the parameter N adopted in the FFMT method.

4.5.1 Truncated Normal Distribution

Assuming random variable V follows a truncated normal distribution. Employing the direct integration method computes the value of $E[(V)^{\lambda}]$, which is regarded as the True Values. Specifying the distribution characteristics of V, denoted as $V \sim \mathrm{TN}(10, 3)$, and truncation interval is $[0, 30]$. Then as the fractional order λ varies, the computational results $E[(V)^{\lambda}]$ obtained via FFMT method and Taylor expansion, respectively. The results are compared with the True Values and errors of the two methods are illustrated in the Figure 4-2. The figure demonstrates that the FFMT method exhibits minimal error fluctuations, consistently maintaining a very low level of error. This stability indicates that the FFMT method reliably produces highly accurate fractional order moment results, irrespective of the value of λ. In contrast, the Taylor expansion method also maintains high accuracy when λ is less than 3. However, when λ exceeds 4, the Taylor expansion method's error increases sharply with higher λ values, showing significant fluctuations. This suggests that the Taylor expansion method lacks the stability and accuracy of the FFMT method for higher-order moment calculations. This observation highlights the superiority of the FFMT method in handling high-order moments.

Figure 4-3 illustrates the error fluctuations of the FFMT method and the Taylor expansion method as λ varies, corresponding to changes in the standard deviation of a truncated normal distribution with a mean of 10 and a truncation range of $[0, 30]$. Figure 4-4 shows the error fluctuations of both methods as λ changes, corresponding to variations in the mean of a truncated normal distribution with a standard deviation of 5 and the same truncation range. The patterns observed in Figures 4-3 and 4-4 indicate that the overall error level of the FFMT method is directly related to the coefficient of variation of the random distribution. A higher coefficient of variation, indicating greater data dispersion, results in larger errors for the FFMT method. This is because higher data dispersion means the information contained in the same number of integer order moments is less effective at reflecting the corresponding fractional order moments. Thus, using these integer order moments to form a linear combination to obtain fractional order moments leads to increased errors. However, even when the coefficient of variation reaches 0.6, indicating significant data dispersion, the FFMT method's error remains controlled within 1%. Furthermore, regardless of changes in the coefficient of variation, the FFMT method

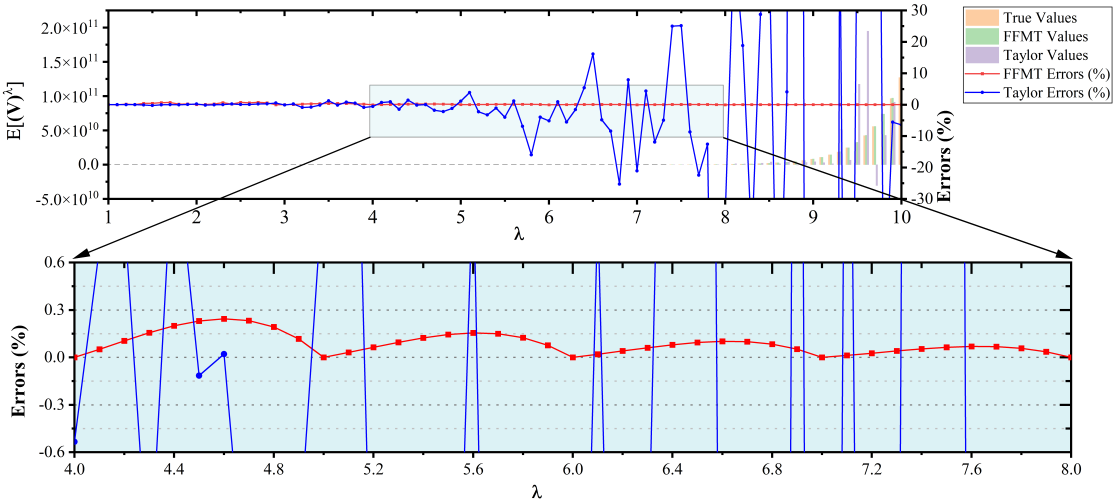


Figure 4-2: The errors of FFMT method and the Taylor expansion method compared to the True Values as λ varies, where the distribution is $V \sim \mathrm{TN}(10, 3)$ and truncation interval is $[0, 30]$.

maintains stable error levels as λ varies. In contrast, the Taylor expansion method's stability and accuracy are limited to lower fractional orders. As λ increases, the Taylor expansion method exhibits sharp error fluctuations and significant error increases. Therefore, the FFMT method demonstrates clear advantages over the Taylor expansion method for practical engineering applications.

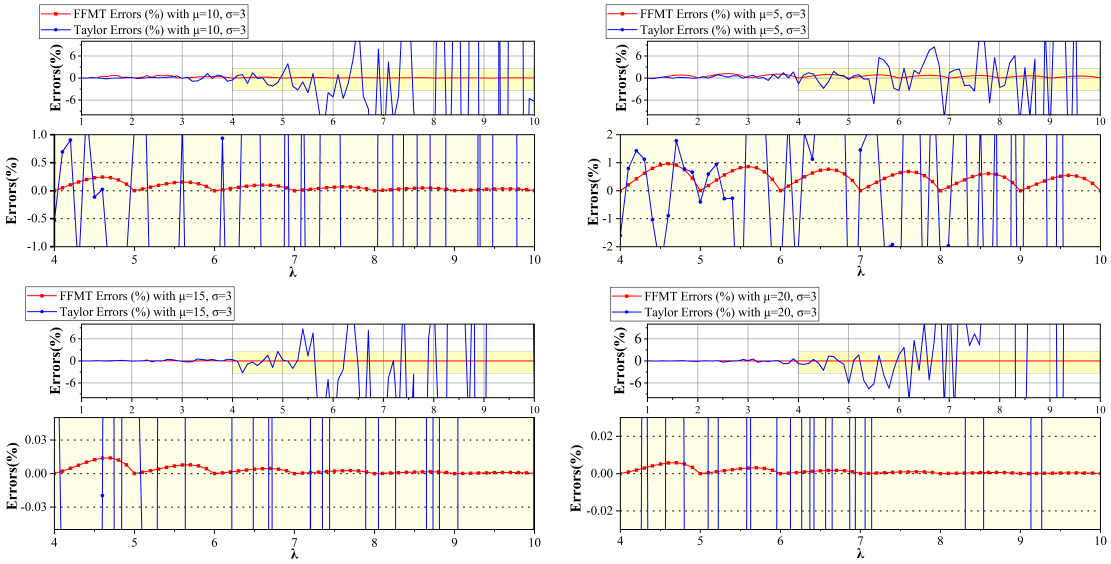


Figure 4-3: Errors of the FFMT method and the Taylor expansion method compared to the True Values as λ varies, considering different μ, denoted as $V \sim \mathrm{TN}(\mu, 3)$, and truncation interval is $[0, 30]$.

4.5.2 Lognormal Distribution

Assuming the random variable V follows a lognormal distribution, denoted as $V \sim \mathrm{LN}(1, 0.5)$. The corresponding fractional moments of the specified order are computed directly using analytical expressions, which are regarded as the True Values. The expressions are presented as follows:

$$E[(V)^{\lambda}] = e^{\frac{1}{2}\cdot\lambda^2\cdot\sigma^2+\lambda\cdot\mu}$$

Figure 4-5 illustrates the results of $E[(V)^{\lambda}]$ calculated using the FFMT and Taylor expansion methods as the lognormal distribution varies with fractional order λ, along with the corresponding error levels compared to the True Values. From the Figure 4-5, it can be observed that although the Taylor expansion method no longer exhibits drastic errors when faced

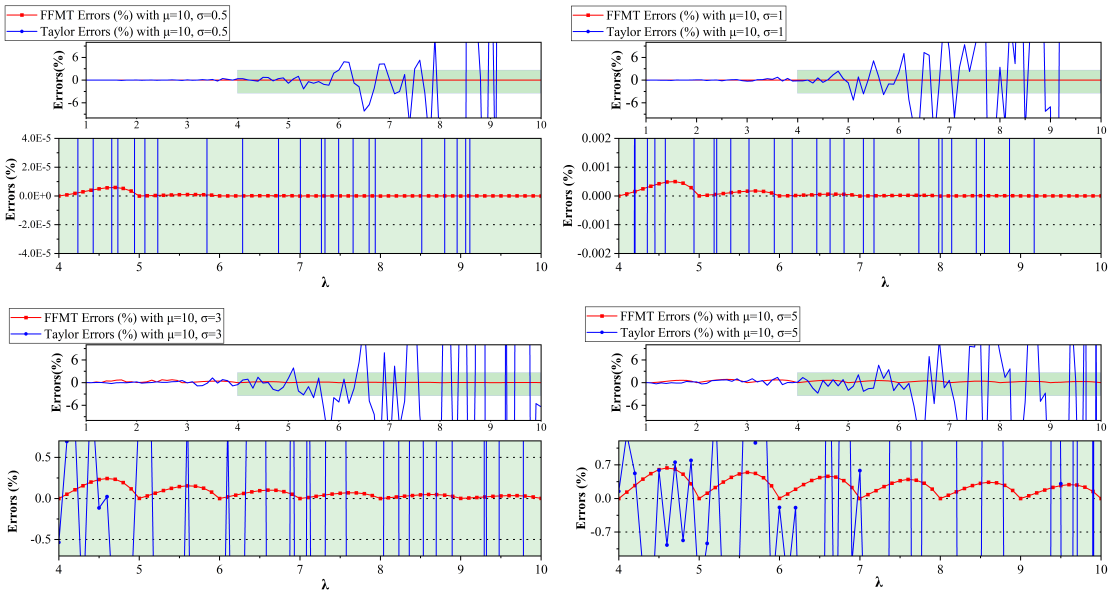


Figure 4-4: Errors of the FFMT method and the Taylor expansion method compared to the True Values as λ varies, considering different σ, denoted as $V \sim \mathrm{TN}(10, \sigma)$, and truncation interval is $[0, 30]$.

with the lognormal distribution, its error levels remain consistently high, averaging over 20% regardless of the variation in λ. In contrast, the FFMT method demonstrates excellent stability in error levels, coupled with high accuracy in results. The standard deviation of this lognormal distribution has already reached 50% of the mean, indicating a substantial degree of dispersion. However, even with such a large dispersion, the error in the results obtained using the FFMT method remains within 0.8% regardless of the variation in λ, demonstrating remarkably high accuracy.

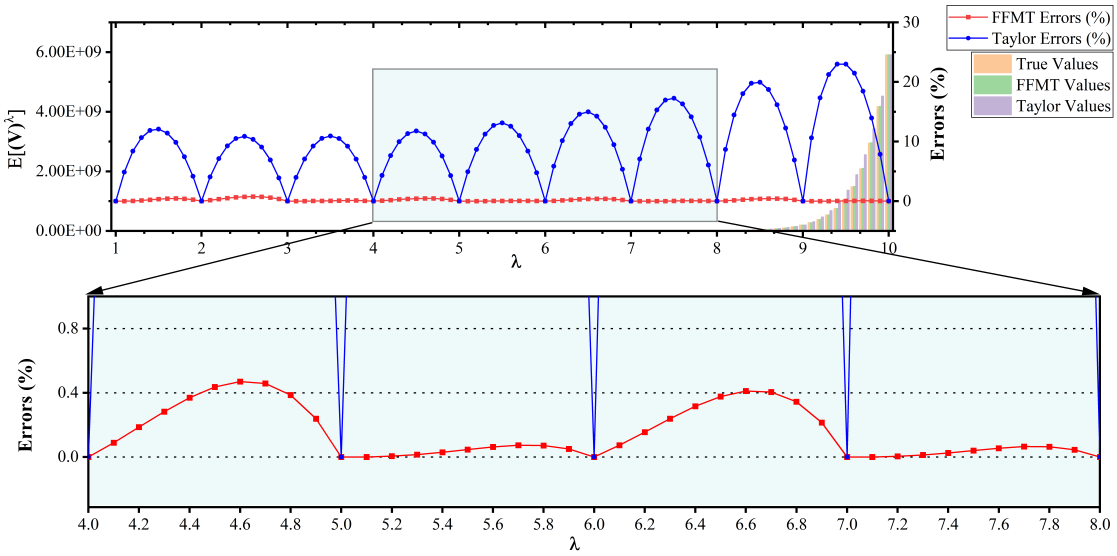


Figure 4-5: The errors of the FFMT method and the Taylor expansion method compared to the True Values as the distribution is $V \sim \mathrm{LN}(1, 0.5)$, while λ varies.

Figure 4-6 illustrates the error fluctuations of the FFMT method and the Taylor expansion method for lognormal distributions with varying means and standard deviations. The FFMT method consistently maintains a very low level of error regardless of changes in the mean and standard deviation of the log-normal distribution. Additionally, as the fractional order λ varies, the FFMT method's error remains stable, underscoring its robustness. In contrast, the Taylor expansion method exhibits significantly higher errors, which are not comparable to those of the FFMT method, demonstrating the superior accuracy of the FFMT method for lognormal distributions. Under the same mean or standard deviation conditions, the result precision of the FFMT method significantly exceeds that of the Taylor expansion method. As the mean of the log-normal distribution increases while the standard deviation remains constant, the error of the Taylor expansion method also increases. This occurs because the accuracy of the Taylor expansion method is influenced

by the expansion point, typically the mean of the distribution in practical applications. Consequently, an increase in the mean results in greater error for the Taylor expansion method. The FFMT method effectively overcomes this limitation, maintaining a low and stable error level regardless of changes in the mean of the log-normal distribution. This stability highlights the FFMT method's reliability in practical engineering applications. As previously noted, increased dispersion of the random variable leads to higher errors for the FFMT method. However, even with greater dispersion, the FFMT method's error remains very low. This further demonstrates the FFMT method's advantage in accuracy.

On the other hand, comparing the error of the FFMT method for the lognormal distribution and the truncated normal distribution reveals that, within the same integer interval corresponding to a given λ, the error for the lognormal distribution is higher than that for the truncated normal distribution. This phenomenon occurs because the growth rate of the real-order moments for the lognormal distribution increases significantly more than that for the truncated normal distribution as the order λ increases. The FFMT method essentially involves linearly combining N integer-order moments with a proportion h to obtain the fractional-order moments within the corresponding interval. When the growth rate of the integer-order moments is higher, the growth rate of the fractional-order moments within the integer interval is also greater. Therefore, using the same optimal h value within the same interval results in increased error for the FFMT method. This phenomenon also explains, in reverse, how different types of random distributions affect the error of the FFMT method. To address this, when the growth rate of the integer-order moments of a random variable is very high, it is necessary to consider variations in the optimal h value within the integer interval. Constructing an analytical expression that allows the optimal h value to change with the order λ can further improve the accuracy of the FFMT method. Given the focus of this study, a more in-depth discussion is not provided here.

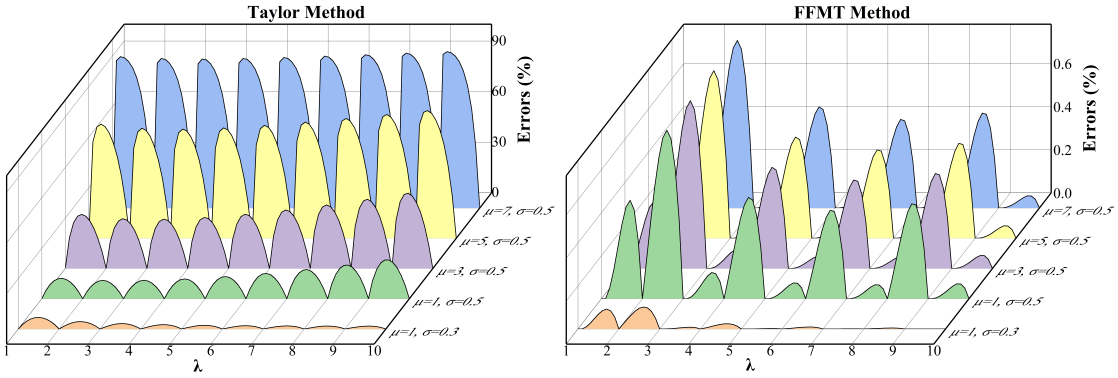


Figure 4-6: Errors of the FFMT method and the Taylor expansion method compared to True Values as λ varies, considering different σ and μ of the log-normal distribution.

4.5.3 Gamma Distribution

As a typical example of a non-Gaussian distribution, the Gamma distribution is considered as the third case. Assuming the random variable V follows a Gamma distribution, denoted as $V \sim \Gamma(k, \theta)$. The True Values of different order moments are computed according to the following formula:

$$E[(V)^{\lambda}] = \theta^{\lambda} \frac{\Gamma(k+\lambda)}{\Gamma(k)}$$

Figure 4-7 depicts the error fluctuations of the FFMT method and the Taylor expansion method as the parameters k and θ of the Gamma distribution vary. The FFMT method consistently maintains a very low and stable error level, regardless of the distribution characteristics of the random variable. In comparison, the Taylor expansion method exhibits errors that are several orders of magnitude higher than those of the FFMT method under identical distribution conditions. As the fractional order λ increases, the FFMT method's error fluctuations remain stable within a presentable range, avoiding increases with λ. In contrast, the Taylor expansion method's error fluctuations increase with λ, potentially causing negative impacts in practical engineering applications. This clearly demonstrates the FFMT method's superior output

stability. When focusing on a specific integer interval of λ, the FFMT method's error increases as λ moves away from the interval boundary and decreases as λ approaches the boundary. This behavior is due to the FFMT method's reliance on linear combinations of integer order moments to obtain corresponding fractional order moments. As λ nears the boundary, the integer order moments more accurately represent the corresponding λ-order moment, resulting in smaller errors. Conversely, as λ moves away from the boundary, the same integer order moments are less effective, leading to increased errors. Nevertheless, within any integer interval, the FFMT method controls error fluctuations within a small range, ensuring highly accurate results.

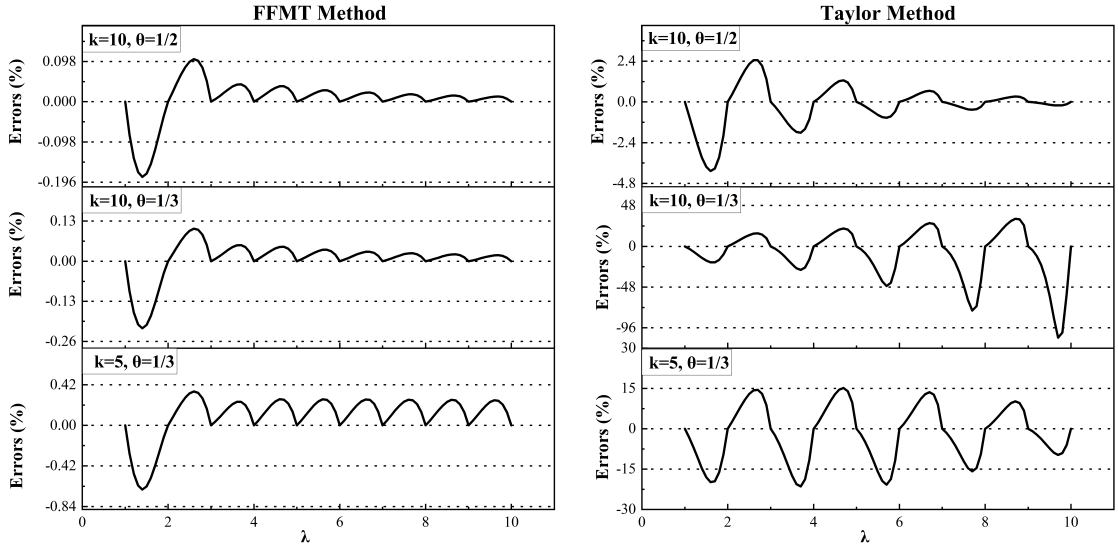


Figure 4-7: Errors of the FFMT method and Taylor expansion method compared to True Values as λ varies, considering different k and θ of gamma distribution.

The results demonstrate the feasibility and effectiveness of the FFMT method for calculating fractional order moments of random variables in the engineering field. The FFMT method exhibits two key advantages: accuracy and stability. The accuracy of the FFMT method ensures that highly precise fractional order moments can be obtained in practical applications, supporting the feasibility of subsequent research utilizing these moments. Stability refers to the method's ability to maintain errors within a very low and stable range, preventing abnormal fluctuations in the results. This stability ensures that the fractional order moments derived from the FFMT method will not cause aberrant outcomes in subsequent studies, thereby providing reliable data for further research.

4.5.4 Real-world Application Case

To demonstrate the advantages of the FFMT method in practical engineering applications, a real-world example is added here for further analysis. In the stochastic traffic assignment problem, the BPR function is used to obtain the corresponding stochastic link travel time T_a (Sheffi, 1984), and its form is given as Equation (4-1). When the link capacity follows a certain random distribution and parameter λ takes a non-integer value, calculating the corresponding T_a leads to fractional moment problems. For the fractional moment problems in stochastic traffic assignment, the most used approach for solving these problems is the Taylor series expansion method (Shao et al., 2006). However, in real-world networks, due to the large scale of the traffic network and the numerous links involved, the Taylor expansion method often cannot use adequate integer-order moments when considering computational costs, which results in inaccurate calculation outcomes. Based on this, a comparison between the FFMT method and the Taylor expansion method is conducted here, with both methods applied to stochastic traffic assignment to compare the traffic assignment results when the network is in equilibrium. To ensure a fair comparison, both methods use $N = \lceil \lambda \rceil$ integer-order moments, allowing for a performance comparison while minimizing computational costs. The case uses the Nguyen and Dupuis network, which includes 13 nodes and 19 links, as illustrated in Figure 4-8.

The free travel times for the links are set to 3. It is assumed that the link capacities follow a lognormal distribution,

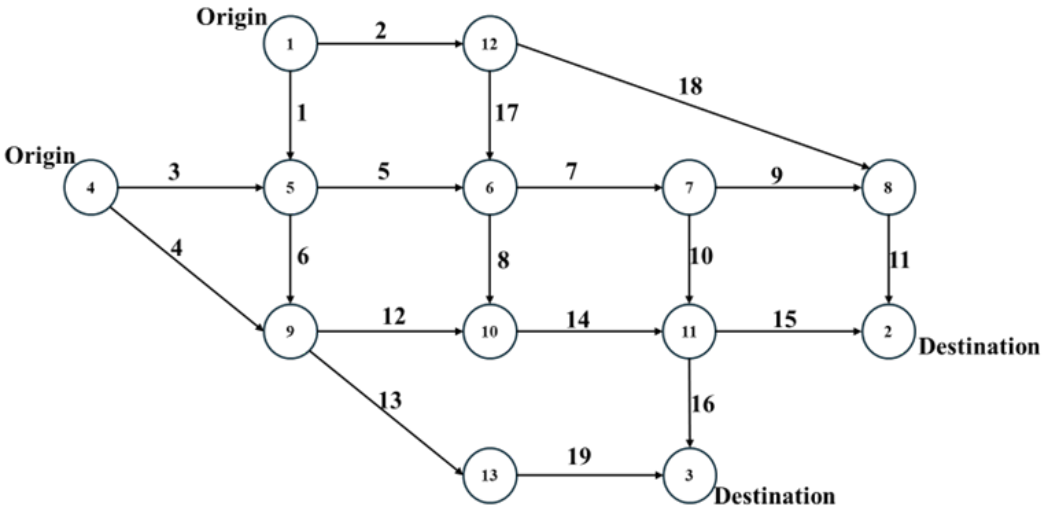


Figure 4-8: The Nguyen and Dupuis Network

Table 4-1: Random Link Capacity

Link	Mean	CV	Link	Mean	CV	Link	Mean	CV
1	2.0	0.3	8	2.7	0.2	15	3.4	0.1
2	2.1	0.3	9	2.8	0.2	16	3.5	0.1
3	2.2	0.3	10	2.9	0.2	17	3.6	0.1
4	2.3	0.3	11	3.0	0.2	18	3.7	0.1
5	2.4	0.3	12	3.1	0.2	19	3.8	0.1
6	2.5	0.3	13	3.2	0.1			
7	2.6	0.2	14	3.3	0.1			

Table 4-2: Path and link sequences

O-D pair	Path number	Link sequence
(1, 3)	1	1-6-13-19
	2	2-17-8-14-16
	3	2-17-7-10-16
	4	1-6-12-14-16
	5	1-5-7-10-16
	6	1-5-8-14-16

with the specific distribution parameters for each link shown in Table 4-1, where CV represents coefficient of variation. In this stochastic traffic assignment, $(1, 3)$ is used as the O-D pair, with a total demand of 40. The link and path sequences in the network are provided in Table 4-2. The traffic assignment method follows the classical User Equilibrium (UE) principle (WARDROP, 1952), and the corresponding assignment algorithm is the Method of Successive Averages (MSA) (Sheffi, 1984). In the BPR function, parameter β is set to 0.15, and parameter λ is set to 5.5. After the network reaches equilibrium, the path flows and average travel times are shown in Table 4-3.

Since the fractional moments of a lognormal distribution have an exact analytical solution, the results obtained using the analytical method are also included for comparison. Results of analytical method represent the fully accurate traffic assignment and are used to compare with the outcomes of the FFMT method and the Taylor expansion method. A comparison of the network assignment results shows that, after reaching equilibrium with the three different methods, the path flows obtained using the FFMT method are very close to those from the analytical method. The errors between the two are well within acceptable limits for practical applications of traffic assignment, indicating that the FFMT method ensures accuracy while controlling computational costs. However, when comparing the results from the Taylor expansion method, it is evident that there is a significant deviation from the analytical solution. Such a level of error is unacceptable in real-world applications. This demonstrates that the Taylor expansion method, when limited by the number of integer-order moments, leads to inaccurate results, and increasing the number of moments would require excessive computational resources. In contrast, the FFMT method manages to maintain accuracy while controlling computational costs, further highlighting its advantages in practical applications.

Table 4-3: Path flow and travel time values for the stochastic traffic assignment model at equilibrium using the Taylor expansion method, the analytical method, and the proposed method.

Path	Analytical Method		Proposed Method		Taylor Expansion Method	
	Flow	Time	Flow	Time	Flow	Time
1	27.72	15.01219	27.76	15.00779	29.72	15.00021
2	6.42	15.01089	6.38	15.01087	5.34	15.00259
3	5.86	15.01089	5.86	15.01087	4.94	15.00259
4	0	17.82058	0	17.81618	0	17.76587
5	0	17.81223	0	17.80790	0	17.76126
6	0	17.81223	0	17.80789	0	17.76126

4.6 Chapter Summary

This chapter focused on the second core research direction of the dissertation—mathematical characterization and numerical estimation of travel-time distributions under uncertainty in transportation networks. The objective was to develop a unified and stable approach for computing arbitrary-order fractional moments using limited integer-moment information, thereby providing a theoretical and computational foundation for modeling the stochastic characteristics of travel times in complex networks.

First, based on the Laplace transform and fractional calculus theory, a unified analytical framework for fractional-moment computation was established. By introducing the concepts of fractional differentiation and integration, this framework derived an analytical relationship between the fractional moments of a random variable and its probability density function, forming the theoretical basis of the Fractional-Folding Moment Transform (FFMT). The framework reveals that the fractional-order moments of travel-time variables can be directly obtained through fractional differentiation of their Laplace transforms, thus achieving a theoretical bridge between the probability density representation and its statistical moments.

Second, on the numerical side, the analytical formulation was transformed into a computationally feasible discrete expression using the Grünwald–Letnikov approximation. The associated error bounds were derived, ensuring both convergence and numerical stability for all positive random variables. Through a detailed analysis of the step parameter

h and truncation order N, the existence and uniqueness of the optimal step size were demonstrated, guaranteeing stable numerical performance across various computational settings.

In the application stage, the FFMT method was validated using real-world traffic data. The results confirm that the proposed method can stably estimate fractional moments under limited sample conditions and accurately capture non-Gaussian and heavy-tailed characteristics of empirical travel-time distributions. Compared with traditional integer-moment approaches, the FFMT exhibits higher robustness and precision when the underlying distribution is unknown or data availability is constrained, providing a reliable numerical foundation for uncertainty representation in transportation systems.

Overall, this chapter bridges the methodological transition from behavioral-level uncertainty to statistical-level stochastic representation. The behavioral heterogeneity and disturbance responses analyzed in Chapter 3 serve as the source of uncertainty, while the FFMT method developed in this chapter provides a mathematical tool to quantify and represent such uncertainty. The study establishes the mathematical basis for stochastic propagation and enables a systematic mapping from behavioral variability to statistical characterization, thereby supplying essential stochastic inputs for subsequent reliability-based optimization.

In summary, this chapter completes the methodological middle layer of uncertainty-aware transportation modeling and lays the theoretical and data-driven foundation for the next chapter. Chapter 5 will further extend this research by exploring reliability-oriented path optimization under link correlation, utilizing the travel-time distributions and covariance structures derived through the FFMT framework to achieve optimal and reliable decision-making in uncertain network environments.

Chapter 5

Reliable Shortest Path Optimization Model Under Relevant Risks

5.1 Overview and Research Objectives

In complex and uncertain transportation networks, path optimization remains one of the core issues in system analysis and management. Conventional shortest-path models typically assume statistical independence among link travel times and aim to minimize expected travel time. However, in real-world networks, travel times on adjacent links often exhibit significant correlations arising from spatial proximity, shared environmental disturbances such as rainfall, flooding, or incidents, and synchronized fluctuations in traffic flow. When such correlations exist, the total travel time along a path becomes a joint random variable with interdependent components rather than a simple additive sum. Neglecting these dependencies can lead to systematic underestimation of path unreliability and consequently to optimization results that deviate from actual network performance.

Under uncertain conditions, travelers and network planners are concerned not only with minimizing expected travel time but also with maintaining travel-time stability and predictability, collectively referred to as reliability. Reliable-path problems have therefore emerged as a major research theme in transportation reliability analysis, focusing on the trade-off between efficiency and stability in travel decisions. Among various formulations, two representative reliability measures are the Mean–Variance (M–V) and Mean–Standard-Deviation (M–S) models, which incorporate variance and standard deviation, respectively, to represent the degree of uncertainty associated with path travel times. Despite their widespread use, most existing studies still rely on the assumption of independent link travel times and rarely capture the joint risk effects introduced by link correlations, limiting the applicability of these models to real, complex networks.

To address these limitations, this chapter investigates the reliable shortest-path optimization problem under correlated link conditions, establishing a unified modeling framework that simultaneously accounts for expected travel time, reliability risk, and link correlation structures. By introducing a travel-time covariance matrix, the proposed framework explicitly incorporates joint risk propagation effects arising from spatial dependencies or common disturbances. Based on this formulation, two complementary models are developed: the Mean–Variance (M–V) model and the Mean–Standard-Deviation (M–S) model, each providing a distinct yet consistent representation of reliability-oriented path optimization. Corresponding solution algorithms are designed to analyze how optimal paths and reliability indicators evolve under varying risk preferences and correlation strengths.

Within the overall structure of the dissertation, this chapter constitutes the system-decision layer of the research framework. Chapter 3 revealed how risk perception and external disturbances generate behavioral heterogeneity and stochastic flow distributions at the network level. Chapter 4 provided a fractional-moment-based approach for estimating travel-time distributions, enabling stable numerical representation of stochastic characteristics. Building upon these foundations, the present chapter integrates uncertainty representation into the decision-making process, completing the methodological progression from risk perception to stochastic characterization and ultimately to reliability-oriented optimization. Through the formulation and analysis of reliable shortest-path models under correlated link conditions, this chapter provides both theoretical and computational foundations for reliable route planning in uncertain transportation networks and serves as a bridge to the integrative discussion presented in Chapter 6.

5.2 Theoretical Framework and Model Formulation

5.2.1 Notation and assumptions

The following notations are used in this chapter.

A: set of links in the network.

$|A|$: number of links in A.

N: set of nodes in the network.

$|N|$: number of nodes in N.

o: origin node.

d: destination node.

T_j: stochastic travel time of path j.

μ_a: mean of the stochastic travel time of link a.

σ_a: standard deviation of the stochastic travel time of link a.

ρ_{ab}: coefficient of correlation between travel times of links a and b.

L_n^{in}: set of links whose head (destination) node is n.

L_n^{out}: set of links whose tail (origin) node is n.

$\omega_{\text{a\^{}b}}$: flow which passes through both links a and b in the network ($\omega_{\text{a\^{}b}} = \omega_{\text{b\^{}a}}$) if $a \neq b$ (or flow of hyperlink a^b in the hypergraph).

$\omega_{\text{a\^{}a}}$: flow of link a (or flow of hyperlink a^a in the hypergraph).

The following assumptions are employed in this study. Only one link is directed from an origin node. In a similar way, only one link is directed to a destination node in a network. These two assumptions are always true if we add two nodes and two links, i.e., the origin and destination nodes and the corresponding two links, to a network to be analyzed.

5.2.2 Shortest path problem

The shortest path search problem in an uncorrelated network formulated based on linear programming is:

$$\min \sum_{a \in A} \mu_a x_a \tag{5-1}$$

s.t.

$$\sum_{a \in L_n^{in}} x_a - \sum_{b \in L_n^{out}} x_b = \begin{cases} -1, & \text{if } n = o, \\ 1, & \text{if } n = d, \\ 0, & \text{otherwise,} \end{cases} \qquad \forall n \in N \tag{5-2}$$

$$x_a \geq 0 \quad \forall a \in A$$

The constraints of (5-2) for an example network shown in Figure1 are expressed by using a coefficient matrix **A** and two row vectors, **x** and **b**, as follows

$$Ax^T = b^T \tag{5-3}$$

where

$$\mathbf{A} = \begin{pmatrix} -1 & 0 & 0 & 0 \\ 1 & -1 & -1 & 0 \\ 0 & 1 & 1 & -1 \\ 0 & 0 & 0 & 1 \end{pmatrix}$$

$$\mathbf{x} = \begin{pmatrix} x_1 & \dots & x_4 \end{pmatrix}$$

$$\mathbf{b} = \begin{pmatrix} -1 & 0 \\ 0 & 1 \end{pmatrix}$$

The objective function is linear, and **b** is a vector with integer entries. The node-link incidence matrix of the directed network, **A**, is known as a totally unimodular matrix. Additionally, since the objective function is linear, this means that the shortest path problem without considering link covariance is essentially a linear programming problem without binary integer constraints, for which there are numerous well-established solution methods. However, when the covariance between links is considered, both the m-v and m-s problems become highly complex nonlinear binary integer programming problems, which will be discussed later.

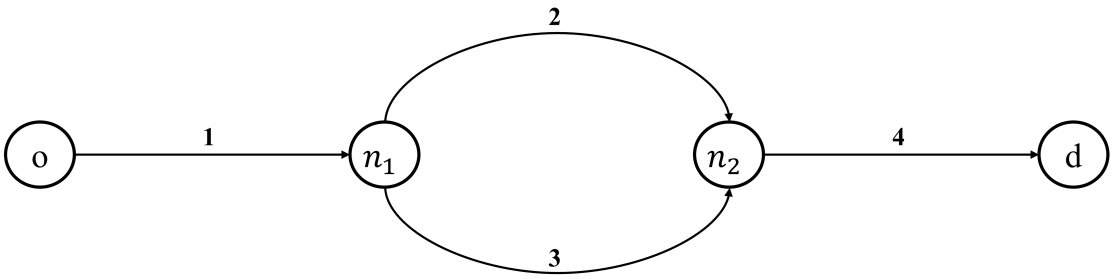


Figure 5-1: An example network

5.3 Mean-Variance (M-V) Reliable Path Problem

The m-v shortest path problem in a correlated network can be formulated as the following Nonlinear binary integer programming (NL-BIP):

$$\min\ g_1 = \sum_{a\in A} \mu_a x_a + \gamma_1 \cdot \sum_{a\in A}\sum_{b\in A} \psi_{ab} x_a x_b \tag{5-4}$$

s.t.

$$\sum_{a\in L_n^{in}} x_a - \sum_{b\in L_n^{out}} x_b = \begin{cases} -1, & \text{if } n = o, \\ 1, & \text{if } n = d, \\ 0, & \text{otherwise,} \end{cases} \qquad \forall n \in N \tag{5-5}$$

$$x_a = \{0, 1\} \quad \forall a \in A \tag{5-6}$$

where

$$\psi_{ab} = \rho_{ab}\,\sigma_a\sigma_b, \qquad \psi_{aa} = \sigma_a^2$$

γ_1 in (5-4) represents the value of path travel time reliability (measured by variance) relative to the expected travel time. x_a is a binary decision variable that equals one if link a is part of the m-v shortest path, and zero otherwise. The NL-BIP problem presents a dual complexity of nonlinearity and integer constraints, which not only results in the lack of convexity and the presence of multiple local optima but also increases combinatorial complexity due to the binary integer constraints. This causes the solution space to grow exponentially with the number of variables, requiring the evaluation of a large number of potential solutions, leading to significant computational overhead. Additionally, the NL-BIP problem is typically classified as NP-hard, meaning that there is currently no known polynomial-time algorithm capable of finding the optimal solution within a reasonable timeframe. Therefore, solving the m-v problem is generally highly complex and requires substantial computational resources, particularly in the practical application of large-scale road networks.

A continuous relaxation problem of the NL-BIP for example network in which integer constraint of (5-5) is relaxed to $x_a \in [0, 1]$ was then solved by assuming $\gamma_1 = 1$, $\mu_a = 0$ ($a = 1, \ldots, 4$) and the variance and covariance matrix of link travel times below:

$$\Sigma = \begin{pmatrix} 5 & 3 & 5 & 4 \\ & 7 & 0 & 3 \\ & & 10 & 4 \\ & & & 4 \end{pmatrix}$$

The solution is $x_2 = 0.765$, $x_3 = 0.235$, $x_1 = x_4 = 1$, at which g_1 is calculated as 35.06. This solution is an interior solution of the quadratic objective function (4) and is not a feasible solution for the NL-BIP. Figure 5-2 shows the relationship between x_2 and g_1. This nonlinear relationship shown in the figure makes the NL-BIP for a large network

difficult to solve. The optimum solution of the NL-BIP is $x_1 = x_2 = x_4 = 1, x_3 = 0$, at which g_1 is calculated as 36.

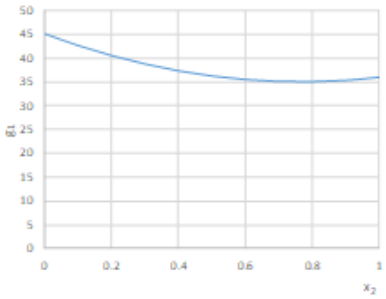


Figure 5-2: Relationship between x_2 and g_1

5.3.1 The m-v shortest path problem expressed in a hypergraph

(1) Graph-Driven Variable Substitution

One of the challenges of the m-v problem in a correlated network lies in the nonlinearity of its objective function, which arises from the quadratic terms of decision variables introduced by considering the covariance between correlated links. In this study, a graph-driven variable substitution method is employed to reformulate the objective function. By ensuring flow conservation—i.e., preserving the properties of the constraint conditions—this approach transforms the original objective function into a linear form through variable substitution. Consequently, the m-v shortest path problem is converted into the following form:

$$\min\ g_2 = \sum_{a \in A} \mu_a \cdot \omega_{a\hat{}a} + \gamma_1 \cdot \sum_{a \in A} \sum_{b \in A} \psi_{ab} \cdot \omega_{a\hat{}b} \tag{5-7}$$

s.t.

$$\begin{aligned} &\sum_{b \in L_n^{in}} \omega_{b\hat{}b} - \sum_{c \in L_n^{out}} \omega_{c\hat{}c} = -1, \quad \text{if } n = o, \\ &\sum_{b \in L_n^{in}} \omega_{b\hat{}b} - \sum_{c \in L_n^{out}} \omega_{c\hat{}c} = 1, \quad \text{if } n = d, \\ &\sum_{b \in L_n^{in}} \omega_{a\hat{}b} - \sum_{c \in L_n^{out}} \omega_{a\hat{}c} = 0, \quad \forall a \in A, \text{ otherwise} \end{aligned} \tag{5-8}$$

$$\omega_{a\hat{}b} = 0 \quad \text{if } \{a, b\} \subseteq L_n^{out}, \qquad \forall n \in N \tag{5-9a}$$

$$\omega_{a\hat{}b} = 0 \quad \text{if } \{a, b\} \subseteq L_n^{in}, \qquad \forall n \in N \tag{5-9b}$$

$$\omega_{a\hat{}b} = \omega_{b\hat{}a} \qquad \forall\, a, b(\neq a) \in A \tag{5-10}$$

$$\omega_{a\hat{}b} \in \{0, 1\} \qquad \forall\, a, b \in A \tag{5-11}$$

The m-v shortest path problem in this study can be addressed by assigning the origin-destination (o-d) demand of one to the shortest path between the o-d pair in the network. The linear function (5-7) represents the total m-v travel time cost to be minimized. The o-d demand assigned to a path or a link can be interpreted as path choice probability or link choice probability, respectively. The total m-v travel time cost is computed using the given mean link travel times and variance and covariance of link travel times in the network.

On (5-8), the first and second equality constraints indicated that the o-d demand flows out from the origin node o

via links in the set L_o^{out} and flows into the destination node d via links in the set L_d^{out}. The third equality constraint is introduced for the calculation of travel time covariance. It specifies that the sum of link flows passing through link $a \in A$ and flowing into node n via links in the set L_n^{in} must flow out from the node via links in the set L_n^{out}, c.f., (5-14) in (Uchida*, 2015). Accompanied with two boundary conditions which are the first and second equality constraints of (8), the third equality constraint enables to calculate the flow that passes through two different links a and b, $\omega_{a\hat{}b}$ for all $a, b(\neq a) \in A$, without enumerating paths from the origin node to the destination node. Such flow costs $\gamma_1 \cdot \psi_{ab} \cdot \omega_{a\hat{}b}$ in the objective function. On the other hand, the flow on link a, $\omega_{a\hat{}a}$ for all $a \in A$, costs $(\mu_a + \gamma_1 \cdot \psi_{aa}) \cdot \omega_{a\hat{}a}$ in the objective function. The number of equality constraints in (5-8) is $2 + |A| \cdot (|N| - 2)$. The number of equality constraints from the third constraint in (5-8) can be large if a network is large. However, in such networks, for most links in A that seem not to be used by the virtual o-d demand, both sides of the equality condition become zero. Therefore, depending on the predefined virtual o-d demand, one can reduce network size to reduce the number of equality constraints denoted by the third constraint in (5-8).

(5-9) shows that no flow passes through different two links in the set of L_n^{in} or L_n^{out} which is defined at node $n \in N$. The number of equality constraints by (5-9) is determined depending on the network topology addressed. (5-10) represents that the symmetric elements have the same value. From (5-10), if (5-9) is not considered, the number of unknown variables of this problem is $\sum_{k=1}^{|A|} k = \frac{1}{2}|A|(|A|+1)$ where $|A|$ is the number of links in the network.

(2) Structure-Preserving Linearization

After the variable substitution, the objective function of the m-v shortest path problem is transformed from a non-linear to a linear form. However, the problem still contains binary integer constraints, making it a linear binary integer programming (L-BIP) problem, which remains NP-hard. Therefore, a structure-preserving linearization approach is employed, utilizing hypergraphs to further reformulate the m-v problem. This transformation ensures that the original traffic network flow structure remains unchanged while simplifying the problem into a linear programming (LP) formulation.

Each hyperlink in the hypergraph considered in this study includes at most three nodes, categorized as tail node(s) and head node(s). The constraints shown by (5-8) and (5-9) for the example network in Figure 5-1 shown as:

$$H_p\,\omega^T = h_p^T \tag{5-12}$$

where

$$H_p = \begin{pmatrix} H_1 & \cdots & 0 \\ \vdots & \ddots & \vdots \\ 0 & \cdots & H_4 \end{pmatrix}$$

$$H_1 = \begin{pmatrix} -1 & 0 & 0 & 0 \\ 1 & -1 & -1 & 0 \\ 0 & 1 & 1 & -1 \end{pmatrix}$$

$$H_a = \begin{pmatrix} 1 & -1 & 0 \\ 0 & 1 & -1 \end{pmatrix} \qquad \forall a \in \{2,3\}$$

$$H_4 = \begin{pmatrix} 1 & -1 & -1 & 0 \\ 0 & 1 & 1 & -1 \\ 0 & 0 & 0 & 1 \end{pmatrix}$$

$$\omega = \begin{pmatrix} \omega_1 & \cdots & \omega_4 \end{pmatrix}$$

$$\omega_a = \begin{pmatrix} \omega_{a\hat{}1} & \cdots & \omega_{a\hat{}4} \end{pmatrix} \qquad \forall a \in \{1,4\}$$

$$\omega_2 = \begin{pmatrix} \omega_{2\hat{}1} & \omega_{2\hat{}2} & \omega_{2\hat{}4} \end{pmatrix}$$

$$\omega_3 = \begin{pmatrix} \omega_{3\hat{}1} & \omega_{3\hat{}3} & \omega_{3\hat{}4} \end{pmatrix}$$

$$h_p = \begin{pmatrix} h_1 & \cdots & h_4 \end{pmatrix}$$

$$h_1 = \begin{pmatrix} -1 & 0 & 0 \end{pmatrix}$$

$$h_a = \begin{pmatrix} 0 & 0 \end{pmatrix} \qquad \forall a \in \{2, 3\}$$

$$h_4 = \begin{pmatrix} 0 & 0 & 1 \end{pmatrix}$$

H_p is the node-hyperlink incidence matrix of the hypergraph shown in Figure 5-3. The coefficient matrix H_p for the network depicted in Figure 5-1 is summarized in Table 5-1. The hypergraph in Figure 5-3 is composed of four sub-hypergraphs, each of which is disconnected from the others. In this study, the sub-hypergraph at the top of the figure is referred to as link1-specific hypergraph, while the one at the bottom is referred to as link4-specific hypergraph. The second and third sub-hypergraphs are referred to as link2-specific and link3-specific hypergraphs, respectively. H_p is a block diagonal matrix composed of H_1, H_2, H_3, and H_4, where H_a is the node-hyperlink incidence matrix of the link$a$-specific hypergraph ($a \in A$). The link$a$-specific hypergraph ($a \in \{2, 3\}$) consists of three hyperlinks, i.e., a^1, a^2 (or a^3) and a^4, and two nodes, i.e., a^n_1 and a^n_2. The link1-specific hypergraph or link4-specific hypergraph includes an additional node, o or d, respectively. The flow on hyperlink a^b ($b \in \{1, \ldots, 4\}$) is $\omega_{a\hat{}b}$, representing the flow passing through both links a and b in the network shown in Figure1. Since $\omega_{2\hat{}3} = \omega_{3\hat{}2} = 0$ from (5-9a) or (5-9b), there is no corresponding hyperlink in the link$a$-specific hypergraph ($a \in \{2, 3\}$) for these flows.

Table 5-1: Node-hyperlink incidence matrix of the hypergraph

	1^1	1^2	1^3	1^4	2^1	2^2	2^4	3^1	3^3	3^4	4^1	4^2	4^3	4^4
o	-1													
1_ n_1	1	-1	-1											
1_ n_2		1	1	-1										
2_ n_1					1	-1								
2_ n_2						1	-1							
3_ n_1								1	-1					
3_ n_2									1	-1				
4_ n_1											1	-1	-1	
4_ n_2												1	1	-1
d														1

For expressing the constraints shown by (5-10), we introduce the following matrix:

$$J = \begin{pmatrix} J_{12} \\ J_{13} \\ J_{14} \\ J_{24} \\ J_{34} \end{pmatrix}$$

where

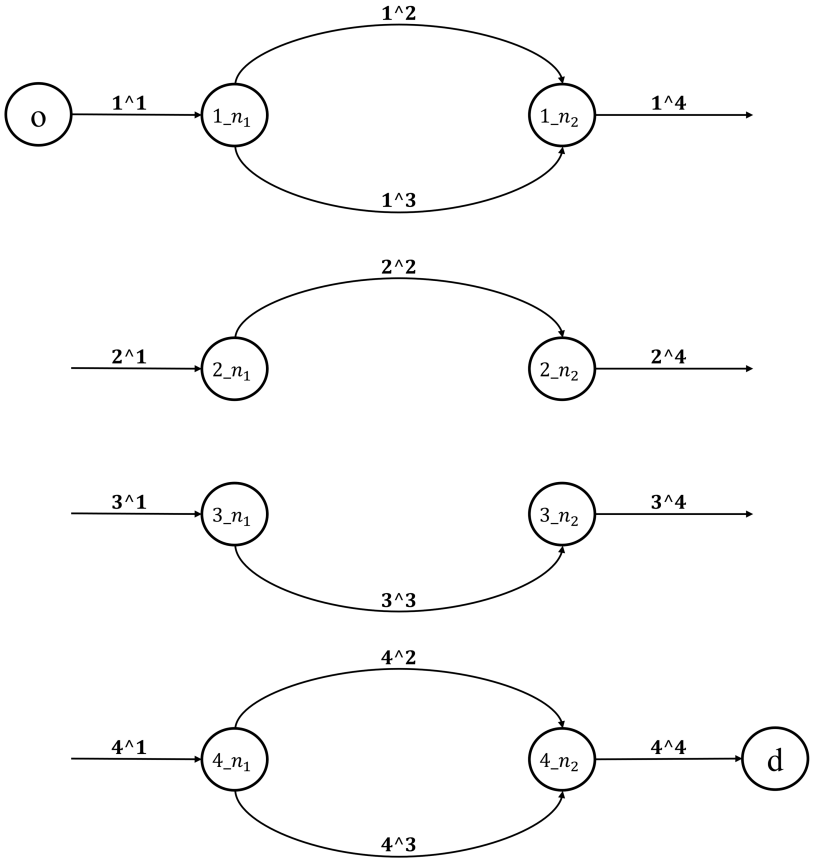


Figure 5-3: Hypergraph

$$J_{ab} = \begin{pmatrix} 0 & \underbrace{1}_{\text{a\^{}b}} & 0 & \underbrace{-1}_{\text{b\^{}a}} & 0 \end{pmatrix} \qquad \{a,b\} \subseteq A;\ \{a,b\} \nsubseteq L_n^{in},\ \{a,b\} \nsubseteq L_n^{out},\ \forall n \in N.$$

Note that, J_{23} is not shown in J since $\omega_{2\hat{}3} = \omega_{3\hat{}2} = 0$ from (5-9a) or (5-9b). Finally, the constraints shown by (5-8), (5-9) and (5-10) are denoted as:

$$H\,\omega^T = h^T \tag{5-13}$$

where

$$H = \begin{pmatrix} H_p \\ J \end{pmatrix}$$

$$h = \begin{pmatrix} h_p & 0 \end{pmatrix}.$$

The coefficient matrix H for the network shown in Figure1 is summarized in Table 5-2. H can be regarded as the node-hyperlink incidence matrix of the directed hypergraph shown in Figure 5-4. We refer to this directed hypergraph as the augmented hypergraph. Each link-specific hypergraph is now connected to the others by the hyperlinks and nodes added by (5-10). Additionally, each link-specific hypergraph appears to have an origin node and a destination node. For example, the link1-specific hypergraph has the origin node o and the destination node C, while the link4-specific hypergraph has the origin node C and the destination node d. Each hyperlink in the augmented hypergraph has at most three nodes, which can be head node(s) and tail node(s). For example, hyperlink 1^2 has one tail node 1_ n_1 and two head nodes 1_ n_2 and A. A hyperlink in the augmented hypergraph is represented by each column of H or Table 5-2, where tail node(s) and head node(s) are denoted by -1 and 1, respectively.

We now suppose that each hyperlink flow in the augmented hypergraph is either zero or one. The augmented hypergraph and (5-13) show that the o-d flow of one is generated from the origin node o and flows into link1-specific

Table 5-2: The coefficient matrix of *H*

	1^1	1^2	1^3	1^4	2^1	2^2	2^4	3^1	3^3	3^4	4^1	4^2	4^3	4^4
o	-1													
1_ n_1	1	-1	-1											
1_ n_2		1	1	-1										
2_ n_1					1	-1								
2_ n_2						1	-1							
3_ n_1								1	-1					
3_ n_2									1	-1				
4_ n_1											1	-1	-1	
4_ n_2												1	1	-1
d														1
A		1			-1									
B			1					-1						
C				1							-1			
D							1					-1		
E										1			-1	

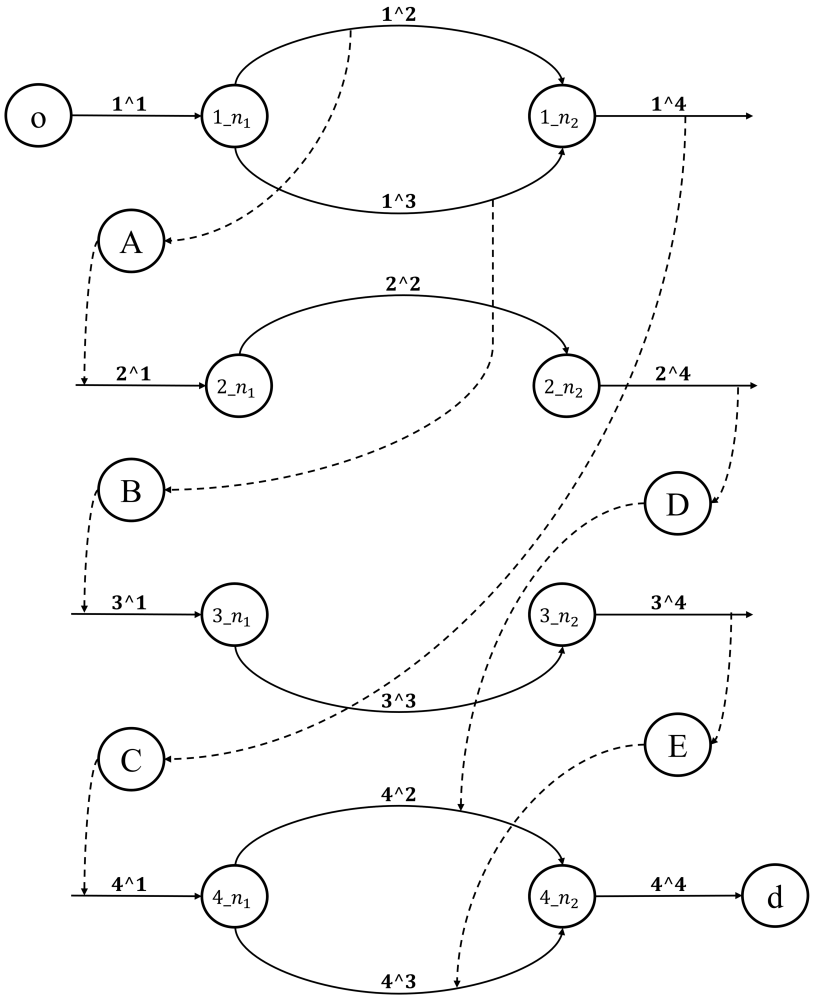


Figure 5-4: Augmented hypergraph

hypergraph via hyperlink 1^1. The o-d flow then reaches its destination node B. If each hyperlink 1^a ($a \in \{2, \ldots, 4\}$) in link1-specific hypergraph carries flow, such hyperlink flow $\omega_{1\hat{}a}$ becomes the o-d flow for link$a$-specific hypergraph via the hyperlinks added by (5-10). For example, if hyperlink 1^2 carries flow, the corresponding hyperlink flow $\omega_{1\hat{}2} = 1$ flows into both nodes 1_ n_2 and A. Thus, the hyperlink flow flowing into node A becomes the o-d flow for the link2-specific hypergraph, $\omega_{2\hat{}1}$, and reaches its destination node D. Since hyperlink 1^3 carries no flow, in this case, all hyperlink flows in link3-specific hypergraph carry no flow, i.e., $\omega_{3\hat{}a} = 0$ for all $a \in \{1, 3, 4\}$. All hyperlink flows in link4-specific hypergraph are determined by the hyperlink flows $\omega_{a\hat{}4}$ for all $a \in \{1, 2, 3\}$ that are calculated in link$a$-specific hypergraph. For example, if hyperlink 2^4 in link2-specific hypergraph carries the flow, i.e., $\omega_{2\hat{}4} = 1$, such flow becomes the hyperlink flow $\omega_{4\hat{}2}$ in link4-specific hypergraph. As mentioned earlier, when the o-d demand of zero is assigned to the link$a$-specific hypergraph for all $a \in \{2, 3, 4\}$, every hyperlink flow in link$a$-specific hypergraph is zero, i.e., $\omega_{a\hat{}b} = 0$ for all $b \in \{1, \ldots, 4\}$, and that becomes the hyperlink flows in the other link-specific hypergraphs, i.e., $\omega_{b\hat{}a} = 0$ for all $b \in \{1, \ldots, 4\}$.

5.3.2 Optimality of the integer relaxation

For an L-BIP problem, if the constraint matrix is totally unimodular and the right-hand side vector consists of integers, the problem possesses integrality property. In this case, the binary integer constraints can be omitted, and the solution remains an integer optimal solution. Regarding the transformed mathematical formulation of the m-v shortest path problem using hypergraphs in this study, integer feasibility is ensured. This is because the objective function in Equation (5-7) is linear, and for the constraint Equation (5-13), the right-hand side vector h consists entirely of integers, while the constraint matrix H is totally unimodular. This study adopts a graph transformation approach embedded in matrix representation to prove the total unimodularity of the constraint matrix H, i.e., the coefficient matrix.

The network example from Figure1 is still used as a carrier to demonstrate that the coefficient matrix H is totally unimodular. Based on this network example, the augmented hypergraph shown in Figure4 can be constructed, and the matrix H serves as node-link incidence matrix for this augmented hypergraph. This augmented hypergraph is a directed network, where the links possess directional properties. To prove that matrix H is totally unimodular, the augmented hypergraph is transformed into an undirected network representation without altering connection characteristics of the original augmented hypergraph.

Two sets, U and V, are defined, each consisting of nodes. All nodes in the original augmented hypergraph are duplicated into two copies, denoted by subscripts u and v, and are assigned to the corresponding sets U and V, as shown by

$$U = \{\, o_u,\ 1_\ n_{1u},\ \ldots,\ 4_\ n_{2u},\ E_u,\ d_u \,\}$$

and

$$V = \{\, o_v,\ 1_\ n_{1v},\ \ldots,\ 4_\ n_{2v},\ E_v,\ d_v \,\}.$$

The nodes in set U represent inputs, while the nodes in set V represent outputs. In this way, the directed augmented hypergraph can be represented by a new undirected graph, as illustrated in Figure 5-5.

Due to the presence of loops in the original augmented hypergraph, two distinct hyperlinks, such as hyperlinks 1^3 and 1^2, simultaneously connect nodes 1_ n_{1v} and 1_ n_{2u}. A similar situation occurs between nodes 4_ n_{1v} and 4_ n_{2u}, where hyperlinks 4^3 and 4^2 simultaneously connect these two nodes. Then further modifications are applied to the undirected graph in Figure 5-5, the hyperlinks that caused repeating connections are removed from the graph. As an example, all instances of hyperlinks 1^3 and 4^3 are eliminated. Consequently, a bipartite graph is derived, as illustrated in Figure 5-6.

Let the node-hyperlink incidence matrix of the undirected graph in Figure 5-5 be denoted as $Q_{(p\times q)}$, where p represents the number of nodes and q represents the number of hyperlinks. Here, the use of p and q is for the convenience of presenting the proof of total unimodularity. For all bipartite graphs, the node-link incidence matrix is totally unimodular. Figure 6 illustrates a typical bipartite graph, with its node-hyperlink incidence matrix denoted as $R_{(p\times(q-2))}$. The matrix

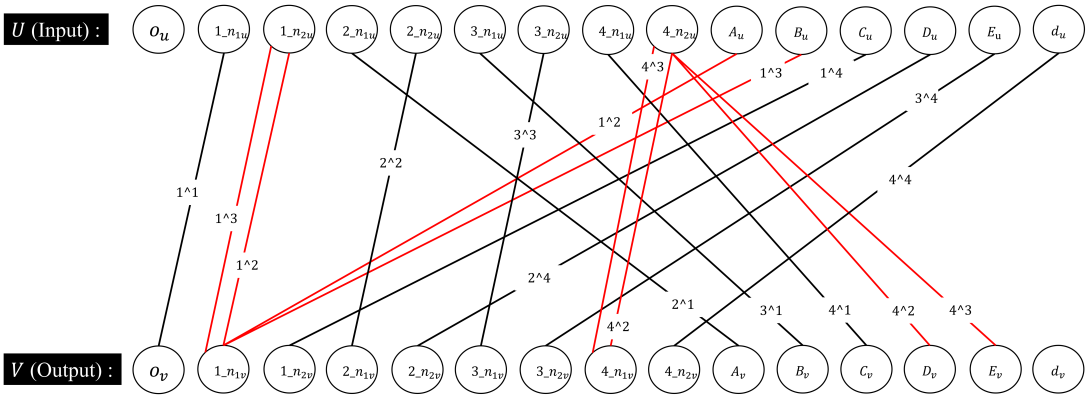


Figure 5-5: Undirected graph transformed from the augmented hypergraph

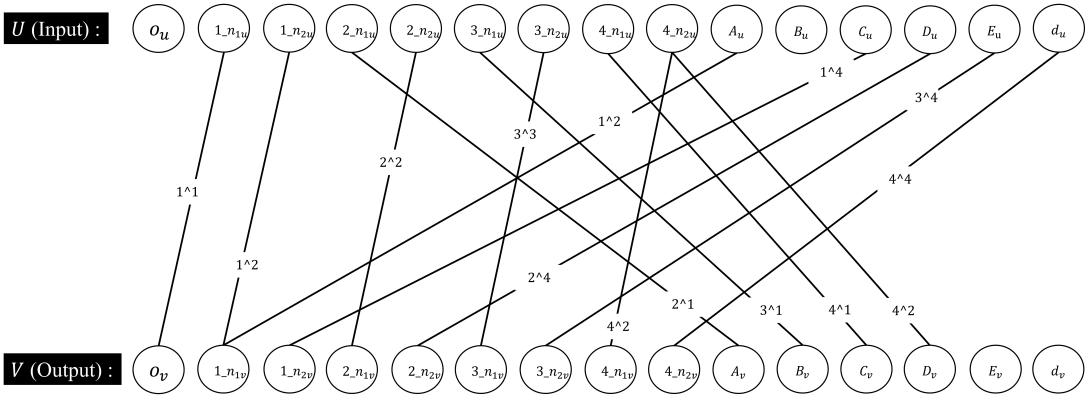


Figure 5-6: The bipartite graph derived from the Undirected graph

R is guaranteed to be totally unimodular. The matrix R is a strict submatrix of Q, with the sole difference being the node-hyperlink incidence matrix of the removed hyperlinks, represented as Z, specifically the node-hyperlink incidence matrix $Z_{(p\times 2)}$ for hyperlinks 1^3 and 4^3. The essence of matrix Z lies in its role as a node-hyperlink incidence matrix. Each hyperlink in Figure 5-5 necessarily connects only two nodes and there are no hyperlinks between nodes within the same set U or set V, therefore each column of matrix Z consists solely of 0 or 1. Let E be an elementary matrix used to represent elementary transformations. Given the identity matrix I_p, after applying an elementary column transformation, the resulting matrix can always be ensured to contain a submatrix equal to matrix Z. Then matrix $Z_{(p\times 2)}$ holds the relationship:

$$Z_{(p\times 2)} \subset (I_p \cdot E)$$

A totally unimodular matrix possesses three properties: (1) a totally unimodular matrix remains totally unimodular after being combined with an identity matrix, (2) a totally unimodular matrix remains totally unimodular after undergoing elementary transformations, and (3) any submatrix of a totally unimodular matrix is itself a totally unimodular matrix. Based on these properties of totally unimodular matrix, the matrix Q can be derived as a totally unimodular matrix through the following relationship (TU means the totally unimodular matrix):

$$Q_{(p\times q)} = [R, Z]_{(p\times q)} \subset [R, (I_p \cdot E)]_{(p\times(p+q-2))}$$

$$R \in \mathrm{TU} \Rightarrow [R, I_p] \in \mathrm{TU} \Rightarrow [R, (I_p \cdot E)] \in \mathrm{TU} \Rightarrow [R, Z] \in \mathrm{TU} \Rightarrow Q \in \mathrm{TU}$$

After proving that the matrix Q is totally unimodular, it can further be demonstrated that the coefficient matrix H is also totally unimodular. The matrix Q represents the node-hyperlink incidence matrix for the undirected graph shown in Figure 5-5, while H represents the node-hyperlink incidence matrix for the augmented hypergraph depicted

in Figure 4. By duplicating the nodes in the directed augmented hypergraph, designating them as inputs and outputs, an undirected graph can be obtained. The connection relationships between nodes and links in the traffic network, as expressed by these two graphs, remain consistent. Therefore, the undirected graph can be reconverted into the original augmented hypergraph through a reverse operation. This involves considering the hyperlink directions represented by the input and output nodes and overlapping them to reconstruct the directed augmented hypergraph from the undirected graph. Given that in this paper, the head node of a hyperlink in the augmented hypergraph is assigned a value of +1 and the tail node a value of −1, the matrix transformation process corresponding to the conversion from the undirected graph to the augmented hypergraph is illustrated in Figure 5-7. Then the following relationship can be derived to prove that the coefficient matrix H is totally unimodular:

$$H_{((p/2)\times q)} \subset E \cdot Q_{(p\times q)}$$

$$Q \in \mathrm{TU} \;\Rightarrow\; (E \cdot Q_{(p\times q)}) \in \mathrm{TU} \;\Rightarrow\; H \in \mathrm{TU}$$

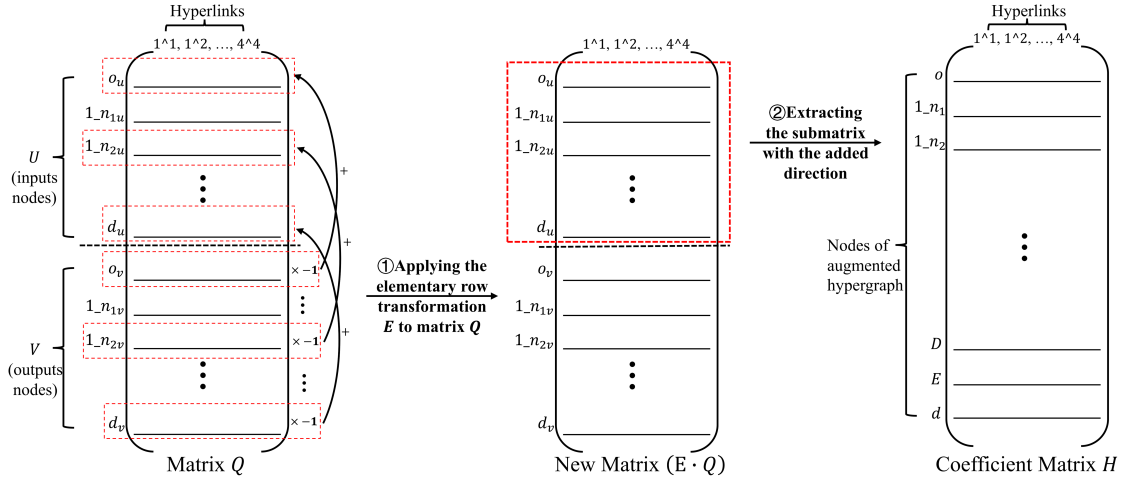


Figure 5-7: Matrix operations correspond to the reverse conversion of the undirected graph into the augmented hypergraph

After proving that the coefficient matrix H is totally unimodular, the m-v shortest path problem under the hypergraph representation possesses the integrality property. Consequently, the binary integer constraints can be entirely omitted, transforming the original NL-BIP formulation of the m-v shortest path problem into an LP problem. This reformulation enables the application of numerous well-established and efficient solution methods to rapidly obtain the global optimal solution. The LP-formulated m-v shortest path problem is presented as follows:

$$\min\; g_2 = \sum_{a\in A} \mu_a \cdot \omega_{\hat{}\mathrm{a}} \;+\; \gamma_1 \cdot \sum_{a\in A}\sum_{b\in A} \psi_{ab} \cdot \omega_{\hat{}\mathrm{b}}$$

s.t. (5-13)

5.4 Mean-Standard-Deviation (M-S) Reliable Path Problem

The m-s shortest path problem in a correlated network can be formulated as the following NL-BIP problem:

$$\min\; g_3 = \sum_{a\in A} \mu_a x_a \;+\; \gamma_2 \cdot \sqrt{\sum_{a\in A}\sum_{b\in A} \psi_{ab} x_a x_b} \qquad (5-14)$$

s.t. (5-5)–(5-6)

γ_2 in (5-14) represents the value of path travel time reliability (measured by standard deviation) relative to the expected travel time. Similarly, by adopting the hypergraph-based formulation of the m-v shortest path problem, the

m-s shortest path problem is transformed accordingly. The resulting optimization problem remains an NL-BIP, which is formulated as follows:

$$\min\ g_4 = \sum_{a\in A} \mu_a \cdot \omega_{\hat{a}a} \ +\ \gamma_2 \cdot \sqrt{\sum_{a\in A}\sum_{b\in A} \psi_{ab} \cdot \omega_{\hat{a}b}} \tag{5-15}$$

s.t. (5-11), (5-13)

The constraint (5-11) represents the binary integer constraints, while constraint (5-13) corresponds to the flow conservation constraints given by equations (5-8) – (5-10). Although the objective function (5-15) is nonlinear, the constraint matrix H in (5-13) remains totally unimodular. Therefore, if the objective function retains linear characteristics, the optimization problem possesses the integrality property. Consequently, the binary integer constraints (5-11) can be ignored, and the original NL-BIP m-s shortest path problem can be transformed into an LP problem for solving. Drawing on the branch-and-bound method proposed by (Horst and Thoai, 1992) and (Frank, 1969b), along with the global optimization algorithm framework suggested by (Soland, 1974), this study employs convex relaxation techniques to transform the objective function into a linear form. The branch-and-bound method is then utilized to iteratively approximate the global optimal solution, ultimately determining the shortest path.

To ensure the validity of the convex relaxation and the fast iteration in the branch-and-bound process, the mathematical formulation of the m-s shortest path problem is further restructured, as shown below:

$$\min\ g_4 = \sum_{a\in A} \mu_a \cdot \omega_{\hat{a}a} + f(\eta) \tag{5-16}$$

s.t. (5-11), (5-13)
where

$$f(\eta) = \gamma_2 \cdot \sqrt{\eta}$$

$$\eta = \sum_{a\in A}\sum_{b\in A} \psi_{ab} \cdot \omega_{\hat{a}b}$$

During the branch-and-bound process, the range of the decision variable η is iteratively optimized until the optimal value of η is obtained. Therefore, an initial interval of η, where its optimal value is located, denoted as M in (5-16), is first established by determining both a lower bound l and an upper bound u as follows:

$$M:\ [l,\ u] \tag{5-17}$$

It is worth noting that the decision variable η is determined by $\omega_{\hat{a}b}$, and a good initial M is crucial for quickly obtaining the global optimal solution through branch-and-bound. In this case, based on the binary nature of $\omega_{\hat{a}b}$, the initial lower bound l is set to 0, meaning that all $\omega_{\hat{a}b}$ take the value of 0, while the initial upper bound u corresponds to the value when all $\omega_{\hat{a}b}$ take the value of 1.

Additionally, to ensure that the relaxed problem maintains the integrality property during the iteration process, allowing it to be relaxed into an LP problem for efficient solving, the following relaxed problem formulation is provided:

$$\min\ \hat{g}_3 = \sum_{a\in A} \mu_a \cdot \omega_{\hat{a}a} + h(\eta) \tag{5-18}$$

s.t. (5-13)
where

$$h(\eta) = \frac{f(u) - f(l)}{u - l}\,\eta + \frac{f(l) - f(u)}{u - l} + f(l) \tag{5-19}$$

The relaxed optimization problem has effectively transformed into an LP problem, where the original binary integer

constraint (5-11) can now be ignored. At this stage, the global optimal solution can be obtained under the given constraints (5-13) and the interval constraint M. By continuously branching the interval M based on the obtained results, the global optimal solution of the relaxed problem will ultimately converge to the global optimal solution of the original problem while satisfying the binary integer constraints.

In each iteration, the interval M from the previous iteration is partitioned based on the current optimal value η^*, as follows:

$$M_1 : [\, l_1\ (= l),\ u_1\ (= \eta^*)\,]$$

$$M_2 : [\, l_2\ (= \eta^*),\ u_2\ (= u)\,]$$

A better interval is selected based on the optimal solutions obtained from both boundaries. For instance, if M_1 yields a better solution, then M_2 is discarded, and M_1 is used as the new search interval for the next iteration of the branch-and-bound process until convergence is achieved. The convergence criterion can be defined based on the change in the interval M or the variation in the optimal solution of the relaxed problem.

The original m-s shortest path problem is an NP-hard NL-BIP problem, making it highly complex to solve. In this chapter, through variable substitution, combined with convex relaxation and the branch-and-bound method, the optimization problem is transformed into an LP problem. In each iteration, only an LP problem needs to be solved, ensuring the practical solvability of the m-s shortest path problem in real-world road networks.

5.5 Numercial Experiments

To better demonstrate the effectiveness of the proposed method in addressing the two types of shortest path problems (m-v and m-s) in practical road networks, the widely used real traffic network known as the Sioux Falls network is employed. This transportation network comprises 24 nodes and 76 links, as illustrated in Figure 5-8. To ensure that the random travel times on the network links better reflect real-world conditions, the average travel time for each link is assumed to range from 10 to 30, with the corresponding variance set between 0.1 and 0.3 times the mean. The values for the mean, variance, and correlation coefficients of the random travel times are generated randomly within these specified ranges.

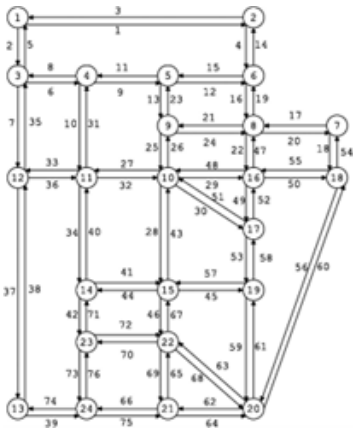
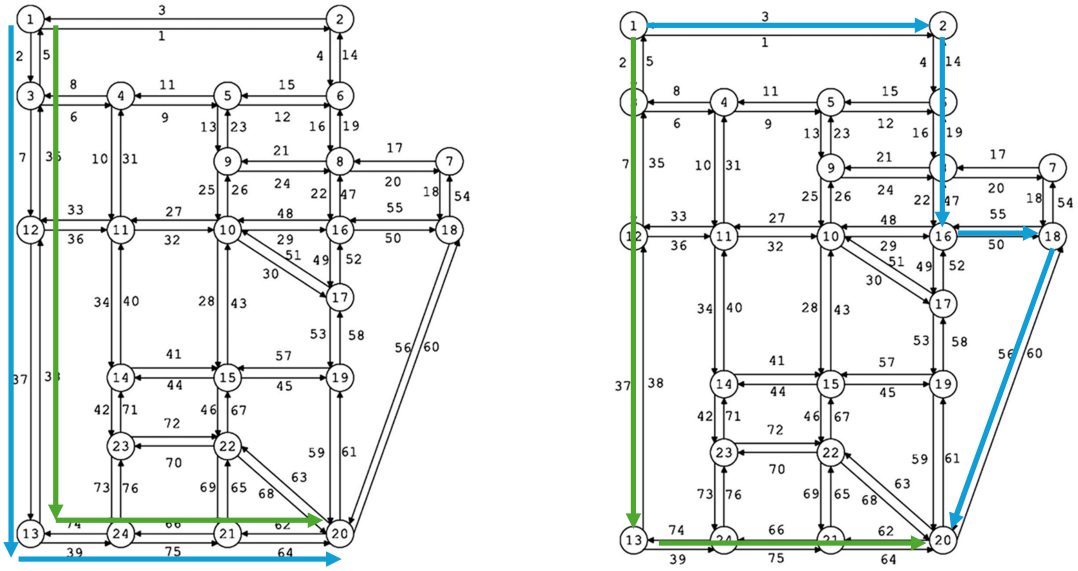


Figure 5-8: The Sioux-Falls Network

The origin-destination (OD) pair for both the m-v and m-s problems is set to $(1, 20)$, and the parameters γ_1 and γ_2 are both assigned a value of 6. It is assumed that the random travel times on the links follow a multivariate normal distribution. Assuming that loops are not permitted (i.e., a path does not revisit the same node), there exist $3,165$ paths between the OD pair $(1, 20)$. Based on the requirement for the shortest reliable path, and considering the correlation between links, the unique shortest path for each of the m-v and m-s problems will be identified from these $3,165$ paths.

According to the proposed method, the shortest paths for the m-v and m-s problems for the OD pair $(1, 20)$ are depicted in Figure 5-9(a). Specifically, the blue line represents the shortest path under the m-v problem, with the global optimal solution of the corresponding optimization problem g_2 being 609.7466; the green route represents the shortest path under the m-s problem, with the global optimal solution of the corresponding optimization problem g_3 being 149.6275. Clearly, under the current distribution of link travel times, the path composed of links 2, 7, 37, 39, 75, and 64 exhibits a significant advantage. Regardless of whether the problem is m-v or m-s, this path is the shortest reliable path.

In the currently used covariance matrix, the variance value of link 2 is 6.9964. When this variance value is amplified by a factor of 10 to 69.964, while all other parameters of the road network remain unchanged, the shortest path problems for both the m-v and m-s models are resolved again. The results of the shortest path problems are illustrated in Figure 5-9(b). The shortest path for the m-s model remains unchanged, as indicated by the green line, with a corresponding global optimal solution value of 167.2205. However, the shortest path for the m-v model changes, as shown by the blue line, with a corresponding global optimal solution value of 722.0160. This outcome arises due to differences in how the two problems handle the correlation within the road network in their respective mathematical formulations. In the m-v problem, the correlation is not subjected to a square root operation. Consequently, when the variance of link 2 increases abruptly, it exerts a substantial impact on the optimal solution of the m-v problem, directly causing a change in both the optimal solution and the corresponding shortest path. In contrast, for the m-s problem, the covariance term in the objective function is processed with a square root operation. As a result, even when the variance of link 2 increases significantly, its influence on the objective function does not exhibit a pronounced increase. Thus, the optimal solution and the corresponding shortest path for the m-s problem remain unchanged. This pattern can also be observed in the changes in the global optimal solution values of the two problems. Regardless, these results demonstrate that the method proposed in this paper effectively addresses both the m-v and m-s problems. Even within a real road network, it can accurately and efficiently identify the corresponding shortest paths.



(a) (b)

Figure 5-9: Shortest Paths between OD Pair (1, 20) for m-v and m-s Problems on the Sioux-Falls Network: (a) Baseline Parameter Settings; (b) Increased Variance for Link 2

Continuing with the random travel time distribution values of the current road network links, the method proposed in this paper is applied to solve the shortest path problems for the m-v and m-s models across different origin-destination (OD) pairs in the Sioux Falls transportation network. Table 5-3 presents the number of acyclic paths, the composition of the shortest paths, and the corresponding global optimal solutions for the optimization problems under different OD pairs. To further validate the accuracy of the proposed method, a branch-and-cut approach, capable of solving the global optimal solution of the NL-BIP problem, is employed to address the m-v and m-s problems in their original NL-BIP form, as specifically outlined in Equations (5-4) – (5-6) and (5-14), and the results are also presented in Table 5-3. The results

in Table 5-3 demonstrate that, even when the OD pairs are varied, this study can accurately identify the shortest paths corresponding to the m-v and m-s problems and achieve highly precise global optimal values. Despite similar path counts in the analyzed cases, the distinct path structures (e.g., variations in node connectivity and link correlations) highlight the method's robustness, as its LP transformation leverages the road network's topological properties. Consequently, neither variations in OD pairs nor path counts affect the method's efficacy. These findings affirm the method's strong applicability in complex road networks.

Table 5-3: Results of different methods for solving the shortest path problems of m-v and m-s under different OD pairs.

OD Pair	Number of Paths	Problem Type	Proposed Method		Branch-and-cut Method	
			Shortest Path (Link Sequence)	Optimal Value	Shortest Path (Link Sequence)	Optimal Value
(13, 2)	4498	m-v	[38, 35, 5, 1]	369.1022	[38, 35, 5, 1]	369.1002
		m-s	[38, 35, 5, 1]	108.6451	[38, 35, 5, 1]	108.6451
(6, 24)	3118	m-v	[15, 11, 10, 34, 42, 73]	523.7684	[15, 11, 10, 34, 42, 73]	523.7684
		m-s	[15, 11, 10, 34, 42, 73]	131.6005	[15, 11, 10, 34, 42, 73]	131.6005
(3, 19)	3705	m-v	[6, 10, 34, 41, 45]	469.9354	[6, 10, 34, 41, 45]	469.9354
		m-s	[6, 10, 34, 41, 45]	135.8708	[6, 10, 34, 41, 45]	135.8708

To conduct a more in-depth analysis of the proposed method, a series of numerical experiments are carried out using arbitrarily generated transportation networks with varying levels of complexity as testbeds. The complexity of each network is controlled by adjusting the number of nodes and links, thereby enabling a systematic validation of the effectiveness of the proposed approach. The travel times of links in all generated transportation networks are assumed to follow a multivariate normal distribution. The corresponding data values are generated as random samples using the same procedure adopted for the Sioux Falls network, ensuring consistency across different experimental settings. Three representative transportation networks with increasing levels of complexity are considered in this study. Specifically, Network (a) consists of 20 nodes and 70 links, Network (b) consists of 30 nodes and 106 links, and Network (c) consists of 40 nodes and 146 links. The topological structures of these networks are illustrated in Fig. 5-10 (a), (b), and (c), respectively.

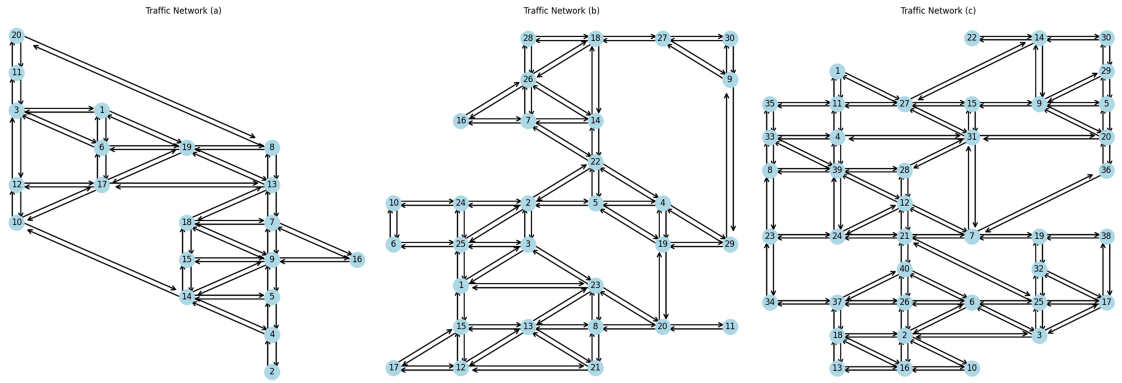


Figure 5-10: Randomly generated transportation networks of varying complexity

The accuracy of the proposed method has been validated using the Sioux Falls transportation network. This section further investigates its practical applicability in more complex settings by employing randomly generated transportation networks. As the scale of a transportation network increases, characterized by a growing number of nodes and links, the original *m–v* and *m–s* problems become increasingly challenging to solve. In such cases, the resulting nonlinear binary integer programming (NL-BIP) problem is often addressed using heuristic algorithms, such as simulated annealing, genetic algorithms, or greedy search methods. However, due to their iterative nature, these approaches are prone to becoming trapped in local optima when dealing with highly complex problem instances. In contrast, the proposed method reformulates the original NL-BIP problem into a linear programming (LP) problem, thereby completely avoiding the issue of local optima. Using the transportation networks illustrated in Fig. 5-10 (a)–(c) as test cases, three solution approaches are evaluated for solving the *m–v* and *m–s* problems between OD pairs: (1) the proposed method; (2) the Branch-and-Cut method, a classical exact optimization technique; and (3) the Simulated Annealing method, a widely

Table 5-4: Optimal *m–v* and *m–s* results for networks (a)–(c) across corresponding OD pairs using different solution methods.

Network	OD pair	Number of Paths	Problem Type	Proposed Method		Branch-and-Cut Method		Simulated Annealing Method	
				Optimal Value	Running Time (s)	Optimal Value	Running Time (s)	Optimal Value	Running Time (s)
(a)	(20, 2)	3173	*m–v*	1883.9511	0.7291	1883.9521	0.5099	1961.6743	0.0322
			m–s	340.7423	3.8061	340.7423	4.0110	600.4269	1.9860
(b)	(17, 30)	141,832	*m–v*	2634.5326	1.8783	2634.5326	2.1179	2959.6096	0.1910
			m–s	454.9855	4.6793	454.9855	5.0120	611.2376	3.6407
(c)	(10, 22)	18,052,844	*m–v*	2725.4066	7.2874	2725.4066	8.2624	2911.0822	0.2958
			m–s	387.4760	8.4163	387.4760	12.4193	671.2628	6.2542

adopted heuristic algorithm. The corresponding numerical results are reported in Table 5-4. All experiments are implemented in Python 3.13 and executed on a Dell OptiPlex 7000 desktop equipped with an Intel Core i7–12900 processor (2.4 GHz), 16 GB RAM, and Microsoft Windows 11 Pro (Version 10.0.22631).

As evidenced in Table 5–4, an increase in the number of links and nodes leads to an exponential surge in the number of paths. For instance, in a network with 40 nodes, the number of acyclic paths between OD pair (10, 22) approaches nearly 20 million. This vast number of paths in such complex networks significantly heightens the computational challenge of solving the original shortest path problem. Nevertheless, analysis of the results demonstrates that, irrespective of increases in the number of network nodes, links, or paths, the method proposed in this study consistently resolves the *m–v* and *m–s* shortest path problems effectively, delivering precise global optimal solutions. In large-scale networks, heuristic algorithms are commonly employed to tackle the NL-BIP problem; however, due to the complexity of such networks, these algorithms often become ensnared in local optima. Taking the simulated annealing method provided in the table as an example, as the network scale expands, its results tend to reflect local optima—a characteristic that proves highly disadvantageous for addressing real-world network challenges. These findings further underscore the efficacy of the proposed method, which successfully reduces the NL-BIP problem in complex networks to a simpler LP problem for resolution, thereby ensuring the identification of global optimal solutions. This capability holds significant practical value for solving shortest path problems in real-world, intricately interconnected networks. From the perspective of computational efficiency, Table 5–4 indicates that for small-scale networks with fewer paths, the running times of the proposed LP-based method, Branch-and-Cut, and Simulated Annealing are comparable for *m–v* and *m–s* problems. In certain cases, such as the *m–v* problem in smaller instances, Branch-and-Cut exhibits shorter running times, likely due to efficient solver optimizations. However, as the network scale grows to include millions of paths, the proposed method demonstrates superior efficiency compared to Branch-and-Cut, reflecting its polynomial complexity in solving the reformulated LP problem. Simulated Annealing requires less time in the tested instances, but its suboptimal solutions highlight a critical trade-off between speed and accuracy. These findings further underscore the efficacy of the proposed method, which successfully reduces the NL-BIP problem in complex networks to a simpler LP problem, ensuring global optimal solutions with competitive computational efficiency. This capability holds significant practical value for solving shortest path problems in real-world, intricately interconnected networks.

5.6 Chapter Summary

This chapter focused on the optimization of reliable shortest paths in transportation networks where statistical correlations exist among link travel times. The main objective was to achieve a balanced consideration between expected travel time and travel-time reliability while explicitly accounting for link interdependencies, thereby providing a robust decision-making foundation for path planning under uncertainty.

The chapter first established a theoretical framework for the reliable shortest-path problem and highlighted the limitations of traditional shortest-path models that assume independence among links. By introducing a travel-time covariance matrix, link correlations were explicitly incorporated into the model formulation. This enhancement enables the framework to capture the joint uncertainty arising from spatial proximity, shared external disturbances, and correlated demand fluctuations, thus offering a more realistic representation of stochastic network behavior.

Two complementary optimization models were then developed based on distinct definitions of reliability: the Mean-

Variance (M-V) and Mean-Standard-Deviation (M-S) formulations. The M-V model measures overall variability through variance, offering analytical tractability and computational efficiency, while the M-S model employs standard deviation to provide a more intuitive behavioral interpretation consistent with risk perception. A comparative analysis of the two approaches demonstrated that the M-V model possesses advantages in mathematical formulation and convergence stability, whereas the M-S model more effectively reflects realistic traveler preferences regarding reliability. Together, these models constitute a unified and flexible system for reliable path optimization.

Subsequently, corresponding algorithms were designed and validated through numerical experiments on benchmark networks. The results confirmed the validity and applicability of the proposed models. When correlations among link travel times were considered, the structure of optimal paths exhibited substantial variation. As correlation intensity increased, the optimal paths identified under the independence assumption no longer remained stable, while the proposed models successfully adapted path selection to balance efficiency and reliability. These findings reveal the systematic influence of correlated risks on route decisions and underscore the necessity of incorporating covariance structures into reliability optimization.

From an overall perspective, this chapter completed the methodological transition from behavioral modeling to stochastic characterization and finally to reliability-oriented decision optimization. Chapter 3 analyzed how risk sensitivity and external disturbances generate behavioral heterogeneity and network-level uncertainty. Chapter 4 introduced a fractional-moment-based approach to represent and quantify stochastic propagation. Building upon these foundations, the current chapter integrated the quantified uncertainty into the decision-making process, thereby establishing a coherent modeling loop that links uncertainty perception, numerical representation, and reliability-based optimization. This integration not only enhances the interpretability of the overall framework but also provides a theoretical and computational basis for reliable route planning in complex, uncertain networks.

In summary, this chapter consolidated the proposed multi-layered modeling framework by bridging behavioral, numerical, and optimization perspectives. It provided a systematic approach to understanding the interactions among uncertainty, correlation, and reliability in transportation systems. Based on these findings, Chapter 6 will further synthesize the three core studies, discuss their interconnections and mutual reinforcement, and explore the potential closed-loop mechanisms that unify behavioral, stochastic, and decision-making processes within uncertainty-aware transportation modeling.

Chapter 6

Integrated Discussion and System Analysis

This chapter provides an integrated examination of the results derived from the three core studies presented in Chapters 3 to 5. The focus is placed on the interconnections, dynamic interactions, and system-level behaviors emerging from the integration of behavioral, numerical, and optimization models. Unlike Chapter 2, which discussed the theoretical and methodological relationships among the three studies, the present chapter emphasizes the empirical and systemic implications of the modeling framework. The aim is to reveal how these models interact to form a cohesive mechanism for representing and managing uncertainty in transportation networks.

6.1 Logical Consistency and Extended Results of the Multi-Layer Framework

The three major studies collectively establish a comprehensive multi-layer framework that progresses from behavioral modeling to stochastic representation and ultimately to reliability-oriented optimization. Beyond their conceptual alignment, the three models exhibit strong logical consistency through continuous information transfer and result-level interdependence. Together, they describe how transportation network operating states evolve under uncertainty through the interaction of traveler behavior, stochastic propagation, and decision-making mechanisms.

At the behavioral layer, the risk-sensitive path choice model captures user heterogeneity and differential responses to uncertainty, generating stochastic and spatially diverse traffic-flow patterns across the network. These heterogeneous behavioral responses serve as the primary source of variability in network operating states.

At the numerical layer, the fractional-moment-based representation framework transforms behavior-induced flow fluctuations into stable statistical descriptors, effectively characterizing non-Gaussianity, skewness, and correlation structures among link travel times. This layer provides a consistent and tractable representation of uncertainty propagation at the network level.

At the optimization layer, the reliable shortest-path model leverages the statistical descriptors derived from the stochastic representation layer to perform risk-informed path selection, balancing expected performance and reliability under correlated link conditions.

Through this sequential integration, behavioral evolution induces uncertainty propagation, which in turn shapes adaptive decision-making outcomes. Consequently, the three models do not operate as isolated components, but rather form an integrated closed-loop system that captures the endogenous evolution of network operating states under uncertainty.

6.2 Interaction among Model Results

A comparative analysis of the results obtained from the three models reveals clear interdependencies and interactive effects, which can be summarized as follows:

a) **Coupling Effects between Risk Behavior and Uncertainty Propagation**
Variations in risk sensitivity alter the distribution of path choice probabilities and reshape the spatiotemporal structure of network flow. As travelers with higher risk aversion concentrate on stable routes, the resulting redistribution of flows amplifies correlations among link travel times. The fractional-moment estimation further indicates that such behavioral adjustments introduce heavier tails and stronger skewness, suggesting that user heterogeneity intensifies non-linear uncertainty propagation through the network topology.

b) **Transmission Effects of Fractional-Moment Representation on Reliable Optimization**
The fractional-moment approach provides a refined statistical basis for reliability-based optimization. When travel-time distributions deviate from normality, variance-based estimators tend to understate risk, whereas fractional moments capture tail behavior and improve robustness. Comparative experiments demonstrate that the covariance structures derived from fractional moments significantly enhance the stability of the Mean–Standard-Deviation (M–S) model in high-correlation scenarios.

c) **Feedback Effects of Reliable Optimization on Behavioral Adjustment**

The outcomes of the reliability optimization—such as the set of optimal paths and reliability indices—can influence travelers' subsequent perception and preference updates. When reliability information is incorporated into behavioral decision-making, users exhibit more stable and consistent path preferences over time. This phenomenon indicates that reliable optimization not only serves as a decision mechanism but also functions as a behavioral regulator, forming the basis of an adaptive feedback process in transportation systems.

6.3 Dynamic Closed-Loop Mechanism

Building on the interdependencies identified in the preceding sections, the three models collectively constitute a dynamic closed-loop mechanism that governs the endogenous evolution of transportation network operating states under uncertainty. This mechanism can be summarized as:

$$\text{Risk-sensitive behavior} \rightarrow \text{Uncertainty propagation} \rightarrow \text{Reliability optimization} \rightarrow \text{Behavioral feedback}$$

Within this closed loop, heterogeneous risk-sensitive behavior generates spatially differentiated traffic-flow patterns, which serve as the primary source of stochastic variability in network operating states. The fractional-moment-based representation framework systematically characterizes how such behavior-induced variability propagates through the network structure, yielding stable statistical descriptors of travel time uncertainty. These descriptors are subsequently utilized by the reliability optimization model to identify robust path decisions that balance efficiency and reliability under correlated network conditions.

Importantly, the feedback in this loop does not correspond to explicit time-dependent traffic evolution or sequential flow propagation. Instead, it reflects an equilibrium-to-equilibrium adjustment process, whereby changes in decision outcomes reshape perceived network conditions and influence travelers' behavioral tendencies under uncertainty. Through repeated behavioral adaptation and redistribution of flows, the network converges to distinct stochastic equilibrium states associated with different uncertainty and risk-perception regimes.

This closed-loop perspective highlights the endogenous nature of uncertainty in transportation systems. Uncertainty is not merely an externally imposed attribute of the environment, but an emergent system property arising from the interaction among traveler behavior, network coupling, and reliability-oriented decision responses. Consequently, the dynamic nature of the transportation network considered in this dissertation lies in the evolution of its operating states under uncertainty, rather than in externally driven time-varying disturbances or dynamic flow propagation.

6.4 Integrated Experiment and Cross-Model Validation

To confirm the practical consistency of the proposed multi-layer framework, this section synthesizes the empirical findings from the three studies rather than introducing new numerical experiments. The goal is to examine whether the behavioral, numerical, and optimization layers collectively form a coherent and operational system. The behavioral experiments in Chapter 3 demonstrated that the risk-sensitive path choice model can reproduce realistic variations in traveler behavior and achieve equilibrium convergence under non-extreme disturbances. The numerical validation in Chapter 4 showed that the fractional-moment estimation method yields highly stable and accurate results even under heavy-tailed or skewed travel-time distributions. The optimization experiments in Chapter 5 further verified that both the M-V and M-S formulations are computationally tractable and globally solvable, providing reliable and interpretable path solutions in correlated networks. Together, these results confirm that each model component performs as designed and that their integration is both theoretically coherent and empirically feasible. The behavioral layer explains the origin of uncertainty, the fractional-moment method quantifies it with precision, and the reliable optimization framework transforms it into actionable decisions. This cross-model validation demonstrates that the overall system can effectively represent, quantify, and manage uncertainty in transportation networks.

6.5 Theoretical and Practical Implications

The integrated analysis of the three models yields several important implications:

a) **Behavior-Driven Uncertainty Generation**
System-level stochasticity originates not solely from external disturbances but also from user risk perception and behavioral heterogeneity. Capturing behavioral drivers is therefore essential for accurately modeling uncertainty.

b) **Cross-Layer Information Transmission as a Stabilizing Mechanism**
The fractional-moment method serves as a bridge that translates behavioral heterogeneity into computable metrics for optimization, ensuring stability and consistency in multi-layer uncertainty modeling.

c) **Reliability Optimization as Both Decision and Regulation Process**
Reliable path optimization provides not only optimal route decisions but also a mechanism for stabilizing user behavior through reliability feedback, contributing to the self-regulation of network systems.

d) **Extensibility of the Closed-Loop Framework**
The proposed multi-layer coupling structure offers general applicability to dynamic traffic assignment, learning-based path planning, and multi-agent interaction models, laying a theoretical foundation for future research on adaptive network systems.

6.6 Summary

This chapter presented an integrated, result-oriented discussion of the three core studies, with a particular focus on the system-level interactions and feedback mechanisms linking behavioral, stochastic, and optimization components. In contrast to the conceptual synthesis in Chapter 2, the discussion here emphasized the emergent patterns and cross-model dependencies revealed through simulation and empirical analysis.

The results demonstrate that uncertainty in transportation networks exhibits endogenous feedback and self-organizing characteristics, arising from the interaction between traveler behavior, stochastic propagation, and reliability-oriented decision-making. Through this lens, the proposed multi-layer framework provides not only theoretical coherence but also a system-level understanding of how network operating states evolve under uncertainty. Moreover, it offers a practical foundation for risk-aware and reliability-oriented network management in complex environments.

Building on these insights, Chapter 7 concludes the dissertation by summarizing the main contributions and methodological innovations, and by discussing potential extensions toward uncertainty-aware dynamic modeling, intelligent decision support, and data-driven optimization.

Chapter 7

Conclusion

7.1 Summary of Findings

This dissertation establishes a comprehensive three-layer framework integrating behavioral modeling, stochastic representation, and reliability-oriented optimization to analyze path choice behavior and network reliability under uncertainty. Rather than treating uncertainty as an exogenous input, the proposed framework systematically captures how uncertainty is generated by traveler behavior, propagated through network structures, and ultimately reflected in reliability-oriented decision-making. Through this integrated perspective, the dissertation provides a coherent mechanism linking individual perception to system-level performance and optimization. The main findings are summarized as follows.

(1) **Development and Validation of a Risk-Sensitive Path Choice Model.**
At the behavioral level, a multi-class risk-sensitive path choice model (BST model) was developed to represent travelers' heterogeneous responses under non-extreme flood disturbances. The model incorporates a risk-aversion coefficient to quantify sensitivity to flood risk and introduces a dual-stochastic generalized cost function integrating travel time, flood risk, and path choice inertia. By employing two independent stochastic components (Gumbel and uniform distributions), the model yields closed-form path choice probabilities and realistically captures behavioral differences among users with varying risk attitudes. Simulation results demonstrate that the proposed model reproduces instinctive risk-avoidance behavior and the resulting redistribution of traffic flows, thereby revealing how heterogeneous behavioral responses reshape network operating states under uncertainty.

(2) **Fractional Moment-Based Representation of Stochastic Travel Time.**
At the stochastic characterization level, a novel method termed the Fractional-Folding Moment Transform (FFMT) was proposed to compute fractional-order moments of random variables using a finite set of integer-order moments. By combining Laplace transforms with fractional calculus, the method derives both analytical and discrete numerical formulations. Theoretical analyses establish error bounds, parameter selection criteria, and the existence and uniqueness of optimal solutions. Numerical experiments confirm that FFMT significantly improves computational stability and accuracy relative to conventional Taylor expansion and Monte Carlo methods, maintaining convergence even under heavy-tailed distributions and high-order conditions. The FFMT framework thus provides a robust and unified tool for characterizing uncertainty structures associated with evolving network states.

(3) **Reliable Path Optimization under Correlated Network Conditions.**
At the optimization level, two classes of reliable path problems—the mean–variance (M–V) and mean–standard deviation (M–S) formulations—were investigated under correlated link travel times. For the M–V problem, traditionally viewed as non-additive and nonlinear, the study reformulates it as a linear programming problem through a flow-conservation-based hypergraph transformation and proves total unimodularity of the constraint matrix, ensuring integer optimal solutions and computational efficiency. For the M–S formulation, a concave minimization problem is established and solved using a globally optimal algorithm grounded in the same linear programming framework. Numerical experiments demonstrate that the proposed models achieve robustness, stability, and scalability in reliable path search under correlated network conditions.

(4) **Integration and Logical Consistency of the Multi-Layer Framework.**
The three studies are tightly interconnected across multiple levels: the behavioral model explains how uncertainty arises from heterogeneous decision-making, the FFMT method translates behavior-induced variability into tractable stochastic descriptors, and the reliable path optimization model utilizes these descriptors to support system-level decision-making. Together, they form a coherent framework that captures the generation, propagation, and control of uncertainty in transportation networks, ensuring logical consistency and continuous information transfer across behavioral, stochastic, and optimization layers.

Overall, this dissertation contributes theoretical and methodological advances in risk-sensitive behavioral modeling, fractional-moment-based stochastic representation, and reliability-oriented network optimization. By integrating these

components into a unified framework, the study provides a systematic foundation for understanding and managing the evolution of transportation network operating states under uncertainty, offering both analytical insights and practical tools for reliability analysis in complex transportation systems.

7.2 Future Research Directions

Although the proposed framework and models have achieved substantial progress in theoretical development and numerical validation, several aspects merit further exploration. Future research can be directed toward the following perspectives:

(1) **Dynamic Behavioral Adaptation and Multi-Source Information Perception.**
The current behavioral model focuses on static risk environments. Future work could extend the model to dynamic decision-making contexts that incorporate information updating, experience-based learning, and real-time perception. This would enable a more realistic representation of travelers' adaptive behavior under evolving environmental and informational conditions.

(2) **Extension of the Fractional Moment Method to Spatiotemporal Stochastic Processes.**
While the FFMT method has demonstrated high precision in single-variable settings, future studies could generalize it to multivariate and spatiotemporally correlated random processes. Integrating sparse reconstruction and machine learning techniques could further enhance the estimation and updating of stochastic travel time distributions in large-scale dynamic networks.

(3) **Intelligent Algorithms for Reliable Path Optimization.**
The current optimization framework relies primarily on mathematical programming. Future research could integrate reinforcement learning, graph neural networks, and metaheuristic algorithms to construct hybrid intelligent optimization models. Such approaches would improve adaptability and computational efficiency in large-scale, high-dimensional, and multi-objective environments.

(4) **System Integration and Policy Applications.**
The multi-layer framework developed in this dissertation could be embedded into real-world transportation management systems for resilience analysis, emergency response, and infrastructure planning. Integrating behavioral, stochastic, and optimization components would allow decision-makers to evaluate policy impacts on network reliability and user welfare, thereby bridging theoretical research and practical decision support.

Appendix A

The Notations Employed in Chapter 3

Table A-1: The Notations Employed in Chapter 3

Notation	Definition	Notation	Definition
A	Set of links in the network	I	Set of O-D pairs in the network
J_i	Set of paths between O-D pair i	M_i	Set of user categories within O-D pair i
δ_{aj}	1 if link a belongs to path j, 0 otherwise	V_a	Stochastic flow on link a
C_a	Capacity of link a	F_{ij}	Stochastic flow on path j for O-D pair i
F_{imj}	Stochastic flow of user type m on path j for O-D pair i	Q_i	Total stochastic O-D flow between O-D pair i
Q_{im}	Demand of user category m in O-D pair i	T_{ij}	Stochastic travel time on path j for O-D pair i
T_a	Stochastic travel time on link a	P_{im}	Proportion of Q_{im} to Q_i
ρ_{im}	Risk sensitivity of user type m in O-D pair i	ϑ_a	Degree of risk of vehicle instability
U_{af}	Flood velocity on link a	U_{ac}	Critical velocity of vehicle instability
w_1, w_2	Parameters related to vehicle appearance, tires, and road roughness	h_{af}	Flood depth on link a
ρ_f	Density of flood water	h_c	Average height of the vehicle
l_c	Average vehicle length	ρ_c	Average density of the vehicle
g	Gravitational acceleration	R_f	Empirical parameter related to flood forces
l_{af}	Proportion of inundated link length to total link length	R_{imj}	Perceived flood risk for user type m on path j

Appendix B

Derivation Process of Calculation Method of t_{ima}

This appendix provides the detailed derivation process of the calculation method of the perceived link travel time t_{ima} for user type m in O–D pair i.

Perceived link travel times of specific user category m within the same O–D pair i can be expressed as:

$$\Pr(T_a < t_{ima}) \geq \rho_{im}, \quad \forall i \in I,\ \forall m \in M_i,\ \forall a \in A. \tag{B-1}$$

The link travel time T_a follows a random distribution, with mean $E[T_a]$ and variance $\mathrm{var}[T_a]$. Applying the conventional one-sided Chebyshev inequality yields:

$$\Pr\big(T_a \geq E[T_a] + k\big) \leq \frac{\mathrm{var}[T_a]}{\mathrm{var}[T_a] + k^2}. \tag{B-2}$$

Inequality (B-2), constructed from Chebyshev's inequality, incorporates the mathematical relationship among k, $E[T_a]$, and $\mathrm{var}[T_a]$. Based on this relationship and the principles of reliability-based travel time, the connection between user risk sensitivity and perceived travel time can be derived.

Let inequality (B-2) be defined as event A. According to the definition of probability, the complementary event $\bar{A}$ satisfies:

$$\Pr(\bar{A}) = 1 - \Pr(A). \tag{B-3}$$

Then the Chebyshev inequality expression for the complementary event $\bar{A}$ becomes:

$$\Pr\big(\bar{A}\big) = \Pr\big(T_a < E[T_a] + k\big) = 1 - \Pr(A) \geq 1 - \frac{\mathrm{var}[T_a]}{\mathrm{var}[T_a] + k^2}. \tag{B-4}$$

Therefore:

$$\Pr\big(T_a < E[T_a] + k\big) \geq 1 - \frac{\mathrm{var}[T_a]}{\mathrm{var}[T_a] + k^2}. \tag{B-5}$$

The objective of deriving an expression for t_{ima} is to directly relate perceived travel time to user risk sensitivity. Thus:

$$1 - \frac{\mathrm{var}[T_a]}{\mathrm{var}[T_a] + k^2} = \rho_{im}. \tag{B-6}$$

Therefore, it naturally follows that:

$$\Pr(T_a < t_{ima}) \geq \rho_{im}. \tag{B-7}$$

where

$$t_{ima} = E[T_a] + \sqrt{\frac{\rho_{im}}{1 - \rho_{im}}}\,\sqrt{\mathrm{var}[T_a]}. \tag{B-8}$$

Appendix C

Proof of the Sub-additivity of Perceived Link Travel Time

For ease of comprehension and elucidation, here assume the path is denoted by j encompassing only two links, namely a and b, as $j = a + b$. Then according to the definition of perceived travel time in this study, perceived travel time of link a, b and path j can be expressed as:

$$t_{ima} = E[T_a] + \lambda \cdot \sqrt{\mathrm{var}[T_a]} \tag{C-1}$$

$$t_{imb} = E[T_b] + \lambda \cdot \sqrt{\mathrm{var}[T_b]} \tag{C-2}$$

$$\hat{t}_{imj} = E[T_{ij}] + \lambda \cdot \sqrt{\mathrm{var}[T_{ij}]} \tag{C-3}$$

where $\lambda = \sqrt{\rho_{im}/(1-\rho_{im})}$.

Then based on the definition of the sub-additivity property of a risk measure, equation (C-1), (C-2) and (C-3) need hold the following relationship:

$$\hat{t}_{imj} \le t_{imj} = t_{ima} + t_{imb} \tag{C-4}$$

Utilizing the $\rho_{(a,b)}$ represents the Pearson product-moment correlation coefficient, considering the transformation trends between path travel time and link travel time, and the value of which always holds: $0 < \rho_{(a,b)} \le 1$. Then the following relationship can be derived:

$$\begin{aligned}
&0 < \rho_{(a,b)} \le 1 \\
&\Rightarrow 0 < \frac{\mathrm{cov}[T_a, T_b]}{\sqrt{\mathrm{var}[T_a] \cdot \mathrm{var}[T_b]}} < 1 \\
&\Rightarrow \mathrm{var}[T_{ij}] - \left(\sqrt{\mathrm{var}[T_a]} + \sqrt{\mathrm{var}[T_b]}\right)^2 \le 0 \\
&\Rightarrow \frac{\mathrm{var}[T_{ij}]}{\left(\sqrt{\mathrm{var}[T_a]} + \sqrt{\mathrm{var}[T_b]}\right)^2} \le 1 \\
&\Rightarrow \left(\frac{\sqrt{\mathrm{var}[T_{ij}]}}{\sqrt{\mathrm{var}[T_a]} + \sqrt{\mathrm{var}[T_b]}}\right)^2 \le 1 \\
&\Rightarrow \lambda \cdot \left(\sqrt{\mathrm{var}[T_{ij}]} - \sqrt{\mathrm{var}[T_a]} - \sqrt{\mathrm{var}[T_b]}\right) \le 0 \\
&\Rightarrow E[T_{ij}] - (E[T_a] + E[T_b]) + \lambda \cdot \left(\sqrt{\mathrm{var}[T_{ij}]} - \sqrt{\mathrm{var}[T_a]} - \sqrt{\mathrm{var}[T_b]}\right) \le 0 \\
&\Rightarrow \hat{t}_{imj} \le t_{imj} = t_{ima} + t_{imb}
\end{aligned} \tag{C-5}$$

Appendix D

Proof of the Expression of P_{imj}

When considering only two paths j and k, the proportion of selecting path j is denoted as P_{imj}. Similarly, within the acceptable path set, the probability that the cost of path j, after applying selection inertia, is less than or equal to the cost of other acceptable paths without selection inertia is denoted as Y_{imj}, expressed as:

$$Y_{imj} = \Pr\left(t_{imj} + R_{imj} - \varepsilon_{imj} \le t_{imk} + R_{imk},\ \forall k \in \bar{J}_{im}\right) \tag{D-1}$$

Using the same criteria for judgment, as outlined in the main text for the definitions of R_{imj} and ε_{imj}, whether R_{imj} or ε_{imj} are mutually independent within the acceptable path set, the derivation of Y_{imj} follows the Random Utility Maximization framework. Here the random disturbance term satisfies the IID and IIA assumptions (McFadden, 1972). When the number of acceptable paths exceeds two, the probability of selecting path j becomes:

$$Y_{imj} = \prod_{\substack{k\in\bar{J}_{im}\\ k\neq j}} \Pr\left(t_{imj} + R_{imj} - \varepsilon_{imj} \le t_{imk} + R_{imk}\right) \tag{D-2}$$

Based on the distributional characteristics of R_{imj}, and for convenience denoting $a_{imj} = -R_{imj}$, the expression for the probability of selecting path j becomes:

$$\begin{aligned}
Y_{imj} &= \prod_{k\neq j} \Pr\left(a_{imk} \le t_{imk} - t_{imj} + a_{imj} + \varepsilon_{imj}\right) \\
&= \frac{1}{\bar{\varepsilon}_{imj}} \int_0^{\bar{\varepsilon}_{imj}} \left[\int_{-\infty}^{\infty} \prod_{k\neq j} e^{-e^{-(t_{imk}-t_{imj}+a_{imj}+\varepsilon_{imj}+r_{imk})}} e^{-e^{-(a_{imj}+r_{imj})}} e^{-(a_{imj}+r_{imj})}\, da_{imj} \right] d\varepsilon_{imj} \\
&= \frac{1}{\bar{\varepsilon}_{imj}} \int_0^{\bar{\varepsilon}_{imj}} \left[\int_{-\infty}^{\infty} \exp\left(-\sum_{k\neq j} e^{-(a_{imj}-t_{imj}+\varepsilon_{imj}+t_{imk}+r_{imk})} \right) \exp\left(-e^{-(a_{imj}-t_{imj}+\varepsilon_{imj}+t_{imj}+r_{imj})} e^{\varepsilon_{imj}} \right) \right. \\
&\qquad \left. \times \exp\left(-(a_{imj}+r_{imj})\right)\, da_{imj} \right] d\varepsilon_{imj} \\
&= \frac{1}{\bar{\varepsilon}_{imj}} \int_0^{\bar{\varepsilon}_{imj}} \left[\int_{-\infty}^{\infty} \exp\left(-e^{-a_{imj}} \sum_{k} e^{t_{imj}-\varepsilon_{imj}-t_{imk}-r_{imk}} \right) \exp\left(e^{-a_{imj}-\varepsilon_{imj}-r_{imj}} - e^{-a_{imj}-r_{imj}} \right) \right. \\
&\qquad \left. \times e^{-(a_{imj}+r_{imj})}\, da_{imj} \right] d\varepsilon_{imj}
\end{aligned} \tag{D-3}$$

Next, substituting $t = e^{-a_{imj}}$ and applying the result from (D-3), the expression becomes:

$$\begin{aligned}
Y_{imj} &= e^{-r_{imj}} \cdot \frac{1}{\bar{\varepsilon}_{imj}} \int_0^{\bar{\varepsilon}_{imj}} \left[\int_0^{\infty} \exp\left(-\left(\sum_k e^{t_{imj}-\varepsilon_{imj}-t_{imk}-r_{imk}} + e^{-r_{imj}} - e^{-\varepsilon_{imj}-r_{imj}} \right) t \right) dt \right] d\varepsilon_{imj} \\
&= \frac{e^{-r_{imj}}}{\bar{\varepsilon}_{imj}} \int_0^{\bar{\varepsilon}_{imj}} \left[\frac{\exp\left(-\left(\sum_k e^{t_{imj}-\varepsilon_{imj}-t_{imk}-r_{imk}} + e^{-r_{imj}} - e^{-\varepsilon_{imj}-r_{imj}}\right) t \right)}{-\left(\sum_k e^{t_{imj}-\varepsilon_{imj}-t_{imk}-r_{imk}} + e^{-r_{imj}} - e^{-\varepsilon_{imj}-r_{imj}}\right)} \right]_0^{\infty} d\varepsilon_{imj} \\
&= \frac{1}{\bar{\varepsilon}_{imj}} \int_0^{\bar{\varepsilon}_{imj}} \frac{1}{e^{-\varepsilon_{imj}} \left(\sum_k e^{t_{imj}+r_{imj}-t_{imk}-r_{imk}} - 1\right) + 1} d\varepsilon_{imj}
\end{aligned} \tag{D-4}$$

Finally, substituting $s = e^{-\varepsilon_{imj}}$, the following closed-form expression is obtained:

$$\begin{aligned}
Y_{imj} &= \frac{1}{\bar{\varepsilon}_{imj}} \int_{e^{-\bar{\varepsilon}_{imj}}}^{1} \frac{1}{s^2 \left(\sum_k e^{t_{imj}+r_{imj}-t_{imk}-r_{imk}} - 1\right) + s} ds \\
&= \frac{1}{\bar{\varepsilon}_{imj}} \ln\left(1 + \frac{(e^{\bar{\varepsilon}_{imj}} - 1) e^{-(t_{imj}+r_{imj})}}{\sum_k e^{-(t_{imk}+r_{imk})}} \right)
\end{aligned} \tag{D-5}$$

Appendix E

Proof of the Expression of Φ_{imk}

The expressions for the unacceptability factors corresponding to path k, compared with path j chosen within the set of acceptable paths are as follows:

$$\Phi_{imk} = \Pr\left(t_{imk} + R_{imk} - \varepsilon_{imk} \geq t_{imj} + R_{imj},\ \forall j \in \bar{J}_{im}\right) = \Pr\left(-R_{imk} \leq t_{imk} - t_{imj} - R_{imj} - \varepsilon_{imk},\ \forall j \in \bar{J}_{im}\right) \tag{E-1}$$

Then considering the distribution characteristics of the R_{imk}, for ease of expression, replacing $-R_{imk}$ with a_{imk}, the Φ_{imk} can be expressed as:

$$\begin{aligned}\Phi_{imk} &= \Pr\left(a_{imk} \leq t_{imk} - t_{imj} + a_{imj} - \varepsilon_{imk}\right) \\ &= \frac{1}{\bar{\varepsilon}_{imk}} \int_0^{\bar{\varepsilon}_{imk}} \left[\int_{-\infty}^{\infty} e^{-e^{-(t_{imk}-t_{imj}+a_{imj}-\varepsilon_{imk}+r_{imk})}} \cdot e^{-e^{-(a_{imj}+r_{imj})}} \cdot e^{-(a_{imj}+r_{imj})}\, da_{imj}\right] d\varepsilon_{imk} \\ &= \frac{1}{\bar{\varepsilon}_{imk}} \int_0^{\bar{\varepsilon}_{imk}} \left[\int_{-\infty}^{\infty} \exp\left(-e^{-a_{imj}}\left(e^{-(t_{imk}-t_{imj}-\varepsilon_{imk}+r_{imk})} + e^{-r_{imj}}\right)\right) \cdot e^{-r_{imj}} \cdot e^{-a_{imj}}\, da_{imj}\right] d\varepsilon_{imk}\end{aligned} \tag{E-2}$$

Given $e^{-a_{imj}} = t$, in conjunction with the results from the equation (E-2), Φ_{imk} can be derived as:

$$\begin{aligned}\Phi_{imk} &= \frac{1}{\bar{\varepsilon}_{imk}} e^{-r_{imj}} \int_0^{\bar{\varepsilon}_{imk}} \left[\int_0^{\infty} \exp\left(-t\left(e^{-(t_{imk}-t_{imj}-\varepsilon_{imk}+r_{imk})} + e^{-r_{imj}}\right)\right) dt\right] d\varepsilon_{imk} \\ &= \frac{1}{\bar{\varepsilon}_{imk}} e^{-r_{imj}} \int_0^{\bar{\varepsilon}_{imk}} \left[\frac{\exp\left(-t\left(e^{-(t_{imk}-t_{imj}-\varepsilon_{imk}+r_{imk})} + e^{-r_{imj}}\right)\right)}{-\left(e^{-(t_{imk}-t_{imj}-\varepsilon_{imk}+r_{imk})} + e^{-r_{imj}}\right)}\right]_0^{\infty} d\varepsilon_{imk} \\ &= \frac{1}{\bar{\varepsilon}_{imk}} \int_0^{\bar{\varepsilon}_{imk}} \frac{e^{-r_{imj}}}{e^{\varepsilon_{imk}} e^{t_{imj}-t_{imk}-r_{imk}} + e^{-r_{imj}}}\, d\varepsilon_{imk}\end{aligned} \tag{E-3}$$

Then, given $e^{\varepsilon_{imj}} = s$, in conjunction with the results from the equation (E-3), the following expression for Φ_{imk} can be obtained:

$$\begin{aligned}\Phi_{imk} &= \frac{1}{\bar{\varepsilon}_{imk}} \int_1^{e^{\bar{\varepsilon}_{imk}}} \frac{1}{\left(s e^{t_{imj}+r_{imj}-t_{imk}-r_{imk}} + 1\right) s}\, ds \\ &= \frac{1}{\bar{\varepsilon}_{imk}} \cdot \frac{e^{\bar{\varepsilon}_{imk}}\left(e^{t_{imj}+r_{imj}-t_{imk}-r_{imk}} + 1\right)}{e^{\bar{\varepsilon}_{imk}} e^{t_{imj}+r_{imj}-t_{imk}-r_{imk}} + 1}\end{aligned} \tag{E-4}$$

Appendix F

Proof of Corollary 2.1

$$
\begin{aligned}
({}_z^{RL}D_t^{\lambda} f(t)) &= \frac{1}{\Gamma(\zeta)} \frac{d^k}{dt^k} \int_z^t (t-\xi)^{\zeta-1} f(\xi)\, d\xi \\
&= \frac{1}{\Gamma(k-\lambda)} \frac{d^k}{dt^k} \left[\frac{(t-\lambda)^{k-\lambda} f(z)}{k-\lambda} + \int_z^t \frac{(t-\xi)^{k-\lambda}}{k-\lambda} f'(\xi)\, d\xi \right] \\
&= \frac{d^k}{dt^k} \left[\sum_{i=0}^{k-1} \frac{(t-\lambda)^{n+i-\lambda} f^{(i)}(z)}{\Gamma(n+i-\lambda+1)} + \frac{1}{\Gamma(2k-\lambda)} \int_z^t (t-\xi)^{2k-\lambda-1} f^{(k)}(\xi)\, d\xi \right] \qquad (A.1) \\
&= \sum_{i=0}^{k-1} \frac{(t-z)^{i-\lambda} f^{(i)}(z)}{\Gamma(i-\lambda+1)} + \frac{1}{\Gamma(k-\lambda)} \int_z^t (t-\xi)^{k-\lambda-1} f^{(k)}(\xi)\, d\xi \\
&= \sum_{i=0}^{k-1} \frac{(t-z)^{i-\lambda} f^{(i)}(z)}{\Gamma(i-\lambda+1)} + ({}_z^{C}D_t^{\lambda} f(t))
\end{aligned}
$$

From the equation (A.1), when $z \to -\infty$, the term $\sum_{i=0}^{k-1} \frac{(t-z)^{i-\alpha} f^{(i)}(z)}{\Gamma(i-\lambda+1)}$ equals to 0, therefore the corollary 2.1 holds true.

Appendix G

Proof of Corollary 2.2

According to the definition of the R-L fractional integral:

$$\begin{aligned}({}_z^{(R-L)}I_t^{\lambda} f(t)) &= \frac{1}{\Gamma(\lambda)} \int_z^t (t-\xi)^{\lambda-1} f(\xi)\, d\xi \\ &= \frac{1}{\Gamma(\lambda)} \int_0^{t-z} \xi^{\lambda-1} f(t-\xi)\, d\xi\end{aligned} \tag{G.1}$$

Given the conditions that $f(t) = e^{\varepsilon t}$, $z \to -\infty$, $\varepsilon > 0$, then:

$$\begin{aligned}({}_z^{(R-L)}I_t^{\lambda} e^{\varepsilon t}) &= \frac{1}{\Gamma(\lambda)} \int_0^{\infty} \xi^{\lambda-1} e^{\varepsilon(t-\xi)}\, d\xi \\ &= \varepsilon^{-\lambda} e^{\varepsilon t}\end{aligned} \tag{G.2}$$

$$({}_z^{C}D_t^{\lambda} e^{\varepsilon t}) = D^k\, \varepsilon^{\lambda-k}\, e^{\varepsilon t} = \varepsilon^{\lambda} e^{\varepsilon t} \tag{G.3}$$

This completes the proof of Corollary 2.2.

Appendix H

Proof of Corollary 2.3

Definition 2.5: Given an arbitrary real number z, $z \in \mathbb{R}$, and a non-integer number λ, $\lambda \in \mathbb{R}^+$ and $\lambda \notin \mathbb{N}$, $m-1 \le \lambda < m \in \mathbb{Z}^+$. The left Grunwald-Letnikov fractional derivatives $({}_z^{GL}D_t^{\lambda} f)$ of order λ of a function $f(t) \in C^m$ is also defined by:

$$({}_z^{GL}D_t^{\lambda} f(t)) = \sum_{i=0}^{m} \frac{f^{(i)}(z)\,(t-z)^{-\lambda+i}}{\Gamma(-\lambda+i+1)} + \frac{1}{\Gamma(-\lambda+m+1)} \int_z^t (t-\xi)^{-\lambda+m} f^{(m+1)}(\xi)\, d\xi \qquad (H.1)$$

Let $k = \lceil \lambda \rceil$, $\zeta = k - \lambda$, $k-1 < \lambda < k$, the following relationship holds:

$$\begin{aligned}
({}_z^{RL}D_t^{\lambda} f(t)) &= \frac{d^k}{dt^k}\left[\frac{1}{\Gamma(\zeta)} \int_z^t (t-\xi)^{\zeta-1} f(\xi)\, d\xi\right] \\
&= \frac{d^k}{dt^k}\left[\sum_{i=0}^{m} \frac{f^{(i)}(z)(t-z)^{k-\lambda+i}}{\Gamma(k-\lambda+i+1)} + \frac{1}{\Gamma(k-\lambda+m+1)} \int_z^t (t-\xi)^{k-\lambda+m} f^{(m+1)}(\xi)\, d\xi\right] \\
&= \sum_{i=0}^{m} \frac{f^{(i)}(z)\,\dfrac{d^k}{dt^k}(t-z)^{k-\lambda+i}}{\Gamma(k-\lambda+i+1)} + \frac{1}{\Gamma(k-\lambda+m+1)} \int_z^t \left[\frac{d^k}{dt^k}(t-\xi)^{k-\lambda+m}\right] f^{(m+1)}(\xi)\, d\xi \\
&= \sum_{i=0}^{m} \frac{f^{(i)}(z)\,(k-\lambda+i)\,\dfrac{d^{k-1}}{dt^{k-1}}(t-z)^{k-\lambda+i-1}}{(k-\lambda+i)\Gamma(k-\lambda+i)} \\
&\quad + \frac{1}{(k-\lambda+m)\Gamma(k-\lambda+m)} \int_z^t \left[(k-\lambda+m)\,\frac{d^{k-1}}{dt^{k-1}}(t-\xi)^{k-\lambda+m-1}\right] f^{(m+1)}(\xi)\, d\xi \\
&= \sum_{i=0}^{m} \frac{f^{(i)}(z)\,\dfrac{d^{k-1}}{dt^{k-1}}(t-z)^{k-\lambda+i-1}}{\Gamma(k-\lambda+i)} + \frac{1}{\Gamma(k-\lambda+m)} \int_z^t \left[\frac{d^{k-1}}{dt^{k-1}}(t-\xi)^{k-\lambda+m-1}\right] f^{(m+1)}(\xi)\, d\xi \\
&= \cdots \\
&= \sum_{i=0}^{m} \frac{f^{(i)}(z)\,(t-z)^{k-\lambda+i-k}}{\Gamma(k-\lambda+i+1-k)} + \frac{1}{\Gamma(k-\lambda+m+1-k)} \int_z^t (t-\xi)^{k-\lambda+m-k} f^{(m+1)}(\xi)\, d\xi \\
&= ({}_z^{GL}D_t^{\lambda} f(t))
\end{aligned} \qquad (H.2)$$

This completes the proof of the corollary 2.3.

Appendix I

Proof of Corollary 2.4

For sufficiently small h, according to the definition of integer-order derivatives, the following expansion can be obtained:

$$f^{(n)}(t) = \frac{(-1)^0 C_n^0 f(t-0h) + (-1)^1 C_n^1 f(t-1h) + (-1)^2 C_n^2 f(t-2h) + \cdots + (-1)^n C_n^n f(t-nh)}{h^n} \tag{I.1}$$

Performing the inverse transformation on Equation (I-1) yields:

$$\begin{aligned} f(t-nh) &= h^0(-1)^0 C_n^0 f^{(0)}(t) + h^1(-1)^1 C_n^1 f^{(1)}(t) + h^2(-1)^2 C_n^2 f^{(2)}(t) + \cdots \\ &\quad + h^n(-1)^n C_n^n f^{(n)}(t) \\ &= \sum_{i=0}^{n} h^i(-1)^i C_n^i f^{(i)}(t) \end{aligned} \tag{I.2}$$

According to Definition 2.5, combined with (I-2), the following relationship can be further derived:

$$\begin{aligned} E[(V)^\lambda] &= \left({}_{s-L}^{GL}D_s^\alpha\right)\left(\mathcal{L}\{p(V)\}(s)\right)\Big|_{s=0} \\ &= \sum_{i=0}^{N}(-1)^i\binom{\lambda}{i}\sum_{j=0}^{i}(-1)^j\binom{i}{j}h^{j-\lambda}\,\frac{d^j}{ds^j}\left(\mathcal{L}\{p(V)\}(s)\right)\Big|_{s=0} \\ &= \sum_{i=0}^{N}\sum_{j=0}^{i}(-1)^{i-j}\binom{\lambda}{i}\binom{i}{j}h^{j-\lambda}\,\frac{d^j}{ds^j}\left(\mathcal{L}\{p(V)\}(s)\right)\Big|_{s=0} \\ &= \sum_{j=0}^{N}\sum_{i=j}^{N}(-1)^{i-j}\binom{\lambda}{i}\binom{i}{j}h^{j-\lambda}\,\frac{d^j}{ds^j}\left(\mathcal{L}\{p(V)\}(s)\right)\Big|_{s=0} \\ &= \sum_{j=0}^{N}(-1)^{N-j}\frac{\lambda-N}{\lambda-j}\binom{\lambda}{N}\binom{N}{j}h^{j-\lambda}\,\frac{d^j}{ds^j}\left(\mathcal{L}\{p(V)\}(s)\right)\Big|_{s=0} \\ &= \sum_{j=0}^{N}(-1)^{N-j}\frac{\lambda-N}{\lambda-j}\binom{\lambda}{N}\binom{N}{j}h^{j-\lambda}\,E[(V)^j] \end{aligned} \tag{I.3}$$

This completes the proof of Corollary 2.4.

Appendix J

Proof of Corollary 2.5

Given $|f(t)| \leq M$, $a + L < b$, L is the memory length, and $\Delta(t)$ denotes the error, then the following inequality holds:

$$\begin{aligned}
\Delta(t) &= \left|({}_{-\infty}^{GL}D_t^{\lambda} f(t)) - ({}_{t-L}^{GL}D_t^{\lambda} f(t))\right| \\
&= \left|\frac{1}{\Gamma(-\lambda)}\left[\int_{-\infty}^{t} \frac{f(\xi)}{(t-\xi)^{\lambda+1}}\, d\xi - \int_{t-L}^{t} \frac{f(\xi)}{(t-\xi)^{\lambda+1}}\, d\xi\right]\right| \\
&\leq \left|\frac{1}{\Gamma(-\lambda)}\left[\int_{-\infty}^{t} \frac{f(\xi)}{(t-\xi)^{\lambda+1}}\, d\xi - \int_{-\infty}^{t-L} \frac{f(\xi)}{(t-\xi)^{\lambda+1}}\, d\xi\right]\right| \\
&= \left|\frac{1}{\Gamma(-\lambda)} \int_{t-L}^{t} \frac{f(\xi)}{(t-\xi)^{\lambda+1}}\, d\xi\right| \\
&\leq \left|\frac{1}{\Gamma(-\lambda)} \int_{t-L}^{t} \frac{M}{(t-\xi)^{\lambda+1}}\, d\xi\right| \\
&= \frac{ML^{-\lambda}}{|\Gamma(1-\lambda)|}
\end{aligned} \tag{J.1}$$

Given a required accuracy ε, ε can impose a direct impact on the memory length. If $\Delta(t) \leq \varepsilon$, then ε further determines the memory length L:

$$L \geq \left(\frac{M}{\varepsilon\,|\Gamma(1-\lambda)|}\right)^{1/\lambda} \tag{J.2}$$

References

[Acosta-Coll et al.(2018)] Acosta-Coll, M., Ballester-Merelo, F., Martinez-Peiró, M., and De la Hoz-Franco, E. (2018). Real-Time Early Warning System Design for Pluvial Flash Floods—A Review. *Sensors*, 18. https://doi.org/10.3390/s18072255

[Benouini et al.(2019)] Benouini, R., Batioua, I., Zenkouar, K., Zahi, A., Najah, S., and Qjidaa, H. (2019). Fractional-order orthogonal Chebyshev moments and moment invariants for image representation and pattern recognition. *Pattern Recognition*, 86, 332–343. https://doi.org/10.1016/j.patcog.2018.10.001

[Boyles and Waller(2010)] Boyles, S.D., and Waller, S.T. (2010). A mean-variance model for the minimum cost flow problem with stochastic arc costs. *Networks*, 56, 215–227. https://doi.org/10.1002/net.20374

[Chen and Zhou(2010a)] Chen, A., and Zhou, Z. (2010a). The α-reliable mean-excess traffic equilibrium model with stochastic travel times. *Transportation Research Part B: Methodological*, 44, 493–513. https://doi.org/10.1016/j.trb.2009.11.003

[Chen and Zhou(2010b)] Chen, A., and Zhou, Z. (2010b). The α-reliable mean-excess traffic equilibrium model with stochastic travel times. *Transportation Research Part B: Methodological*, 44, 493–513. https://doi.org/10.1016/j.trb.2009.11.003

[Chen et al.(2017)] Chen, B.Y., Shi, C., Zhang, J., Lam, W.H.K., Li, Q., and Xiang, S. (2017). Most reliable path-finding algorithm for maximizing on-time arrival probability. *Transportmetrica B: Transport Dynamics*, 5, 248–264. https://doi.org/10.1080/21680566.2016.1169953

[Chen et al.(2022)] Chen, J., Wang, Y., Ou, J., Fan, C., Lu, X., Liao, C., Huang, X., and Zhang, H. (2022). ALBRL: Automatic load-balancing architecture based on reinforcement learning in software-defined networking. *Wireless Communications and Mobile Computing*, 2022, 3866143.

[Consigli(2002)] Consigli, G. (2002). Tail estimation and mean–VaR portfolio selection in markets subject to financial instability. *Journal of Banking & Finance*, 26, 1355–1382. https://doi.org/10.1016/S0378-4266(02)00267-4

[Cottone and Di Paola(2009)] Cottone, G., and Di Paola, M. (2009). On the use of fractional calculus for the probabilistic characterization of random variables. *Probabilistic Engineering Mechanics*, 24, 321–330. https://doi.org/10.1016/j.probengmech.2008.08.002

[de Palma and Picard(2005)] de Palma, A., and Picard, N. (2005). Route choice decision under travel time uncertainty. *Transportation Research Part A: Policy and Practice*, 39, 295–324. https://doi.org/10.1016/j.tra.2004.10.001

[Di et al.(2013)] Di, X., Liu, H., Pang, J.-S., and Ban, X. (Jeff) (2013). Boundedly rational user equilibria (BRUE): Mathematical formulation and solution sets. *Transportation Research Part B: Methodological*, 57, 300–313. https://doi.org/10.1016/j.sbspro.2013.05.014

[Dremin(1994)] Dremin, I. (1994). Fractional moments of distributions. *ZhETF Pisma Redaktsiiu*, 59.

[Fan et al.(2005a)] Fan, Y.Y., Kalaba, R.E., and Moore, J.E. (2005a). Arriving on time. *Journal of Optimization Theory and Applications*, 127, 497–513. https://doi.org/10.1007/s10957-005-7498-5

[Fan et al.(2005b)] Fan, Y.Y., Kalaba, R.E., and Moore, J.E. (2005b). Shortest paths in stochastic networks with correlated link costs. *Computers & Mathematics with Applications*, 49, 1549–1564. https://doi.org/10.1016/j.camwa.2004.07.028

[Feng et al.(2024)] Feng, C., Valdebenito, M.A., Chwała, M., Liao, K., Broggi, M., and Beer, M. (2024). Efficient slope reliability analysis under soil spatial variability using maximum entropy distribution with fractional moments. *Journal of Rock Mechanics and Geotechnical Engineering*, 16, 1140–1152. https://doi.org/10.1016/j.jrmge.2023.09.006

[Fosgerau and Small(2013)] Fosgerau, M., and Small, K. (2013). Hypercongestion in downtown metropolis. *Journal of Urban Economics*, 76. https://doi.org/10.1016/j.jue.2012.12.004

[Frank(1969a)] Frank, H. (1969a). Shortest paths in probabilistic graphs. *Operations Research*, 17, 583–599. https://doi.org/10.1287/opre.17.4.583

[Frank(1969b)] Frank, H. (1969b). Shortest paths in probabilistic graphs. *Operations Research*, 17, 583–599. https://doi.org/10.1287/opre.17.4.583

[Frey and Burmaster(1999)] Frey, H.C., and Burmaster, D.E. (1999). Methods for characterizing variability and uncertainty: Comparison of bootstrap simulation and likelihood-based approaches. *Risk Analysis*, 19, 109–130. https://doi.org/10.1023/A:1006962412150

[Gelman(1995)] Gelman, A. (1995). Method of moments using Monte Carlo simulation. *Journal of Computational and Graphical Statistics*, 4, 36–54. https://doi.org/10.1080/10618600.1995.10474664

[Gradeci et al.(2018)] Gradeci, K., Labonnote, N., Sivertsen, E., and Time, B. (2018). The use of insurance data in the analysis of surface water flood events – A systematic review. *Journal of Hydrology*. https://doi.org/10.1016/j.jhydrol.2018.10.060

[Gzyl and Tagliani(2010)] Gzyl, H., and Tagliani, A. (2010). Hausdorff moment problem and fractional moments. *Applied Mathematics and Computation*, 216, 3319–3328. https://doi.org/10.1016/j.amc.2010.04.059

[Haas and Pigorsch(2009)] Haas, M., and Pigorsch, C. (2009). Financial economics, fat-tailed distributions. In: Meyers, R.A. (Ed.), *Encyclopedia of Complexity and Systems Science*, pp. 3404–3435. Springer, New York, NY. https://doi.org/10.1007/978-0-387-30440-3_204

[Hall(1983)] Hall, R.W. (1983). Travel outcome and performance: The effect of uncertainty on accessibility. *Transportation Research Part B: Methodological*, 17, 275–290. https://doi.org/10.1016/0191-2615(83)90046-2

[Horst and Thoai(1992)] Horst, R., and Thoai, N.V. (1992). Conical algorithm for the global minimization of linearly constrained decomposable concave minimization problems. *Journal of Optimization Theory and Applications*, 74, 469–486. https://doi.org/10.1007/BF00940322

[Hutson and Shier(2009)] Hutson, K.R., and Shier, D.R. (2009). Extended dominance and a stochastic shortest path problem. *Computers & Operations Research*, 36, 584–596. https://doi.org/10.1016/j.cor.2007.10.016

[Jackson and Jucker(1982)] Jackson, W.B., and Jucker, J.V. (1982). An empirical study of travel time variability and travel choice behavior. *Transportation Science*, 16, 460–475. https://doi.org/10.1287/trsc.16.4.460

[Biyari and Lindsey(1993)] Biyari, K.H., and Lindsey, W.C. (1993). Statistical distributions of Hermitian quadratic forms in complex Gaussian variables. *IEEE Transactions on Information Theory*, 39, 1076–1082. https://doi.org/10.1109/18.256521

[Khani and Boyles(2015)] Khani, A., and Boyles, S.D. (2015). An exact algorithm for the mean–standard deviation shortest path problem. *Transportation Research Part B: Methodological*, 81, 252–266. https://doi.org/10.1016/j.trb.2015.04.002

[Lam et al.(2008)] Lam, W.H.K., Shao, H., and Sumalee, A. (2008). Modeling impacts of adverse weather conditions on a road network with uncertainties in demand and supply. *Transportation Research Part B: Methodological*, 42, 890–910. https://doi.org/10.1016/j.trb.2008.02.004

[Laue(1980)] Laue, G. (1980). Remarks on the relation between fractional moments and fractional derivatives of characteristic functions. *Journal of Applied Probability*, 17, 456–466. https://doi.org/10.2307/3213035

[Liu et al.(2004)] Liu, H., Recker, W., and Chen, A. (2004). Uncovering the contribution of travel time reliability to dynamic route choice using real-time loop data. *Transportation Research Part A: Policy and Practice*, 38, 435–453. https://doi.org/10.1016/j.tra.2004.03.003

[Lo et al.(2006)] Lo, H.K., Luo, X.W., and Siu, B.W.Y. (2006). Degradable transport network: Travel time budget of travelers with heterogeneous risk aversion. *Transportation Research Part B: Methodological*, 40, 792–806. https://doi.org/10.1016/j.trb.2005.10.003

[Lo and Tung(2003)] Lo, H.K., and Tung, Y.-K. (2003). Network with degradable links: Capacity analysis and design. *Transportation Research Part B: Methodological*, 37, 345–363. https://doi.org/10.1016/S0191-2615(02)00017-6

[Luchko(2023)] Luchko, Y. (2023). Fractional integrals and derivatives: "True" versus "false." *Mathematics*, 11. https://doi.org/10.3390/math11133003

[Mahmassani and Liu(1999)] Mahmassani, H.S., and Liu, Y.-H. (1999). Dynamics of commuting decision behaviour under advanced traveller information systems. *Transportation Research Part C: Emerging Technologies*, 7, 91–107. https://doi.org/10.1016/S0968-090X(99)00014-5

[Martínez-Gomariz et al.(2023)] Martínez-Gomariz, E., Barbero, C., Sanchez-Juny, M., Forero-Ortiz, E., and Sanz-Ramos, M. (2023). Dams or ponds classification based on a new criterion to assess potential flood damage to roads in case of failure. *Natural Hazards*, 117, 625–653.

[Matsui and Pawlas(2013)] Matsui, M., and Pawlas, Z. (2013). Fractional absolute moments of heavy tailed distributions. *Brazilian Journal of Probability and Statistics*, 30. https://doi.org/10.1214/15-BJPS280

[McFadden(1972)] McFadden, D. (1972). Conditional logit analysis of qualitative choice behavior.

[Nie and Fan(2006)] Nie, Y., and Fan, Y. (2006). Arriving-on-time problem: Discrete algorithm that ensures convergence. *Transportation Research Record*, 1964, 193–200. https://doi.org/10.3141/1964-21

[Nie and Wu(2009)] Nie, Y., and Wu, X. (2009). Shortest path problem considering on-time arrival probability. *Transportation Research Part B: Methodological*, 43, 597–613. https://doi.org/10.1016/j.trb.2009.01.008

[Nikolova and Stier-Moses(2014)] Nikolova, E., and Stier-Moses, N. (2014). A mean-risk model for the traffic assignment problem with stochastic travel times. *Operations Research*, 62. https://doi.org/10.1287/opre.2013.1246

[Nonnenmacher and Metzler(1995)] Nonnenmacher, T.F., and Metzler, R. (1995). On the Riemann-Liouville fractional calculus and some recent applications. *Fractals*, 3, 557–566. https://doi.org/10.1142/S0218348X95000497

[Novák et al.(2024)] Novák, L., Valdebenito, M., and Faes, M. (2024). Fractional moment estimation from polynomial chaos expansions.

[Podlubny(1998)] Podlubny, I. (1998). *Fractional Differential Equations: An Introduction to Fractional Derivatives, Fractional Differential Equations, to Methods of Their Solution and Some of Their Applications*. Elsevier.

[Remmert(1998)] Remmert, R. (1998). The Gamma function. In: Remmert, R. (Ed.), *Classical Topics in Complex Function Theory*, pp. 33–72. Springer, New York, NY. https://doi.org/10.1007/978-1-4757-2956-6_2

[Rostami et al.(2018)] Rostami, B., Chassein, A., Hopf, M., Frey, D., Buchheim, C., Malucelli, F., and Goerigk, M. (2018). The quadratic shortest path problem: Complexity, approximability, and solution methods. *European Journal of Operational Research*, 268, 473–485. https://doi.org/10.1016/j.ejor.2018.01.054

[Salvat et al.(1999)] Salvat, F., Fernández-Varea, J.M., Sempau, J., and Mazurier, J. (1999). Practical aspects of Monte Carlo simulation of charged particle transport: Mixed algorithms and variance reduction techniques. *Radiation and Environmental Biophysics*, 38, 15–22. https://doi.org/10.1007/s004110050133

[Sandev et al.(2011)] Sandev, T., Metzler, R., and Tomovski, Z. (2011). Fractional diffusion equation with a generalized Riemann-Liouville time fractional derivative. *Journal of Physics A: Mathematical and Theoretical*, 44, 255203. https://doi.org/10.1088/1751-8113/44/25/255203

[Sen et al.(2001)] Sen, S., Pillai, R., Joshi, S., and Rathi, A.K. (2001). A mean-variance model for route guidance in advanced traveler information systems. *Transportation Science*, 35, 37–59. https://doi.org/10.1287/trsc.35.1.37.10141

[Shahabi et al.(2015)] Shahabi, M., Unnikrishnan, A., and Boyles, S.D. (2015). Robust optimization strategy for the shortest path problem under uncertain link travel cost distribution. *Computer-Aided Civil and Infrastructure Engineering*, 30, 433–448. https://doi.org/10.1111/mice.12103

[Shahabi et al.(2013)] Shahabi, M., Unnikrishnan, A., and Boyles, S.D. (2013). An outer approximation algorithm for the robust shortest path problem. *Transportation Research Part E: Logistics and Transportation Review*, 58, 52–66. https://doi.org/10.1016/j.tre.2013.07.002

[Shao et al.(2006)] Shao, H., Lam, W.H.K., and Tam, M.L. (2006). A reliability-based stochastic traffic assignment model for network with multiple user classes under uncertainty in demand. *Networks and Spatial Economics*, 6, 173–204. https://doi.org/10.1007/s11067-006-9279-6

[Sheffi(1984)] Sheffi, Y. (1984). *Urban Transportation Networks: Equilibrium Analysis with Mathematical Programming Methods*.

[Simon(1955)] Simon, H.A. (1955). A behavioral model of rational choice. *The Quarterly Journal of Economics*, 69, 99–118. https://doi.org/10.2307/1884852

[Siri et al.(2022)] Siri, E., Siri, S., and Sacone, S. (2022). A topology-based bounded rationality day-to-day traffic assignment model. *Communications in Transportation Research*, 2, 100076. https://doi.org/10.1016/j.commtr.2022.100076

[Siu and Lo(2014)] Siu, B.W.Y., and Lo, H.K. (2014). Punctuality-based route and departure time choice. *Transportmetrica A: Transport Science*, 10, 585–621. https://doi.org/10.1080/18128602.2012.751681

[Soland(1974)] Soland, R. (1974). Optimal facility location with concave costs. *Operations Research*, 22, 373–382. https://doi.org/10.1287/opre.22.2.373

[Sullivan et al.(2023)] Sullivan, J., Sentoff, K, Segale, J., Marshall, N., Fitzgerald, E., and Schiff, R. (2023). A new risk-based measure of link criticality for flood risk planning. *Transportation*, 51, 2051–2071. https://doi.org/10.1007/s11116-023-10396-y

[Sumalee et al.(2011)] Sumalee, A., Uchida, K., and Lam, W.H.K. (2011). Stochastic multi-modal transport network under demand uncertainties and adverse weather condition. *Transportation Research Part C: Emerging Technologies*, 19, 338–350. https://doi.org/10.1016/j.trc.2010.05.018

[Lefebvre(2021)] Lefebvre, T. (2021). On moment estimation from polynomial chaos expansion models. *IEEE Control Systems Letters*, 5, 1519–1524. https://doi.org/10.1109/LCSYS.2020.3040851

[Tagliani(2011)] Tagliani, A. (2011). Hausdorff moment problem and fractional moments: A simplified procedure. *Applied Mathematics and Computation*, 218, 4423–4432. https://doi.org/10.1016/j.amc.2011.10.019

[Uchida(2015)] Uchida, K. (2015). Travel time reliability estimation model using observed link flows in a road network. *Computer-Aided Civil and Infrastructure Engineering*, 30, 449–463. https://doi.org/10.1111/mice.12109

[Wang et al.(2021)] Wang, N., Hou, J., Du, Y., Jing, H., Wang, T., Xia, J., Gong, J., and Huang, M. (2021). A dynamic, convenient and accurate method for assessing the flood risk of people and vehicle. *Science of The Total Environment*, 797, 149036. https://doi.org/10.1016/j.scitotenv.2021.149036

[Wang et al.(2014)] Wang, X., Jian-yun, Z., Shahid, S., Guan, E., Wu, Y., Gao, J., and He, R. (2014). Adaptation to climate change impacts on water demand. *Mitigation and Adaptation Strategies for Global Change*, 21. https://doi.org/10.1007/s11027-014-9571-6

[Wardrop(1952)] Wardrop, J.G. (1952). Road paper: Some theoretical aspects of road traffic research. *Proceedings of the Institution of Civil Engineers*, 1, 325–362. https://doi.org/10.1680/ipeds.1952.11259

[Watling(2006)] Watling, D. (2006). User equilibrium traffic network assignment with stochastic travel times and late arrival penalty. *European Journal of Operational Research*, 175, 1539–1556. https://doi.org/10.1016/j.ejor.2005.02.039

[Xing and Zhou(2011)] Xing, T., and Zhou, X. (2011). Finding the most reliable path with and without link travel time correlation: A Lagrangian substitution based approach. *Transportation Research Part B: Methodological*, 45, 1660–1679. https://doi.org/10.1016/j.trb.2011.06.004

[Xu and Dang(2019)] Xu, J., and Dang, C. (2019). A novel fractional moments-based maximum entropy method for high-dimensional reliability analysis. *Applied Mathematical Modelling*, 75, 749–768. https://doi.org/10.1016/j.apm.2019.06.037

[Xu et al.(2017)] Xu, X., Chen, A., Cheng, L., and Yang, C. (2017). A link-based mean-excess traffic equilibrium model under uncertainty. *Transportation Research Part B: Methodological*, 95, 53–75. https://doi.org/10.1016/j.trb.2016.10.018

[Ye and Kim(2019)] Ye, Q., and Kim, H. (2019). Assessing network vulnerability of heavy rail systems with the impact of partial node failures. *Transportation*, 46. https://doi.org/10.1007/s11116-018-9859-6

[Zeng et al.(2015)] Zeng, W., Miwa, T., Wakita, Y., and Morikawa, T. (2015). Application of Lagrangian relaxation approach to α-reliable path finding in stochastic networks with correlated link travel times. *Transportation Research Part C: Emerging Technologies*, 56, 309–334. https://doi.org/10.1016/j.trc.2015.04.018

[Zhang and Pandey(2013)] Zhang, X., and Pandey, M.D. (2013). Structural reliability analysis based on the concepts of entropy, fractional moment and dimensional reduction method. *Structural Safety*, 43, 28–40. https://doi.org/10.1016/j.strusafe.2013.03.001

[Zhang and Khani(2019)] Zhang, Y., and Khani, A. (2019). An algorithm for reliable shortest path problem with travel time correlations. *Transportation Research Part B: Methodological*, 121, 92–113. https://doi.org/10.1016/j.trb.2018.12.011

[Zhang et al.(2017)] Zhang, Y., Max Shen, Z.-J., and Song, S. (2017). Lagrangian relaxation for the reliable shortest path problem with correlated link travel times. *Transportation Research Part B: Methodological*, 104, 501–521. https://doi.org/10.1016/j.trb.2017.04.006

[Zhao et al.(2021)] Zhao, H., Li, S., and Zhu, C. (2021). Uncertainty analysis of rock tunnel based on fractional moment and dimensional reduction method. *International Journal of Rock Mechanics and Mining Sciences*, 139, 104656. https://doi.org/10.1016/j.ijrmms.2021.104656

[Zhou et al.(2022)] Zhou, R., Zheng, H., Liu, Y., Xie, G., and Wan, W. (2022). Flood impacts on urban road connectivity in southern China. *Scientific Reports*, 12. https://doi.org/10.1038/s41598-022-20882-5

Acknowledgments

This dissertation was completed with the support and encouragement of many individuals and institutions, to whom sincere appreciation is hereby expressed.

First and foremost, sincere gratitude is extended to Professor Kenetsu Uchida of Hokkaido University for his continuous guidance and invaluable support throughout the doctoral studies. His rigorous academic standards, insightful perspectives, and persistent pursuit of excellence have profoundly shaped scholarly development and research capabilities.

Heartfelt thanks are also extended to Associate Professor Ryuichi Tani for his constructive advice and generous assistance in research methodologies, experimental design, and academic writing. His precise feedback and constant encouragement have been essential to the successful progress of this work.

Appreciation is further given to all members of the laboratory for their collaborative support and kindness during both research activities and daily life. Their insightful discussions and shared experiences have greatly enriched the academic journey.

Acknowledgment is also given to Hokkaido University for providing an outstanding research environment and comprehensive institutional resources. Special gratitude is extended to the EXEX Scholarship Program, whose support has enabled full dedication to academic and research work.

To all those who have contributed to this dissertation in various ways, your support is sincerely appreciated.